University of Valladolid

Faculty of Sciences

Department of Theoretical, Atomic and Optical Physics

Experimental transition probabilities and Stark parameters of singly ionized noble gases.

Thesis submitted by

María Teresa Belmonte Sainz-Ezquerra

as part of the requirements for the degree of Doctor in Physics

supervised by

Santiago Mar Sardaña
Stevica Djurović
Juan Antonio Aparicio Calzada

May 2016

A mis padres, mi hermana y Ewan,

por iluminar mi vida.

Para mis abuelos,

por ser el origen de todo.

"The imagination of nature is far, far greater than the imagination of man."

- Richard P. Feynman -

Agradecimientos - Acknowledgement

"The teacher who walks in the shadow of the temple, among his followers,
gives not of his wisdom, but rather of his faith and his lovingness.
If he is indeed wise, he does not bid you enter the house of his wisdom,
but rather leads you to the threshold of your own mind."

- Khalil Gibran, *The Prophet-*

Pocos lugares hay tan mágicos como los pasillos de una facultad de ciencias. Casi una década ha pasado ya desde que recorrí por primera vez la antigua Facultad de Ciencias de Valladolid y varios pasillos se han sucedido, no sólo en distintas facultades sino también en diferentes países. Pasillos llenos de gente curiosa que siempre quiere aprender, puertas tras las cuales he encontrado ayuda, consejo, apoyo, sabiduría y amistad. A todas esas personas escondidas detrás de puertas con o sin nombre va mi más profundo agradecimiento. Esta tesis no es más que el resultado de muchos esfuerzos conjuntos y nunca podría haber llegado a puerto sin TODOS vosotros.

Nunca habrá visitado todos esos pasillos si no fuese por los dos físicos a los que más admiro: mis padres. Horas de dedicación y esfuerzo que durante muchos años habéis invertido en mí y que me han hecho amar este campo del conocimiento. Siempre habéis mantenido mi mente abierta, inquieta y ansiosa por entender y no he podido tener mejores maestros. Sabéis que ese 'cuando estudies física lo entenderás' tiene la culpa de todo. Esta tesis es, sin ninguna duda, otro de nuestros 'trabajos en equipo'.

Si hay alguien con quien he compartido puertas y habitaciones y que tiene la culpa de que esta tesis se materialice, esa es sin duda mi hermana. Pau, gracias por romper puertas, por sacarme de la "torre de marfil" de la facultad y hacerme ver que siempre hay

más. Ya sabes, ¡aún puedes volver al camino del bien, ingeniera de la familia!

Las primeras puertas del departamento a las que uno, tímidamente, se atreve a llamar son las de sus tutores. A mis tres directores de tesis, Santiago, Apa y Stevica, va mi agradecimiento más sincero. Habéis sido el equilibrio perfecto de personalidades y entre los tres me habéis enseñado mucho más de lo que jamás esperé aprender, no solo de Física sino de la vida en general. Si de algo me he dado cuenta es de que no hay nada más satisfactorio que navegar en un barco capitaneado por un equipo de personas buenas, sensatas y valiosas de las que uno puede aprender. Es el mejor legado que podríais haberme dejado y lo llevaré siempre conmigo, allá donde vaya.

La siguiente puerta que uno atraviesa es la de su propio despacho y en ese sentido no he podido ser más afortunada, ya que he tenido la suerte de compartir espacio con amigos más que con compañeros. El tiempo se ha pasado muy rápido a vuestro lado, Ale y Diego. Muchas gracias por tantas y tantas conversaciones sobre lo humano y lo divino, kitkats de los que le alegran a uno el día y cocina de alto nivel. No podría haber escogido mejores amigos, de verdad. ¡Espero que la distancia no sea más que un muy buen motivo para organizar cenas internacionales!

No podría olvidarme de mi última compañera de despacho, que me acogió tras su puerta y me puso las pilas en el momento en que más lo necesitaba, cuando escribir parecía una tarea imposible. Irene, has sido el mejor modelo que podía tener. Sólo espero tener esa fuerza y determinación que siempre me asombran de ti.

Hay ciertas puertas tras las cuales uno se siente siempre en casa y esa es sin duda la tuya, Carlos. Hace ya 8 años que llamé vergonzosamente en busca de ayuda con los misterios de la óptica, que luego se convirtieron en los de la cuántica y finalmente en los más importantes, los de la vida. No hay un gracias suficiente para agradecerte toda tu ayuda y apoyo durante estos años. Y qué decir de esos nudillos que llaman cuidadosamente a mi puerta y sobre todo de ese '¡Teruu!' que tanto me ha acompañado. Ra, gracias por iluminar todos estos años. No habría sido lo mismo sin tí.

Puertas y más puertas que siempre me sacan una sonrisa o me enseñan algo. Fernando, no hay nada más inspirador que ser asaltado en el pasillo con los misterios de los factoriales o la siempre fascinante historia de los calendarios. Eres el encargado de mantener nuestros cerebros en marcha, ¡no pares nunca! Y puertas tras las cuales se esconden sonrisas radiantes como las vuestras, Concha e Inma, que iluminan todo el pasillo. Qué haríamos sin vuestra fortaleza y tenacidad, habéis sido un gran ejemplo de lucha constante para

mí. Y a las otras chicas del pasillo, Bea e Isa, a Marco, a Ángel y a Carlos y al resto de profesores del departamento, muchas gracias por la ayuda que siempre me habéis prestado.

Algunos hemos compartido muchos años de camino, ya desde la carrera. No me olvido de ti, Alberto, mi amigo sensato y compañero de horas de laboratorios y conversaciones. Gracias por estar siempre ahí. Y a todos vosotros, Bea, Alejandra, todos los miembros del GOA, Vero: ha sido un placer.

Y sin dejar la facultad, no puedo olvidarme de tres personas sin las cuales nunca habría llegado hasta aquí y que permanecerán siempre en mi recuerdo aunque ya no estén con nosotros. A Mauricio Pardos, que con tanta paciencia y con el espíritu de un verdadero maestro fue forjando mi mente para la física. A Carlos de Francisco, incansable en sus intentos por hacernos ver que la física no estaba reñida con el humor. Y finalmente para Diego, sin cuyo consejo puede que no estuviese aquí. Siempre apareciste en el momento oportuno y aún no sé por qué...

I can not forget all the fantastic people I met in Serbia during my 6 months in Novi Sad. Thank you so much for welcoming me so warmly and helping me so much. You made me feel at home. Stevica, I can not express my gratitude in words. You have always helped me a lot more than was necessary. I just hope to reciprocate someday: hvala. Lazar, thank you so much for your infinite help and friendship during my time there and apologies for all the work I gave you. An important part of this thesis would had never existed without you. To Igor, Zoran, Teodora, Kristina, Ines and all the people in the Science Faculty and of course, to Tamara: hvala. I am looking forward to seeing all of you in Spain!

I would also like to thank all the fantastic people in the Space and Atmospheric Physics Department at Imperial College in London, especially my supervisor Juliet C. Pickering, who welcomed me and taught me so much during the 3 months I spent there. I can not forget you, Isabel, for all your help and constant support not only during this British adventure, but during all these years.

Finalmente, para la persona que día tras día ha estado a mi lado durante todos estos años de tesis, apoyándome cuando las fuerzas flaqueaban. Ewan, not only I own you the fact that the English in this manuscript is understandable, but also the necessary strength to write it. Thank you for transforming Valladolid into the most magical of the places and opening with me a door into the future...

"When I got to him, Feynman was gazing at a rainbow. He had an intense look on his face, as if he were concentrating. As if he had never seen one before. Or maybe as if it might be his last. I approached him cautiously.

'Professor Feynman. Hi', I said.

'Look, a rainbow', he said without looking at me. I was relieved that I didn't detect any residual annoyance in his voice.

I joined him in staring at the rainbow. It appeared pretty impressive, if you stopped to look at it. It wasn't something I normally did-in those days.

'I wonder what the ancients thought of rainbows', I mused. There were many myths based on the stars, but I thought rainbows must have seemed equally mysterious.

'That's a question for Murray', he said. 'All I know', Feynman continued, 'is that according to one legend angels put gold at its ends and only a nude man can reach it. As if a nude man doesn't have better things to do', he said with a sly smile.

'Do you know who first explained the true origin of the rainbow?' I asked.

'It was Descartes', he said. After a moment he looked me in the eye. 'And what do you think was the salient feature of the rainbow that inspired Descartes' mathematical analysis?' he asked.

'Well, the rainbow is actually a section of a cone that appears as an arc of the colors of the spectrum when drops of water are illuminated by sunlight behind the observer.'

'And?'

'I suppose his inspiration was the realization that the problem could be analyzed by considering a single drop, and the geometry of the situation.'

'Youre overlooking a key feature of the phenomenon', he said.

'Okay, I give up. What would you say inspired his theory?'

'I would say his inspiration was that he thought rainbows were beautiful.'

- Leonard Mlodinow, *Feynman's Rainbow-*

"Me dirigí hacia Feynman. Cuando llegué a él, Feynman estaba observando un arco iris. Tenía una intensa mirada en su rostro, como si se estuviera concentrando, como si nunca hubiera visto uno antes. O quizá como si pudiera ser el último que viera. Me acerqué a él cautelosamente.

'Hola, profesor Feynman', dije.

'Mira, un arco iris', dijo sin mirarme. Observé el arco iris. Parecía muy impresionante, si te parabas a considerarlo. No era algo que yo hiciera normalmente en esta época.

'Me pregunto qué pensaban los antiguos del arco iris', dije en voz baja. Había muchos mitos basados en las estrellas, pero pensaba que el arco iris debió de haber parecido igualmente misterioso.

'Esa es una pregunta para Murray', dijo. 'Todo lo que sé', siguió diciendo Feynman, 'es que según una leyenda los ángeles ponen oro en sus extremos y sólo un hombre desnudo puede alcanzarlo. Como si un hombre desnudo no tuviera cosas mejores que hacer', dijo con una sonrisa pícara.

'¿Sabes quién explicó por primera vez el verdadero origen del arco iris?', pregunté.

'Fue Descartes', dijo. Después de un rato me miró a los ojos. '¿Y cuál piensas tú que fue la principal característica del arco iris que inspiró el análisis matemático de Descartes?', preguntó.

'Bien, el arco iris es en realidad una sección de un cono que aparece como un arco con los colores del espectro cuando las gotas de agua son iluminadas por la luz del sol que procede de detrás del observador.'

'¿Y?'

'Supongo que lo que le inspiró fue el darse cuenta de que el problema podía analizarse considerando una única gota y la geometría de la situación.'

'Estás pasando por alto un aspecto clave del fenómeno', dijo.

'Muy bien, me rindo. ¿Qué diría usted que inspiró su teoría?'

'Yo diría que lo que le inspiró fue el pensamiento de que el arco iris era bello...'"

-Leonard Mlodinow, *El arco iris de Feynman*-

Introduction.

Knowledge of atomic parameters, such as transition probabilities and Stark widths and shifts, is of great importance not only in the field of theoretical atomic physics, but also for the diagnosis of any radiation emitting source such as conventional lamps, lasers, industrial and fusion plasmas. It is also of considerable use in the field of Astrophysics, where transition probabilities and Stark parameters are necessary for the calculation of data such as chemical abundances of the different elements in stars. However, current needs are not covered by the data available, especially in the ultraviolet region, where there is an absence of accurate experimental data for ionized atoms.

The subject of this thesis is the measurement of new atomic data by means of a plasma emission spectroscopy technique. In particular, this work has focused on the measurement of accurate new transition probabilities of singly ionized Argon and Krypton in the ultraviolet region, paying special attention to the calculation of their uncertainties, and the measurement of Stark widths and shifts of Ar II spectral lines in the ultraviolet. A significant quantity of new data and their uncertainties has been reported and analyzed, contributing to the upgrading of atomic databases with new, high quality data.

The research of this doctoral thesis was conducted in the Plasma Spectroscopy Laboratory at the University of Valladolid. The group has been working on the measurement of atomic parameters for more than thirty years and has wide experience in the field of plasma spectroscopy, the fruit of many hours of hard work invested by all those who have participated on it. The experimental set-up and plasma diagnostic methods have been carefully developed over the years and a deep knowledge of the experiment has permitted the carrying out of high quality measurements.

The manuscript has been structured into six different chapters. The first three are devoted to the description of the theoretical framework, the experimental set-up and the

processing of the data. The second half consists of three chapters, each of them containing one of three previously published articles and include all the recent developments in the field, a detailed description of the experiments, as well as the results and conclusions.

Chapter 1 summarizes the fundamental theoretical concepts involved in the measurement of transition probability values and Stark parameters and defines the terms that will be used throughout the manuscript. **Chapter 2** contains a thorough description of the experimental set-up, from the generation of the plasma to the acquisition of the spectra, paying special attention to the calibration of the spectroscopic channel. **Chapter 3** focuses on data processing and the study and determination of uncertainty associated with the measured atomic parameters. **Chapters 4**, **5** and **6** contain the experimental details and results of the measurement of Stark parameters in Ar II and transition probabilities in Ar II and Kr II in the ultraviolet respectively. The bibliographies of these chapters are included in each of the articles.

Contents

List of Figures

List of Tables

Chapter 1

Theoretical fundamentals.

"Too see a World in a Grain of Sand,
And a Heaven in a Wild Flower,
Hold Infinity in the palm of your hand
And Eternity in an hour"

- William Blake -

1.1   Plasma definition, parameters and criteria.

A plasma, nowadays considered as the fourth state of matter, can be defined as a quasineutral gas of charged and neutral particles that interact amongst themselves and with the electric field in which they are immersed and where collective effects dominate over collisions (Bittencourt, 2004; Chen, 1974; Spitzer, 1956).

The use of the word plasma, from the Greek $\pi\lambda\alpha\sigma\mu\alpha$("mouldable substance" or "jelly"), was introduced by the Czech medical scientist Johannes Purkinje in the mid-twentieth century to designate the transparent liquid component of the blood that remains once corpuscles have been eliminated.

Plasmas were first identified as "radiant matter" by the British chemist and physicist Sir William Crookes in 1879 , although this term had already been used by Michael Faraday

sixty years before, as Crookes explains by quoting Faraday's notes (Crookes, 1897):

"If we conceive a change as far beyond vaporisation as that is above fluidity, and then take into account also the proportional increased extent of alteration as the changes rise, we shall perhaps, if we can form any conception at all, not fall far short of Radiant Matter; and as in the last conversion many qualities were lost, so here also many more would disappear."

The British physicist Sir Joseph John Thomson identified plasma as a different nature of matter in 1897, but it was the American scientist Irving Langmuir who first used the term "plasma" in 1928 to refer to the ionized gases he was working with. The way in which an electrified fluid carries electrons and ions reminded him of the way plasma carries red and white corpuscles.

When a sufficient quantity of energy is provided to a gas, it will gradually dissociate into an atomic gas. Increasing the quantity of energy even more, some of these particles will start to have enough energy to collide with other ones and ionization will take place. It is important to notice that this change from gas to plasma is not a phase transition in the thermodynamic sense, since it does not take place at a constant temperature as happens with the other phase transitions.

The presence of a significant number of charged particles within a plasma makes it electrically conductive, being strongly influenced by electromagnetic fields and a very good thermal conductor. A plasma can be characterized by the following parameters:

∗ **Degree of ionization**: this parameter can be defined as (Bittencourt, 2004):

$$\alpha = \frac{n_e}{n_e + n_n} \tag{1.1}$$

where n_e is the electron density and n_n is the density of neutral particles.

∗ **Debye length**: the Debye length or shielding radius gives an idea of the distance to which the electric field of a charged particle (electron or ion) extends before being shielded by the surrounding particles of opposite charge (Thorne, 1974). This parameter represents a typical length for collective action, being the individual interactions between different particles only important over distances smaller than this quantity, which is defined as:

$$\lambda_D = \left(\frac{\varepsilon_0 \mathrm{k} T}{n_e e^2}\right)^{\frac{1}{2}} \tag{1.2}$$

where ε_0 is the vacuum permittivity, k is the Boltzmann constant (written in roman to differentiate it from the subscript related to the upper energy level), T is the plasma temperature, n_e is the plasma electron density and e is the electron charge.

∗ **Plasma frequency**: this parameter represents the resonance frequency of the collective oscillations of the electrons around their equilibrium positions. These oscillations take place when a plasma is abruptly removed from its equilibrium condition. In this situation, the internal electric fields will tend to restore the original charge neutrality, which will create collective movements characterized by the plasma frequency:

$$\omega_{pe} = \left(\frac{n_e e^2}{m_e \varepsilon_0}\right)^{\frac{1}{2}} \tag{1.3}$$

where ω_{pe} represents the frequency of the electron oscillations, since they are much lighter than the ions and therefore will determine this parameter. The reciprocal of the plasma frequency establishes a typical timescale within the plasma.

There are certain criteria that an ionized gas, a collection of different charged particles that are free to move in response to either the fields that they generate or those applied from outside, must fulfill in order to be classified as a plasma. A thorough explanation about **plasma criteria** can be found in Bittencourt (2004). Here, the different criteria will only summarize as:

1) The dimensions of the plasma L must be large in comparison to the Debye length λ_D:

$$L >> \lambda_D \tag{1.4}$$

This implies that there is enough 'space' for the collective shielding effect to happen.

2) The average distance between electrons, which is roughly given by $n_e^{\frac{1}{3}}$, must be very small compared to the Debye length:

$$n_e \lambda_D^3 >> 1 \tag{1.5}$$

where n_e is the plasma electron density. This condition is also expressed as $g << 1$ by defining the so-called **plasma parameter** as:

$$g = \frac{1}{n_e \lambda_D^3} \tag{1.6}$$

This parameter is a measure of the ratio between the average inter-particle potential energy and the average plasma kinetic energy.

3) Macroscopic neutrality: in absence of any external disturbance, a plasma is macroscopically neutral

$$n_e = \sum_{z=1}^{k} z \, n_z \tag{1.7}$$

If this third criterion was not fullfilled, the potential energy resulting from the Coulomb forces would be much higher than the thermal kinetic energy of the particles. The condition of quasi-neutrality is valid throughout the volume of the plasma if its spatial scale length is much larger than the Debye length, but it is not fulfilled in those regions close to the boundaries.

4) The frequency of the collisions between electrons and neutral atoms ν_{en} must be smaller than the plasma frequency ω_{pe}:

$$\nu_{pe} > \nu_{en} \tag{1.8}$$

where

$$\nu_{pe} = \frac{\omega_{pe}}{2\pi} \tag{1.9}$$

This criterion ensures the independent behaviour of the electrons. Otherwise, they will be forced by the collisions to thermalize with the neutrals and being in complete equilibrium the medium could be treated as a gas, as stated in Bittencourt (2004).

This collective of electrons, ions and neutral atoms and the radiation field are in constant interaction. The light electrons are accelerated in the electric field until they collide

with an atom or ion, transferring all or part of their energy and exciting or ionizing the other particle. The main processes that are likely to happen amongst the different kind of particles (Marr, 1968) within the plasma are:

a) Collisional excitation and de-excitation:

$$X(n) + e^- \rightleftharpoons X(n') + e^- \tag{1.10}$$

b) Collisional recombination and ionization:

$$X^+ + e^- + e^- \rightleftharpoons X(n) + e^- \tag{1.11}$$
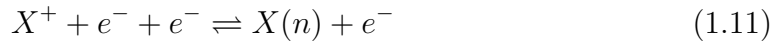
c) Radiative recombination and photoionization:

$$X^+ + e^- \rightleftharpoons X(n) + h\nu \tag{1.12}$$

d) Photo-excitation and emission:

$$X(n) + h\nu \rightleftharpoons X(n') \tag{1.13}$$

In the previous expressions, $X(n)$ represents an atom in a given configuration, $X(n')$ the same atom in an excited state, X^+ an ion and $h\nu$ is the energy of a given photon. Some of the previous processes, such as the radiative recombination (1.12), emit continuous radiation due to the fact that free electrons can have any energy and therefore, the photons emitted can also have a wide range of energies, creating a continuum spectrum. The deceleration of the electron also produces a continuum radiation known as Bremsstrahlung.

However, other processes such as spontaneous emission produce spectral radiation, which can be used to obtain a great deal of information about the plasma conditions and different properties of the atoms and ions present within it. The analysis of this radiation coming from the plasma is the field of study of Plasma Spectroscopy.

1.2   The main plasma balance processes and plasma equilibrium.

1.2.1   Balance processes.

A classic and complete description of a plasma would necessitate a knowledge of the position and velocity of every particle, as well as of the electromagnetic fields within it. This approach is highly complex and therefore a use of the probabilistic methods of statistical mechanics is far more convenient. The statistical description of a plasma is complete when all the distribution functions of every kind of particle and physical processes taking place within it are known.

There are four main processes involving charged, neutral particles and photons, each of them being described by one of the following equations:

* **The Maxwell equation**: it determines the quantity of particles of mass m and temperature T_c with velocities ranging between v and $v + dv$ out of the total density of particles n. It can be written as:

$$\frac{n(v)}{n} = 4\pi \left(\frac{m}{2\pi k T_c} \right)^{\frac{3}{2}} v^2 e^{\frac{-\frac{1}{2}mv^2}{k T_c}} \tag{1.14}$$

   where k is the Boltzmann constant. This balance mechanism is based on the exchange and conservation of kinetic energy during the collisions between particles.

   When collisions take place between particles of the same variety, the energy and distribution functions tend to be equilibrated, as analyzed in Spitzer (1956). However, when collisions take place between electrons and other species in the plasma, the electrons thermalize very rapidly into a Maxwellian distribution, but do not thermalize as quickly with neutral particles and ions due to the large mass difference. This leads to a resistivity and provides a mechanism for heating, often called *ohmic heating* or *Joule heating*.

* **The Boltzmann equation**: it establishes the occupation of the excited states of atoms and ions as a function of the temperature. The proportion of the total density of particles that are in the state of energy E_k is:

$$\frac{n_k}{n} = \frac{g_k}{Z(T)} \; e^{\frac{-E_k}{\mathrm{k}T_{exc}}} \tag{1.15}$$

where g_k is the statistical weight or degeneracy of the energy level k (defined as $2J_k + 1$), T_{exc} is the excitation temperature and $Z(T)$ is the partition function of the considered atom, given by:

$$Z(T) = \sum_k g_k \; e^{\frac{-E_k}{\mathrm{k}T_{exc}}} \tag{1.16}$$

Therefore, the relative population of the excited states k and i can be written as:

$$\frac{n_k}{n_i} = \frac{g_k}{g_i} \; e^{-\frac{E_k - E_i}{\mathrm{k}T_{exc}}} \tag{1.17}$$

* **The Saha equation**: this expression is an application of the general equilibrium relation for atomic dissociation and it provides the plasma degree of ionization by giving the ratio between the densities of two successive ions of the same element, n_z and n_{z+1}:

$$\frac{n_{z+1}}{n_z} = \frac{2}{n_e} \left(\frac{2\pi m_e \mathrm{k}T_S}{h^2} \right)^{\frac{3}{2}} \frac{Z_{z+1}(T_S)}{Z_z(T_S)} \; e^{-\frac{E_z^\infty - \Delta E_z^\infty}{\mathrm{k}T_S}} \tag{1.18}$$

z being the charge of the ions, T_S the so-called Saha's temperature, Z_{z+1} and Z_z the partition functions of the ionic species, E_z^∞ the ionization energy of the ion with charge z and ΔE_z^∞ the reduction of the ionization potential as a result of the interaction between the ion and the other charged particles present within the plasma. For the kind of plasmas generated in our laboratory, the reduction of the ionization potential can be described by using the Debye-Hückel model (Griem, 1964):

$$\Delta E_z^\infty = \frac{1}{4\pi\varepsilon_0} \frac{e^2}{\lambda_D} z \sqrt{1 + \frac{< z^2 >}{< z >}} \tag{1.19}$$

where z represents the charge of the next ion (i.e., $z = 1$ for a neutral atom), ε_0 the vacuum permittivity, e the electron charge, λ_D the Debye lenght, $< z >$ and $< z^2 >$ correspond to the average values of z and z^2 over the different ionic species present in the plasma, it being possible to approximate their ratio by z. Introducing this supposition and the expression (1.2) for the Debye length, we can write:

$$\Delta E_z^\infty = 2.09 \cdot 10^{-11} \sqrt{\frac{n_e}{T}} \; z \; \sqrt{1+z} \tag{1.20}$$

with n_e expressed in m^{-3}, T in K and ΔE_z^∞ in eV.

* **The Planck equation**: the last of the balance processes is based on the conservation of the plasma radiation (Lochte-Holtgreven, 1968) and it establishes a balance between the processes of absorption and emission of radiation. The Planck function governs the distribution of radiative energy as a function of the frequency :

$$U(\nu) = \frac{8\pi\nu^2}{c^3} \frac{h\nu}{e^{\frac{h\nu}{kT_{rad}}} - 1} \tag{1.21}$$

where ν is the frequency of the radiation and T_{rad} is the parameter that characterizes the Planck equation.

1.2.2   Plasma equilibrium.

Depending on which of the previous balance processes are verified, the plasma will be in a different thermodynamic state. The study of the plasma equilibrium is a complicated task and approximations are made on many occasions to simplify the analysis. Detailed descriptions of this subject can be found in Fantz (2006); Lochte-Holtgreven (1968); Marr (1968); Thorne (1974). We will only focus here on those plasma descriptions which are important for the analysis of the plasma used in this thesis.

a) **Thermodinamic equilibrium (TE)**: a plasma is in complete thermodynamic equilibrium when all forms of energy distribution are described by the same temperature parameter, T:

$$T_{k_e} = T_{k_i} = T_{k_n} = T_{exc} = T_S = T_{rad} = T \tag{1.22}$$

where T_{k_e}, T_{k_i} and T_{k_n} represent the temperatures associated to the kinetic energy of the electrons, ions and neutral atoms, respectively, and T_{exc}, T_S and T_{rad} are the temperature parameters from the Boltzmann, Saha and Planck equations.

Thermodynamic arguments show that the **principle of detailed balance** or microscopic reversibility must then operate: every atomic process is as frequent as its

inverse process, where this frequency is given by the product of the number of particles participating in the process and its probability of occurrence (Lochte-Holtgreven, 1968).

In these circumstances, it is possible to describe the plasma in a simple way as all the interesting magnitudes can be obtained from the TE equations once the temperature, pressure and chemical composition of the plasma are fixed. The plasma will be described by the free electron density n_e, the ion density n_i, the absolute temperature T and the ionization degree α.

b) **Local thermodinamic equilibrium (LTE)**: in this kind of equilibrium it is possible to find a temperature parameter that fits the Maxwell, Boltzmann and Saha relations for every point. In this case, the form of energy which is out of balance with the other three is the radiation energy:

$$T_{k_e} = T_{k_i} = T_{k_n} = T_{exc} = T_S \neq T_{rad} \tag{1.23}$$

This idea does not seem strange if we consider that this radiative equilibrium would require the plasma to be optically thick at all frequencies, which would make it impossible to use an spectroscopic technique as no radiation would leave the plasma source. This LTE is achieved provided the plasma has a sufficiently high electron density, which ensures that collisional processes dominate over the radiative ones (Marr, 1968). This means that the probability of an excited state de-exciting through an inelastic collision is much larger than through spontaneous radiation processes (Thorne, 1974).

Different authors suggest that a criterion for LTE is that the velocity of the electronic collisions must be at least one order of magnitude higher to the speed of the fastest radiative transition. Griem suggests a criterion (Griem, 1963, 1964, 1997) which establishes the threshold value for the electron density from which it is possible to consider that the plasma is in LTE

$$n_e \geq 9.2 \cdot 10^{23} \left(\frac{E_2}{E_H} \right)^3 \sqrt{\frac{kT}{E_H}} \tag{1.24}$$

where n_e is given in m^{-3}, E_2 is the energy of the first excited state and E_H is the Rydberg constant. Fujimoto & Whirter propose a different criterion (Fujimoto & Whirter, 1990) by using a collisional-radiative model given by:

$$n_e \geq 1.5 \cdot 10^{24} z^7 \left(\frac{T}{z^2 10^6} \right)^a \tag{1.25}$$

being

$$a = 0.55 - \left(\frac{0.49}{z} \right)^{\frac{3}{2}} \tag{1.26}$$

where n_e is expressed in m^{-3} and T in K. This criterion is more restrictive that Griems one, establishing a higher threshold value of the electron density.

c) **2-T Local thermodinamic equilibrium**: for dense plasmas, the electron distribution dominates over those from other particles. Due to their small mass, their velocities are high in comparison to those of the other particles and their cross-sections for collisions also tend to be higher. However, the electrons have small cross-sections for the transference of momentum through collisions with particles of very different mass, which leads to a lower efficiency in the transfer of the energy distribution in electron-atom and electron-ion collisions (Marr, 1968). This means that the velocity distributions of electrons, ions and neutral atoms, even if Maxwellian, will be described by a different temperature parameter:

$$T_{k_e} = T_{exc} = T_S > T_{k_i} \approx T_{k_n} \tag{1.27}$$

These kinds of plasmas are referred to as two-temperature plasmas.

d) **Partial local thermodinamic equilibrium (pLTE)**: there are different situations that prevent the plasma from being in a complete LTE. For example, as we descend to lower energy levels of the emitting particle, their collisional excitation cross section decreases and the probability of spontaneous emission increases. This means that the lower energy levels are more likely to be overpopulated. If the deviation from the LTE is not too big, there is generally a certain level of energy from which the distribution of the excited states follows a Saha-Boltzmann distribution. In addition, the temperature which characterizes this function can be considered a good approximation of the kinetic energy of the electrons:

$$T_{c_e} = T_{exc} = T_S = T \tag{1.28}$$

this expression only being valid for energy levels above a certain threshold value. This is the description that adapts better to the plasma generated in our laboratory and is referred to as *partial local thermodinamic equilibrium.*

For hydrogen-like atoms, there are different theoretical estimations of the principal quantum number n_{cr} above which the energy levels are thermalized and therefore, it is possible to consider that LTE exists. Griem provides the following criterion (Griem, 1963, 1964, 1997) for a given electron density and temperature:

$$n_{cr} = 417 \left(\frac{n_e}{z^7}\right)^{-\frac{2}{17}} \left(\frac{T_{k_e}}{z^2}\right)^{\frac{1}{17}} \tag{1.29}$$

where z is the ionization state of the atom and the electron density n_e and temperature T_{k_e} are expressed in m^{-3} and K, respectively. The ratios (n_e/z^7) and (T_{k_e}/z^2) are normally called plasma reduced density and temperature, respectively. Equation (1.29) was obtained by imposing the condition that the rate of de-excitation for collisional processes is at least 10 times higher than the one for radiative processes.

By defining an effective principal quantum number n^*, it is possible to extend the equation (1.29) to non hydrogen-like atoms. This effective principal quantum number appears as a consequence of expressing the energy levels of a non hydrogen-like atom in the manner conventionally used for those of hydrogen:

$$E_{z,n}^\infty = E_H \frac{z^2}{n^{*2}} \tag{1.30}$$

where $E_{z,n}^\infty$ represents the ionization energy of a given energy level n and E_H is the Rydberg constant. It is important to remark that the pLTE will be reached more easily for heavier atoms.

1.3 Plasma light emission and absorption: intensity and shape of spectral lines.

A plasma can be used as an extensive source of light from which it is possible to obtain very interesting atomic information due to the radiation that escapes from it. Analyzing that radiation is the main purpose of any experiment carried out within the field plasma spectroscopy.

1.3.1   Emission and absorption coefficients.   Radiative transfer equation.

In this section, we will describe the physical phenomenon known as radiative transfer, which studies the transference of the energy in the form of electromagnetic radiation. The plasmas generated in our experiment are used as sources of radiation, the intensity of which is the magnitude we are interested in from an spectroscopic point of view. The intensity emitted by a plasma column, I, is the power emitted by a luminous cylinder, l in length and d in diameter. If we look at a differential interval of that cylinder, dx, the relationship between the radiation emitted and absorbed by the plasma at a certain frequency ν is given by the radiative transfer equation (Canon, 1985; Griem, 1997; Lochte-Holtgreven, 1968):

$$\frac{dI(\nu, x)}{dx} = \varepsilon(\nu, x) - \kappa'(\nu, x)\ I(\nu, x) \tag{1.31}$$

where $\varepsilon(\nu, x)$ is the emission coefficient and $\kappa'(\nu, x)$ is the absorption coefficient.

In the case of the radiation corresponding to a spectral line of frequency ν due to the transition between the upper energy level k and the lower energy level i, the **emission coefficient** per volume and solid angle due to the spontaneous transitions is given by the expression:

$$\varepsilon(\nu) = \frac{h\nu}{4\pi}\ A_{ki}\ n_k\ P^{se}(\nu, x) \tag{1.32}$$

h being the Plank constant, A_{ki} is the Einstein coefficient for spontaneous emission between the energy levels k and i, n_k is the population density of the upper energy level and P^{se} is the spontaneous emission normalized profile.

The effective **absorption coefficient** accounts for the quantity of radiation absorbed by the plasma itself, including the true absorption and also the induced emission, which is considered a negative absorption, and is expressed as:

$$\kappa'(\nu, x) = \frac{h\nu}{c}\ B_{ik}\ n_i\ P^a(\nu, x)\left(1 - \frac{g_i\ n_k\ P^{ste}(\nu, x)}{g_k\ n_i\ P^a(\nu, x)}\right) \tag{1.33}$$

where c is the speed of light, B_{ik} is the absorption Einstein coefficient, n_i and n_k are the population densities of the lower and upper energy levels, P^a and P^{ste} are the absorption and stimulated emission normalized profiles, respectively, and g_k, g_i are the statistical weights of the upper and lower energy levels. In the kind of plasma used in our laboratory, where collisions are dominant (Canon, 1985), it is possible to make the following hypothesis:

$$P^{se}(\nu, x) = P^a(\nu, x) = P^{ste}(\nu, x) \tag{1.34}$$

known as the *approximation of complete redistribution*. In these circumstances, it is possible to solve the equation (1.31), obtaining the total intensity measured at the end of the cylinder L in length:

$$I(\nu, L) = I(\nu, 0) \, e^{-\int_0^L \kappa'(\nu,x)dx} + \int_0^L \varepsilon(\nu, x) \, e^{-\int_x^L \kappa'(\nu,p)dp} \, dx \tag{1.35}$$

If we introduce the concepts of differential **optical depth**:

$$d\tau'(\nu, x) = \kappa'(\nu, x)dx \tag{1.36}$$

and **source function**:

$$S(\nu, x) = \frac{\varepsilon(\nu, x)}{\kappa'(\nu, x)} \tag{1.37}$$

and consider that the emission and absorption are spatially homogeneous:

$$\kappa'(\nu, x) = \kappa'(\nu) \tag{1.38}$$

$$\varepsilon(\nu, x) = \varepsilon(\nu) \tag{1.39}$$

the equation (1.35) being possible to simplify and express as:

$$I(\nu, l) = I(\nu, 0) \, e^{-\tau'(\nu)} + S(\nu)(1 - e^{-\tau'(\nu)}) \tag{1.40}$$

In order to obtain the transition probabilities and Stark parameters from the measured intensity, we need to know the emission coefficient $\varepsilon(\nu)$. For optically thin spectral lines ($\tau'(\nu) << 1$) and plasmas where the incident radiation of frequency ν is zero ($I(\nu, 0) = 0$), it is possible to develop the equation (1.40), arriving at:

$$\varepsilon(\nu) = \frac{I(\nu, l)}{L} \tag{1.41}$$

In the case of optically thick spectral lines, the solution for the equation (1.40) is given in Appendix X.

1.3.2   Line intensity and transition probabilities.

We will now focus on the total energy emitted in a radiative transition between an upper energy level, k, and a lower energy level, i. The intensity of this spectral line emitted is determined by two parameters: the population of the upper energy level and the transition probability, A_{ki}, which is also known as the Einstein coefficient for spontaneous emission. The quantum mechanic derivation of this parameter (Ritcher, 1968) in electric dipole approximation leads to the expression:

$$A_{ki} = \frac{64\pi^4\nu^3}{3hg_kc^3} \sum_{m,m'} \left| \int \psi_{k,m}^* \sum_j R_j \psi_{i,m'} d^3r \right|^2 \tag{1.42}$$

where $\psi_{k,m}$ and $\psi_{i,m'}$ are the eigenfunctions corresponding to the different sublevels of the upper and lower energy states, the j-summation extends to all the electrons involved in the transition and R_j is the electric dipole transition moment. It can be seen how this coefficient only depends on intrinsic properties of the atom. More detailed information about the theoretical calculation of transition probabilities can be found in Crossley (1969); Hibbert & Hansen (1994); Kuhn (1969); Layzer & Garstang (1968); Miles & Wiese (1970); Nicholls & Steward (1962); Thorne (1974).

In our case, we obtain the transition probabilities experimentally, the areas under the profiles (considered relative line intensities) being the necessary value for their determination. The intensity of a spectral line emitted by the plasma corresponding to a spontaneous transition between the energy levels k and i can be expressed as (Vujnović & Wiese, 1992;

Wiese, 1988):

$$I_{ki} = \frac{1}{4\pi} A_{ki} \ \hbar \ \omega_{ki} \ N_k = \frac{1}{2} A_{ki} \frac{\hbar c}{\lambda_{ki}} N_k \tag{1.43}$$

where A_{ki} is the transition probability between the states k and i, ω_{ki} is the angular frequency of the radiation emitted and N_k is the population of the upper energy level, which depends on the plasma conditions and is thus different for different sources. In our case, this population can be expressed as (1.15):

$$N_k = N(T) \ \frac{g_k \ e^{-\frac{E_k}{kT}}}{Z(T)} \tag{1.44}$$

$N(T)$ being the total population of atoms in the emitting species, g_k the statistical weight or degeneration of the level k, E_k the energy of that level and $Z(T)$ the partition function of the emitting atom. By combining the equations (1.43) and (1.44), we can express the intensity of a spectral line corrected by the spectrometer response as:

$$I_{ki} = M \frac{A_{ki} \ g_k \ \hbar c}{2\lambda_{ki}} \frac{N(T)}{Z(T)} e^{-\frac{E_k}{kT}} \tag{1.45}$$

where M is a purely geometric factor (a relative calibration being assumed) and T is the excitation temperature which in a collision-dominated plasma (Lochte-Holtgreven, 1968), like the one used in this experiment, is supposed to coincide with the Maxwell and the Saha temperatures.

From the the ratio between the equation (1.45) for the intensity of two spectral lines of the same species and stage of ionization, the line under study and what we will call a *reference line* (a spectral line for which the transition probability is already known) at a given instant, it is possible to obtain the equation 34 in Konjević (1999). Rearranging this equation, we can isolate the unknown transition probability value and express it as a function of known quantities:

$$A_{ki} = A_{ref} \frac{I_{ki}}{I_{ref}} \frac{\lambda_{ki}}{\lambda_{ref}} \frac{g_{ref}}{g_k} e^{\frac{E_{ki} - E_{ref}}{kT}} \tag{1.46}$$

Operating in this way, we eliminate the unknown quantities, such us the geometric

factor M, the total population of the emitting species N and the partition function $Z(T)$.

The transition probabilities can also be obtained by measuring the so-called "branching fractions" BF and the lifetime of the upper energy level τ_k as follows (Huber & Sandeman, 1986):

$$A_{ki} = \frac{BF_{ki}}{\tau_k} \tag{1.47}$$

This technique has the advantage that the branching fractions are independent of the population of the upper level and of the plasma length, it being only necessary to know relative spectral responses:

$$BF_{ki} = \frac{A_{ki}}{\sum_i A_{ki}} = \frac{I_{ki}}{\sum_i I_{ki}} \tag{1.48}$$

The lifetime of the upper level can be measured in different ways (delay time, beam foil spectroscopy, Hanle effect)(Corney, 1970; Thorne, 1974) and be expressed as a function of the Einstein A-coefficients of each of the possible transitions from this upper level to the lower ones:

$$\tau_k = \frac{1}{\sum_i A_{ki}} \tag{1.49}$$

In an emission experiment like ours, the disadvantage of the "branching fraction-lifetime" method lies in the necessity of knowing all the relative intensities of each of the spectral lines coming from a given upper energy level. The wavelengths of these spectral lines can lie within a very wide range of the spectrum, from the UV region to the far-IR, which would require different detectors and optical elements. This technique is currently used in the measurement of transition probabilities in Fourier Transform Spectroscopy experiments, such as those carried out at Imperial College by the FTS group (Ruffoni, 2013), amongst others.

A dimensionless quantity which is also used in the field of spectroscopy is the oscillator strength or f-value of a transition (Marr, 1968; Nicholls & Steward, 1962). This magnitude was introduced before the appearance of the quantum theory and it gives an idea of the ability of an atom to absorb or to emit radiation from a given state. A very interesting description of this magnitude can be found in Thorne (1974). This magnitude is normally defined for absorption measurements f_{ik} between the lower energy level i and the upper k

as (Thorne, 1974):

$$f_{ik} = \frac{mh}{\pi e^2} \nu_{ik} B_{ik} \tag{1.50}$$

where ν_{ik} is the frequency of the radiation absorbed and B_{ik} is the Einstein coefficient for absorption between those two energy levels. This absorption f-value is related to the emission one f_{ki} by:

$$f_{ki} = - \left(\frac{g_i}{g_k} \right) f_{ik} \tag{1.51}$$

In particular, the emission f-value can be related to the transition probability value by using the expression (Thorne, 1974):

$$A_{ki} = \frac{g_i}{g_k} \frac{2\pi e^2 \nu^2}{\varepsilon_0 m c^3} f_{ik} = \frac{6.670 \cdot 10^{15}}{\lambda^2} \frac{g_i}{g_k} f_{ik} \tag{1.52}$$

with A_{ki} being expressed in s^{-1} and λ in ångströms.

In articles related to Astrophysics, it is usual to find the quantity $log(g_i f_{ik})$ (also found as $log(gf)$ in the literature), which is related to the transition probability by the expression:

$$log(g_i f_{ik}) = log[A_{ki} \ g_k \ \lambda^2 \cdot 1.499 \cdot 10^{-14}] \tag{1.53}$$

where λ is expressed in nm.

1.3.3 Measurement of transition probabilities: methods and crit ical factors.

When trying to obtain atomic parameters with a high level of accuracy, it is especially important to have under control all the critical factors that might act as sources of error in our measurements. These critical factors depend on the kind of experiment and have been very clearly explained by Wiese in different publications (Vujnović & Wiese, 1992;

Wiese, 1988; Wiese & Kelleher, 1998; **?**). For emission experiments, we normally find three different types of measurements:

1) **Measurement of "branching ratios"**: this method is based on the measurement of relative intensities for groups of spectral lines coming from a common upper energy level and only the assumption of emission from an optically thin layer is needed (Kock, 1996). The branching fraction has already been defined in (1.48). Combining the BF with the lifetime τ of the upper energy level, it is possible to obtain very reliable transition probability values, as can be seen in (1.47).

2) **Measurement of absolute intensities**: measurements of this kind have the advantage of providing absolute transition probability values. However, very restrictive conditions must be fulfilled, which means that such experiments are not very common. Some of the main difficulties arise from the necessity of carrying out an absolute calibration of the spectral radiances, which is very complicated in experiments where the optical path of light is quite long and normally full of different optical elements necessary to guide the light from the light source to the spectrometer. In addition to this, the plasma source must be in LTE and a it is necessary to know the plasma length (Kock, 1996).

3) **Measurement of relative intensities**: this method is based on the measurement of relative intensities of spectral lines coming from different upper energy levels. A homogeneous plasma column (del Val, 1993), emission from an optically thin layer, as well as some assumption of at least pLTE are required. By using the equilibrium equations to express the population ratios, the transition probabilities can be obtained from equation (1.46) once the temperature is calculated by one of the methods that will be discussed later.

   In order to obtain this excitation temperature, it is necessary to already know the transition probabilities of some of the recorded spectral transitions. This is one of the main disadvantages of this method, as the absolute accuracy of the newly measured A_{ki}-values will always be determined by the uncertainty attributed to these A_{ki}-values taken from the bibliography.

   Since this technique is the one used in this thesis, it is worth analyzing the critical aspects regarding measurements of this variety (Vujnović & Wiese, 1992; Wiese & Kelleher, 1998).

a) **A valid plasma model**: the most suitable models being either local or partial local thermodynamic equilibrium (LTE or pLTE).

b) **Absence of self-absorption**: ideally, the spectral radiation should be emitted by a optically thin plasma layer. However, the very intense lines tend to be slightly self-absorbed, which is acceptable as long as the corrections for this optical depth are small. In our experiment, all the lines the self-absorption of which is higher than 20% are dismissed.

c) **Spectral calibration**: it is very important to calibrate the observed intensities extremely carefully by comparing them with accurate radiometric standards.

d) **Correct determination of the line intensity**: paying special attention to the contributions of the line wings to the total intensity and adequately eliminating the contribution of the background intensity.

e) **Inhomogeneities and boundary layers**: it is important to make sure that the measurements are carried out in a homogenous volume of the plasma, far from the effect caused by the boundary layers, which tend to be colder than the rest of the plasma. The plasma homogeneity in our experiment has been studied in del Val (1993).

f) **Inherent uncertainties in plasma diagnostic methods**: given that there are different sources of uncertainty which are very difficult to eradicate completely from the experiment, it is very important to acknowledge and study how they affect the measurements in order to give at least an estimation of the order of magnitude of these inherent uncertainties.

1.3.4 Line shape and broadening mechanisms.

The experimentally observed spectral lines are usually the result of several broadening mechanisms. The analysis of a spectral line profile is a source of very valuable information regarding the plasma conditions. From the study of the full-width at half-maximum (FWHM) it is possible to calculate the electron density of the plasma under study, which has very interesting applications in many different fields.

The fact that a spectral line is not a Dirac delta function, but has a certain width, is due to different factors such as the interaction of the emitter with the surrounding field of radiation, the self-absorption phenomenon, the thermal motion of the emitter or

its interaction with the neighboring particles. We will describe each of these broadening mechanisms in this section, paying special attention to those more relevant in our experiment. More detailed descriptions of line broadening can be found in Griem (1974); Konjević (1999); Marr (1968); Thorne (1974).

In addition to the previous mechanisms, our spectral lines will present an instrumental broadening arising from factors such as the size of the slit, the diffraction limit of the optical elements, the interference pattern of the dispersive instruments used or the finite spatial resolution of the detector (Thorne, 1974). In our case, with an experiment based on a spectrometer, the instrumental profile can be described by a gaussian profile.

1.3.4.1   The natural broadening.

The natural broadening of a spectral line is due to the finite lifetime of the atomic excited state (Baranger, 1962), which means that the length of the wave train emitted is by an undisturbed, resting atom is finite (Marr, 1968). For a transition between the energy levels k and i, this broadening can be calculated (Konjević, 1999) as:

$$\omega_N(cm) = \frac{\lambda^2(\sum_{i'} A_{i'i} + \sum_{k'} A_{k'k})}{2\pi c} \tag{1.54}$$

where ω_N is the FWHM, $A_{i'i}$ is the transition probability between the state i and any allowed level i'. The highest values of natural broadening appear when one of the two levels is dipole-coupled to the ground state, but even in these cases they are of the order of 10^{-4} nm (Konjević, 1999). Therefore, this broadening is orders of magnitude smaller than the observed one and it can be neglected without introducing a significant error.

1.3.4.2   The Doppler broadening.

The Doppler broadening effect is due to the random motion of the light-emitting particle, the frequency or wavelength of the light radiated by the emitter being shifted as a consequence of the relative velocity emitter-observer. Assuming that the velocity of the emitter is not relativistic and its distribution is maxwellian, the normalized emission profile will be gaussian, following the equation:

$$P_D(\omega) = \frac{1}{\sqrt{\pi}} \frac{e^{-\frac{\Delta\omega}{\Delta\omega_D}^2}}{\Delta\omega_D} \tag{1.55}$$

where the shift in frequencies $\Delta\omega$ is measured with respect to the frequency of the transition in a motionless atom and $\Delta\omega_D$ is the Doppler width defined as:

$$\Delta\omega_D = \left(\frac{2kT}{Mc^2}\right)^{\frac{1}{2}} \omega_0 \tag{1.56}$$

which depends on the mass M and the kinetic temperature of the emitter T. The full-width at half-maximum expressed in units of wavelength is given by the equation:

$$\Delta\lambda_D = \left(\frac{8\ln 2 \; kT}{Mc^2}\right)^{\frac{1}{2}} \lambda_0 = 7.162 \cdot 10^{-7}\lambda_0 \sqrt{\frac{T}{M}} \tag{1.57}$$

with the temperature T given in K and M in atomic mass units. In our case, the Doppler width for a wavelength of $\lambda_0 = 300$ nm ranges between 4.3-5.5 pm in the Argon experiment and between 3.2-3.5 pm in the Krypton experiment, within the temperature interval considered in each case.

1.3.4.3 The pressure broadening.

The pressure broadening is caused by the perturbation of the light-emitting atom by other particles of the plasma. The perturbers might be either neutral or charged particles, but the effect of the charged ones is much greater, so the neutral perturbers can be neglected as soon as there is any appreciable ionization, as happens in our experiment. Depending on the kind of perturber, it is possible to differentiate between three different types of pressure broadening mechanisms:

* **Resonance broadening**: this kind of broadening occurs for transitions involving a level that is dipole-coupled to the ground state (Konjević, 1999). It is possible to find an expression for its evaluation in Ali & Griem (1965, 1966). For the kind of plasmas produced in our laboratory, this width is completely negligible being no higher than a picometre.

* **Van der Waals broadening**: it appears as a result of the short-range dipole

interaction between an excited atom and the induced dipole of a neutral ground-state atom (Konjević, 1999). An estimation for the FWHM can be found in Griem (1964). As happened with the resonance broadening, this mechanism produces broadenings smaller than a picometre and is only relevant in plasmas where the density of neutral particles is, at least, two orders of magnitude higher than that of charged particles.

∗ **Stark broadening**: this broadening mechanism is based on a quantum effect caused by the presence of charged particles (ions and electrons) in the vicinity of the emitting particle that modify its internal states and therefore the frequency of its emissions. It is important to bear in mind that it is a statistical phenomenon that combines the radiation emitted by a collective of atoms or ions, each of them under the effect of a different electric field.

The overall result of the Stark effect is the broadening and shifting of the spectral lines emitted by the plasma. The observed Stark profile does not normally have a simple analytic expression and different models have been developed in order to describe this effect(Griem, 1964, 1974).

1.4   Plasma diagnostics.

Before carrying out any kind of measurement of atomic parameters, it is necessary to characterize the plasma used as a source of radiation by establishing its electron density and temperature. It is possible to find different diagnostic methods for both parameters and the choice of the most appropriate one will depend on the kind of experiment. Extensive revisions about plasma diagnostics can be found in (Huddlestone & Leonard, 1965; Hutchinson, 1987; Marr, 1968; Thorne, 1974)

1.4.1   Plasma temperature.

The excitation temperature of the plasma is an essential parameter in order to obtain the transition probability values by means of the equation (1.46). Different techniques can be found in Marr (1968); Thorne (1974). However, as stated in Marr (1968), the simplest and most direct method of using the intensities of spectral lines in order to determine the temperature of a plasma is by applying the relationship existing between the intensities

of a spectral line and the transition probability associated with that atomic transition between the upper energy level k and the lower i.

As seen before, under the assumption of pLTE (a condition fulfilled by our plasma), we can make use of the Boltzmann distribution for the upper energy levels involved in this work and express this relation as (1.45):

$$I_{ki} = M \frac{A_{ki} \; g_k \; \hbar c}{2\lambda_{ki}} \frac{N}{Z(T)} e^{-\frac{E_k}{kT}} \tag{1.58}$$

By rearranging the previous equation and taking logarithms, we arrive at the expression:

$$\ln\left(\frac{I_{ki}\lambda_{ki}}{g_k A_{ki}}\right) = \ln\left(\frac{\hbar c M N}{2Z(T)}\right) - \frac{E_k}{kT} = a + bE_k \tag{1.59}$$

where I_{ki} is the intensity of the spectral line (area under the profile), λ_{ki} is the wavelength corresponding to the emitted radiation, g_k is the statistical weight of the upper energy level, A_{ki} is the transition probability, E_k is the upper energy level and T is the temperature. The values of the energies, wavelengths and transition probabilities can be obtained from spectroscopic tables (Kramida et al., 2015; Striganov & Sventitskii, 1968).

By representing the left side of equation (1.59) against the energy of the upper level E_k for several spectral lines it is possible to carry out a linear fit, it being possible to obtain the temperature from the slope of this fit as $T = -1/kb$. This is the so-called **Boltzmann-plot** technique and it is the one used in this work.

The accuracy of this method depends on the uncertainties attached to the transition probabilities and especially on the range of energies in the x-axis in comparison to kT (Konjević, 1999). In order to minimize the error of the temperature, it is important to use a set of lines the upper energy levels of which range in as wide an interval as possible, ideally several times larger than kT, that includes all the upper energy levels of the transitions the A_{ki}-values of which are to be obtained. The description of these uncertainties will be developed in more depth in Chapter 3.

1.4.2   Electron density: plasma refractivity.

One of the most reliable techniques with which to determine the electron density of the plasma independently from the spectroscopic measurements is the use of an interferometric method. Many material media, including plasmas created in our laboratory, are strongly dispersive, i.e. their refraction index presents a strong variation depending on the frequency of the radiation passing through it. The low densities of some natural or laboratory-created plasmas allow the refraction of the light to be forgotten due to the very close value of the radiation's phase velocity to c. However, for dense plasmas and wavelengths close to those of very intense spectral lines, the refraction index can show values considerably different from $n = 1$.

According to the classical Lorentz oscillator model, when an electromagnetic wave of amplitude E_0 and frequency ω propagates in a material medium, it polarizes the atoms present in it due to the relative separation between the most external electron and the nucleus. Due to these forces, this external electron acquires a forced harmonic oscillator movement, which in the most general case is damped due to the radiation losses. The nucleus will also be subjected to this movement, but due to their large mass they are not able to follow the high frequency oscillations of the electric field. For our laboratory conditions and considering that n will be close to unity, it is possible to use the following expression (Griem, 1997) for the refractivity:

$$n(\omega) - 1 = \frac{e^2 N}{2m_e\varepsilon_0} \frac{(\omega_0^2 - \omega^2)}{(\omega_0^2 - \omega^2) + \gamma^2\omega^2} \tag{1.60}$$

where N is the dipole density, ω is the frequency of the electromagnetic wave, ω_0 is the natural frequency of the atomic oscillator (which corresponds to the frequencies of the atomic transitions) and γ is the damping constant.

The refractivity of the free electrons is obtained by assuming $\gamma = 0$ and $\omega_0 = 0$ in (1.60), which results in:

$$(n-1)_e = -\frac{e^2 n_e}{2\varepsilon_0 m_e} \frac{1}{\omega^2} = -\frac{1}{2}\left(\frac{\omega_{pe}}{\omega}\right)^2 = -\frac{r_e}{2\pi} \lambda^2 n_e \tag{1.61}$$

ω_{pe} being the plasma frequency already defined in (1.3) and r_e the classical electron radius

expressed as:

$$r_e = \frac{e^2}{4\pi\varepsilon_0 m_e c^2} \tag{1.62}$$

Regarding the refractivity associated with the bound electrons, we will generalize the expression (1.60) and consider each atom or ion as a system of q linear oscillators, obtaining:

$$(n-1)_a = \frac{e^2 n_a}{2 m_e \varepsilon_0} \sum_{j=1}^{q} \frac{(\omega_{0j}^2 - \omega^2) f_j}{(\omega_{0j}^2 - \omega^2) + \gamma_j^2 \omega^2} \tag{1.63}$$

where ω_{0j} and γ_j are the natural frequency and the damping coefficient of the j-th oscillator respectively and f_j is dimensionless factor which characterizes the contribution of the oscillator to the scattering and absorption of light. Assuming a semiclassical approximation, it is possible to express the equation (1.63) as a function of the wavelength:

$$(n-1)_a \simeq \frac{r_e}{2\pi} \sum_{i,k;i\neq k} f_{ki} \frac{\lambda_{ki}^2 \lambda^2}{\lambda^2 - \lambda_{ki}^2} n_i \tag{1.64}$$

where n_i is the density of atoms in each of the upper energy levels of the different transitions, which is given by the Boltzmann distribution if the plasma is, at least, in pLTE. It is a good approximation to assume that the total refractivity of the plasma can be expressed as the addition of the refractivities due to the free electrons and the bound ones associated to each of the species, s (atoms and ions), that compose the plasma (Alpher & White, 1965):

$$n - 1 \simeq (n-1)_e + \sum_{s}(n-1)_s \tag{1.65}$$

The contribution of the free electrons to the refractivity shows linear behaviour with the electron density and it is strongly dependent on the incident wavelength. With regard to the bound electrons, an experiment carried out in our laboratory (de la Rosa, 1989; de la Rosa et al., 1990) proved that their contribution to the total refractivity can be approximated to a constant as it varies very slowly with the wavelength. Due to this fact, it is possible to eliminate the contribution of the non-electronic species by using a two-wavelength interferometry method (Aparicio et al., 1998) and to obtain the electron density value n_e in the plasma column by using the expression:

$$(n-1)_{\lambda_2} - (n-1)_{\lambda_1} = -\frac{r_e}{2\pi}(\lambda_2^2 - \lambda_1^2)n_e \tag{1.66}$$

with λ_1 and λ_2 corresponding to the wavelengths of the two different lasers used in our experiment.

Chapter 2

Experimental apparatus, spectra acquisition and calibration

> *"Quand tu veux construire un bateau,*
> *ne commence pas par rassembler du bois,*
> *couper des planches et distribuer du travail,*
> *mais réveille au sein des hommes*
> *le désir de la mer grande et large."*

> \- Antoine de Saint-Exupéry -

This chapter contains a description of the experimental apparatus used at the Plasma Spectroscopy Laboratory at the University of Valladolid. This complex laboratory is the result of thousands of hours of work invested by all those who have worked on it for the last 30 years. The measurement of atomic parameters with the level of accuracy that we have nowadays would had been absolutely impossible without the effort made by all the Master's and PhD students and their supervisors. From the development of the high voltage source to the careful design of the discharge lamp, all the aspects of this kind of plasma spectroscopy experiment have been carefully studied and characterized, allowing us a deep level of control over our current measurements. This fact enables us, not only to measure with high precision, but also to quantify very accurately the error introduced by our method of measuring. To everyone who has worked in this laboratory, I extend all my gratitude and recognition.

This PhD has not dealt with the development of the experimental setup. However, due to the change of location of our Faculty, the entire laboratory had to be relocated and therefore disassembled and reassembled on new premises. Given the enormous quantity of time consumed by the move, we used the opportunity to improve and replace some apparatus for the experiment such as cables, plugs, electrical and electronic connections and resistors. Reassembling and tuning up the entire experiment took the first year of this PhD.

A detailed description of the experimental apparatus is given in this chapter. The majority of the details included here have been taken from Aparicio (1996); González (1999); Peláez (2008); del Val (1997). Furthermore, the spectra acquisition will be explained, followed by a detailed explanation of the calibration of our spectroscopic system.

2.1   Experimental apparatus

2.1.1   The plasma generation source

2.1.1.1   The Excitation Unit.

The excitation unit, shown in Fig. 2.1, is comprised of the electric and electronic equipment used to produce the discharge that will generate the plasma. This unit can be divided into the charging and the discharge systems and it was designed to produce a current pulse with the following characteristics:

* Maximum intensity values of around kA, with energies of kJ. This enables the production of dense plasmas.

* Lifetime of around 200 μs, with a plateau of 40 μs.

* Smooth temporal variations, within that temporal scale, to avoid plasma instabilities.

* Great repeatability. This allows us to take several measurement series which are possible to compare.

We can distinguish three main parts: the charging and discharge system, both comprised of a power and a control unit, and the preionization circuit. The next paragraphs

describe each of them briefly. The letter in parenthesis corresponds to the diagram of each part in Fig. 2.1.

- Charging System: the Power Unit (A).

  This consists of a transformer T1 220/125 V the aim of which is to isolate the power unit from the electrical grid. It supplies power to a second transformer T2, 3KVA, which raises the voltage from 125 to 15000V. This voltage is then rectified and it feeds a 10 capacitor bank, each 2.5 μF, arranged as a positive grounded delay line. This has been designed so that the current peak presents a 40 μs plateau during the discharge. The high voltage transformer T2 is turned on through a relay (D1) which is activated by the control unit. The capacitors C1 and C2 eliminate the rebound current peaks produced during the discharge, since they might affect the measurement systems.
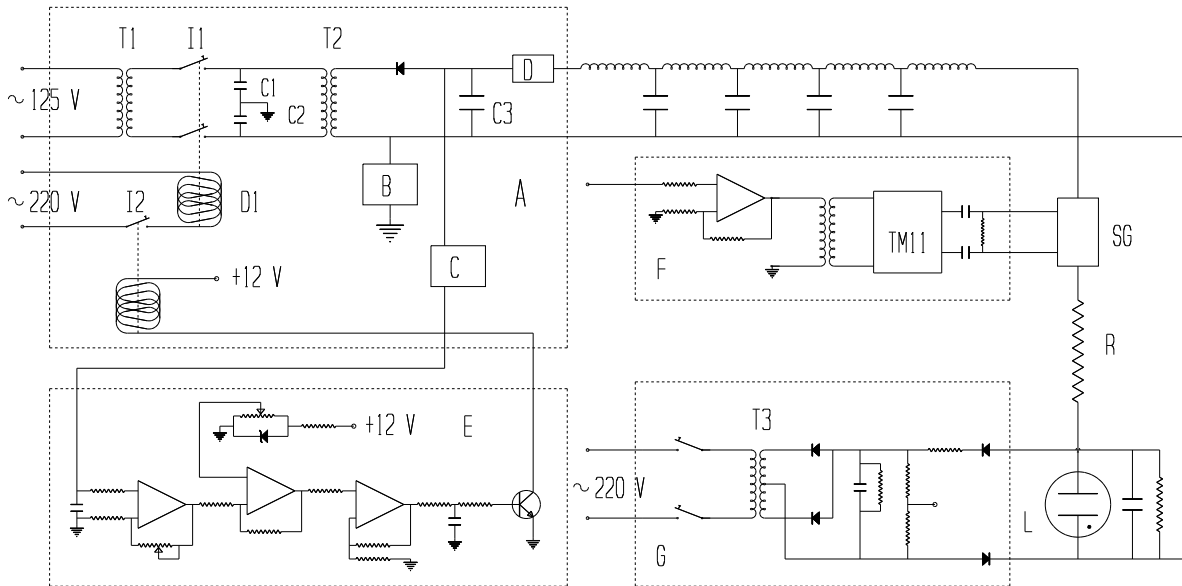
Figure 2.1: Block scheme of the plasma generation unit.

Block B represents a ground connection through a bridge circuit, which causes the circuit to float only during the discharge.

Block C represents a system with which to measure the charging voltage and it has a double purpose. On the one hand, it works as a reference for the control unit, which rules the charging process. On the other hand, it sends a signal which is used as a control signal in another part of the experiment.

Block D represents a decoupling circuit between the charge and the discharge systems. It is based on a RLC circuit which prevents a sudden voltage drop in the charging circuit during the discharge. Finally, capacitor C3 works as a reservoir to stabilize the charging system.

The entire power unit is enclosed within a Faraday cage both for safety reasons and to prevent electrical noise from reaching the measuring systems. This Faraday cage is carefully grounded.

- Charging System: the Control Unit (E).

  The control unit's aim is to open and close the charging circuit through switch I1. The charge takes place if two requirements are fulfilled: a charging instruction is received and the capacitor bank is discharged.

  The circuit is open either when the charging instruction ends, regardless of the capacitors' situation, or when the capacitor bank reaches the desired/programmed voltage. This voltage is controlled by circuit E. The signal received by meter C is filtered, amplified and compared with a reference voltage by a Schmitt trigger. The trigger response is adapted to control switch I2, which activates charging relay D1. The Schmitt trigger reference voltage is what establishes the charging voltage of the capacitors, which in our circuit is 10 000 times the reference voltage.

- Discharge System: the Power Unit.

  The discharge of the capacitor bank takes place when a Spark-gap is activated. Then, a current pulse flows through a resistor R and the lamp L. This resistor bears the high power to which the circuit is subjected during the discharge and it takes the current pulse to the subcritical condition.

- Discharge System: the Control Unit (F).

  The trigger signal, one of the most critical in our experiment, is generated as follows: the central computer, which controls the whole experiment, checks that all the devices are operational. Then, it authorizes the ICCD camera to initiate the experiment. The ICCD waits for the detector to be in its scanning downtime and it sends a signal to F (impedance matching circuit), which also plays a safety role. After this, the circuit F activates a high voltage pulse generator TM-11, which initiates the spark-gap. The pulse produced by the TM-11, of around 30 kV, results in an avalanche of electrons on the spark-gap, which discharges the capacitor bank through the lamp. Three μs elapse between the ICCD signal and the lighting of

the lamp. Once the voltage measured by C falls below a certain threshold switch I2 closes again, which automatically initiates the charging process again.

- The preionization circuit (G).

  The discharge system has a low intensity DC voltage source which keeps the gas inside the lamp slightly ionized. This allows us a small and constant ignition time of 3.3 μs. Due to the fact that this current and the one produced by the power system flow through the same cable to the lamp (the lamp does not have a double electrode), it is absolutely necessary to guarantee the safety of both circuits. This is especially important if we consider that the spark gap cannot tolerate permanent electric current and the preionization circuit is not prepared for high currents. To avoid these possible problems, both circuits are decoupled by using high voltage diodes. In this way, the high power current cannot access the preionization system and the spark gap remains open until the lamp is turned on.

  The preionization system consists of a transformer T3 from 220 to 15000 V with an 8 mA current limit followed by a rectifier and a filter. A voltage divider provides a voltage reading from the lamp working in a preionization regime. Figure 2.2 shows the normalized time evolution of a voltage pulse within the lamp. As happens with the current, the absolute values of the voltage depend on the particular conditions of each experiment (the type of gas used, the pressure, the electrodes, etc.) and the figure only shows the functional dependency voltage/current versus time.

2.1.1.2   The vacuum and gas system.

This part of the experimental set-up is responsible for the control of the gas pressure and the particle flux, which define the particle concentration in our plasma. This system was designed to:

- ∗ Inject a continuous flow of pure or mixed gases in various proportions (finely regulated from 1 to 100 cm^3/min).

- ∗ Achieve controlled and relatively low pressures of around 2 Pa.

The discharge lamp has two gas outlets, one of them connected to the vacuum system and the other to a gas injection system. Fig. 2.3 shows a plan of the setup used. Gas flows
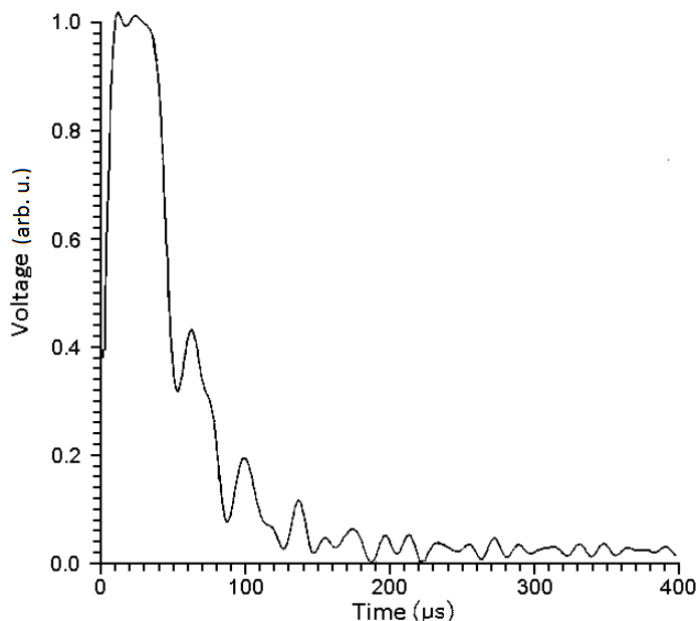
Figure 2.2: Normalized voltage pulse within the lamp over time.

constantly through the lamp for the duration of the experiment and the flux and pressure within the lamp are checked constantly.

A rotatory pump (RV12 from Boc Edwars, model A65501903) with an extraction flow rate of 12 m^3/hour is used to evacuate all the air and gases from the lamp, making it possible to reach pressures of 1 Pa inside it. The pressure within the lamp is regulated by a needle valve placed in its gas outlet pipe (the inlet pipe to the vacuum pump). A thermocouple manometer able to measure in the range of 7 to 70 Pa is positioned at this point. Two piezoelectric manometers measure the pressure at the mixer output. One of them is able to measure pressures between 100 Pa and 1 atm and the other one between 1 Pa and 1 atm.

The gas injection in the lamp is controlled by means of a multichannel mass flow controller (MKS Type 1179A Mass-Flo Controller) with four independent channels which converge at the lamp's inlet pipe. Two out of the four channels inject fluxes ranging from 1 to 100 cm^3/min in a controlled manner and are normally used for the carrier gas if a mixture is being used. The remaining two channels have a much finer flow control, between 0.01 and 1 cm^3/min, and are used to inject the gas we are spectroscopically interested in. The flux can be controlled in an automatic or manual way. The automatic mode is better for small fluxes, whereas the manual one is better for dealing with big fluxes.
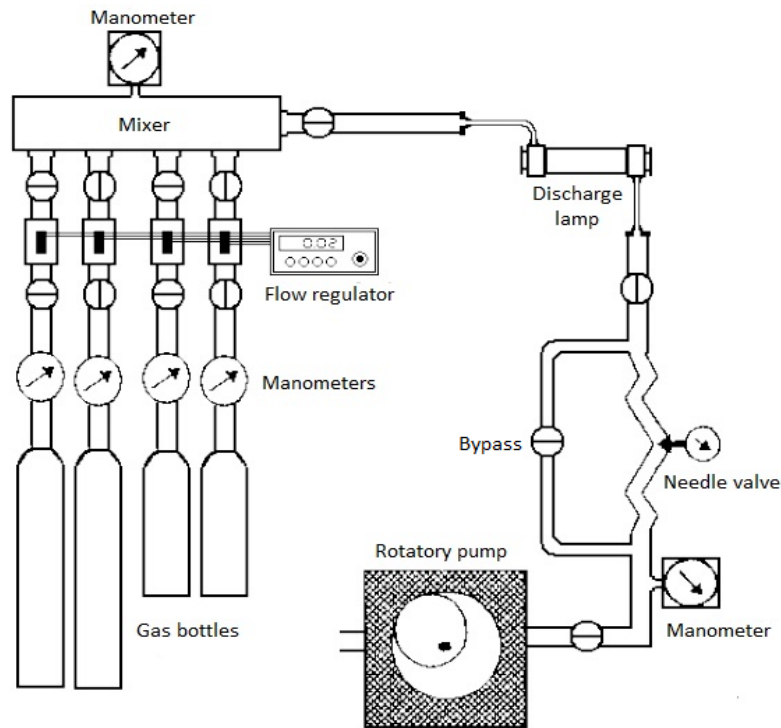
Figure 2.3: Scheme of the vacuum and gas control system.

Although the entire vacuum system has been optimized over the years, a very careful check is performed before carrying out any further measurement. In this way, we can be absolutely certain of the absence of any leak during our experiment. The minimum pressure within the lamp that is possible to maintain in a stable way is 1 Pa. The gas system allows us to maintain constant fluxes and pressures during the experiments for up to 15 consecutive hours.

2.1.1.3 The discharge lamp.

The discharge lamp is the plasma container and it was expressly designed to generate a highly homogeneous plasma without strong spatial or temporal gradients. This homogeneity makes the diagnostics of the plasma much easier, allowing us to have good control over it.

The discharge lamp shown in Fig. 2.4 is the heart of our experiment, as encloses the plasmas generated in our laboratory for spectroscopic purposes. Our lamp consists of a cylindrical Pyrex tube, 175 mm in length and 18 mm in internal diameter. This

tube slightly exceeds the two annular aluminum pieces which constitute the electrodes. This configuration, together with the material chosen for the electrodes, were designed to minimize the ejection of particles from the solid electrodes due to the collisions of the energetic plasma particles produced after each discharge. This phenomenon is known as "sputtering". Two Viton (a material resistant to high temperatures) O-rings are placed on the front faces of the electrodes. Beside each of the O-rings, there is an annular aluminum piece the purpose of which is to extend the length of the lamp 10 mm on each side. Then, over new O-rings, we find the quartz windows that enclose the discharge lamp. In this way, the windows are located far enough from the electrodes to allow for several thousand discharges to take place in the course of an experiment without damage or substantial opacity because of sputtering. In spite of this fact, the quartz windows are replaced every 800 discharges in order to reduce the optical transmittance loss to values under 5%.
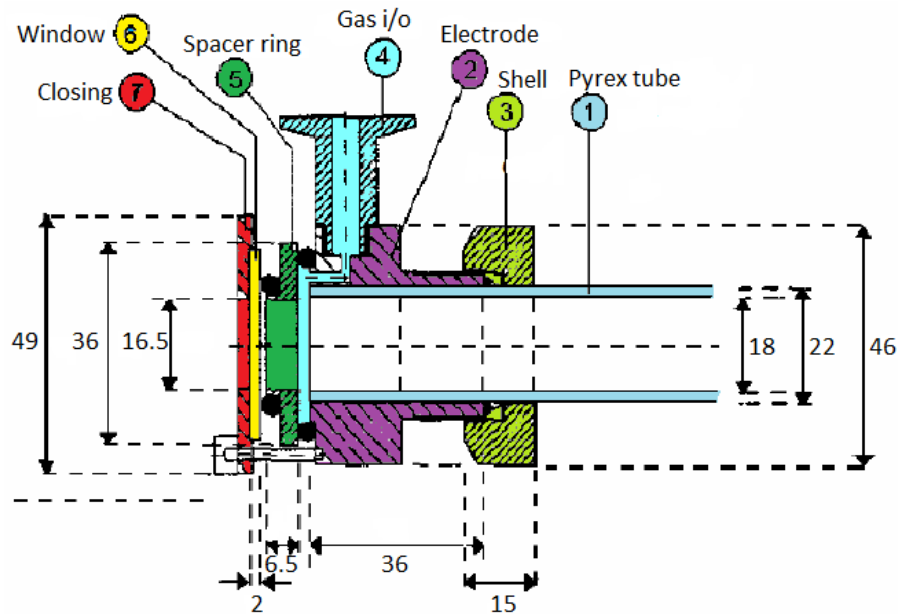
Figure 2.4: Discharge lamp scheme. Sizes are expressed in millimetres.

The interior of the lamp is connected to the vacuum and the gas injection systems through two perforations in the electrodes. All these pipes and connections are made of an isolating material. The gas constantly flowing through the lamp cleans and removes all the impurities from the electrodes

The electrical connection to the electrodes is arranged symmetrically. Three parallel cables, also parallel to the axis of the lamp and arranged in a triangular configuration (120 degrees), connect the cathode. The anode is connected in the same way through three

other cables placed alternately alongside the previous ones. This design eliminates any action of the magnetic field that could appear during the discharge.

2.1.2 Plasma diagnostics.

Two independent optical techniques are used to perform the plasma diagnostics in our laboratory: the interferometric and the spectroscopic technique. The interferometric technique is used to study the plasma refractivity from which it is possible to derive the plasma electronic density, whereas the spectroscopic technique is used to record the different spectral profiles. From these spectra, we are able to obtain information about the plasma excitation temperature, the transition probabilities and the Stark parameters. Both the interferometric and the spectroscopic measurements are made axially in two symmetrical plasma columns parallel to the lamp axis and 2 mm from it.
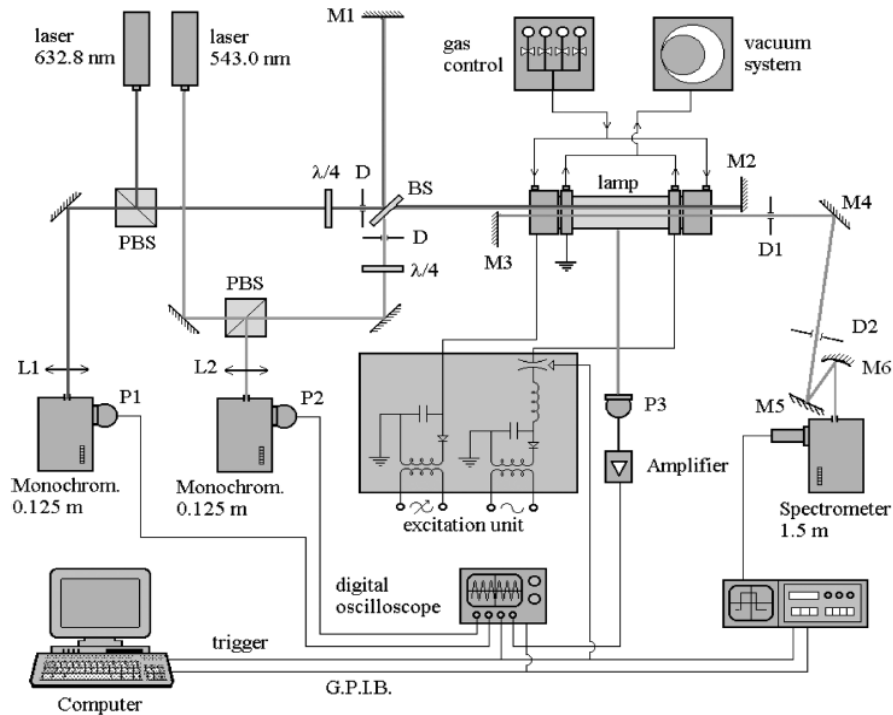
Figure 2.5: Experimental set-up.

2.1.2.1   The interferometric channel.

The lamp is placed in one of the arms of a Michelson interferometer, working in a Twynman-Green configuration. In the Fig. 2.5 the interferometer is comprised of a laser (as a source of coherence light), the beam splitter BS and the two mirrors M1 and M2. The two mirrors have been so positioned that their optical path difference relative to the beam splitter is around zero. This allows us to obtain the maximum contrast in the interference pattern/fringes. The pinholes D, 3 mm in diameter, prevent secondary reflections from the windows enclosing the lamp from entering the detector system, which would reduce the contrast. These pinholes are very useful during the optical alignment.

The polarizing beamsplitter cubes PBS and the quarter waveplates ($\lambda/4$) are introduced to decouple the laser cavity from the interferometer. The light emitted by the laser is reflected by the polarizing cube and it passes through the quarter waveplate, which dephases the two components of the electric field giving as a result circularly polarized light. This light operates inside the interferometer. Once the light leaves the interferometer, the quarter waveplate dephases the two components in $\pi/2$ again, which produces a beam of light linearly polarized in a direction perpendicular to the light emitted by the laser. The PBS cubes do not reflect this light, but transmit it to the detector system minimizing the quantity of light fed back into the laser.

After passing through the polarizing cube, the (light) beam is focused by the objective lenses L1 or L2, 25 mm in focal length, on the entrance slit of each of the monochromators (ORIEL 7240, 1200 lines/mm, f=0.125 m) tuned to the wavelength of the green and red laser radiation, respectively. Two optic fibers guide the light to the photomultipliers P1 (ORIEL 7060) and P2 (Hamamatsu R5928). The output signal of the photomultipliers is displayed by an oscilloscope (Hewlett Packard, model 1741A) and collected by a digital oscilloscope (YOKOGAWA DL1200). Each of these oscilloscope channels can store 10000 points for acquisition. Selecting a temporal resolution of 100 ns per sample, we can register an interferogram of up to 1 ms. This length of time is a sufficient period in which to record the plasma's entire lifespan, which concludes with a relaxation stage. The end of the lifespan will be considered the phase origin when assessing the change on the refractivity and, therefore, electron density. The signal from the oscilloscope is transferred to the computer controlling the experiment through a GPIB (General Purpose Interface Bus). A new digital oscilloscope (Tektronix TDS 1012) has now been installed instead of the YOKOGAWA one.
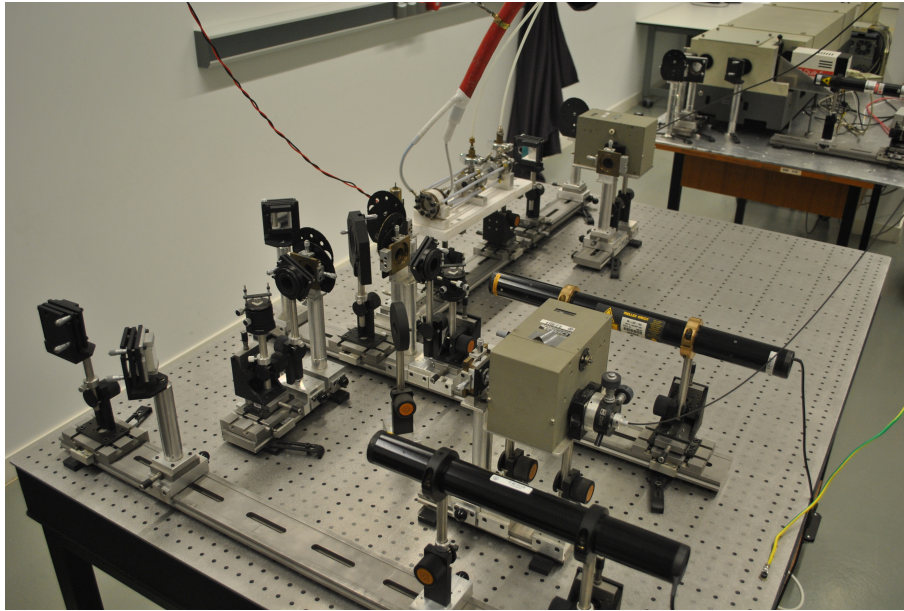
Figure 2.6: General view of the optical part of the experiment.

Due to the fact that the plasma lifetime (ranging from 0.1 to 1 ms) can be comparable to the typical mechanical vibration period, the entire interferometric device is arranged on top of an anti-vibration table. The typical mechanical oscillation period of the optical elements on this table, which is possible to measure with the digital oscilloscope, is of several milliseconds.

2.1.2.2 The spectroscopic channel.

The light beam emitted by the plasma source is analyzed spectroscopically. This channel is parallel to the interferometric one and located symmetrically to it, 2 mm from the lamp axis. The two pihnholes D1 and D2, which are separated by 1.5 m, select a narrow and collimated beam 3 mm in diameter. This beam is focused on the entrance slit of the Jobin-Yvon monochromator through a 150 mm focal length cylindrical mirror, M6. The slit width is usually smaller than 40 μm so that there is enough radiation entering the monochromator while minimum instrumental function is maintained, as can be seen in Fig. 2.7.

The grating monochromator, shown in Fig. 2.8, is based on a Czerny-Turner configuration. It is comprised of two square concave mirrors of 110 mm side length and 1500 mm focal length and a holographic diffraction grating of 2400 lines/mm. This grating
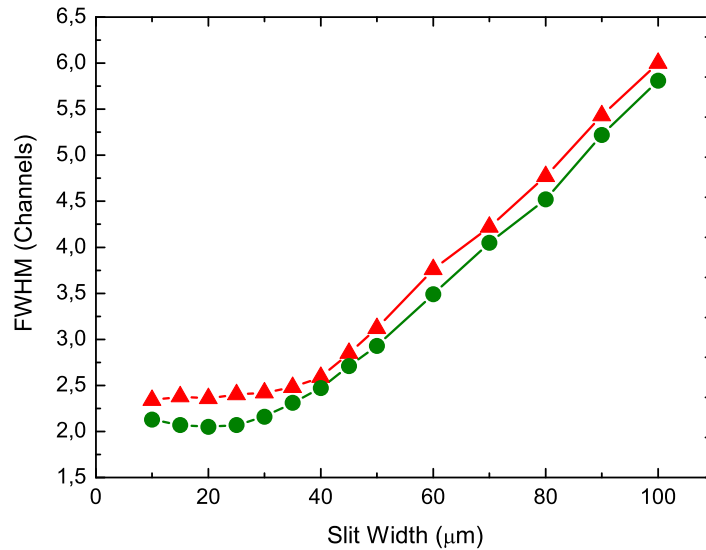
Figure 2.7: Instrumental broadening as a function of the entrance slit width at 632.8 nm (red) and 543.0 nm (green).

is placed on a mobile holder which can be moved either through an external crank with a positioning error of 0.02 nm or through a stepper motor activated from an analogical driver card installed on the main computer. This monochromator works properly up to the third order of diffraction. The image of the entrance slit is formed in the focal plane of the collecting mirror, where an ICCD (Intensified Charge-Coupled Device) camera is placed. Due to the fact that this entrance slit is not rectangular but slightly curved (in order to reduce optical aberrations), the 2-dimensional image provided by the ICCD is integrated by following the curvature of the slit. A detailed description can be found in Peláez et al. (2012).

The camera used to record the spectra is an ICCD 4 Quik E model from Standford Computer Optics Inc, comprised of an image intensifier and a CCD sensor. The image intensifier amplifies the incident photon signal, which eliminates the necessity of actively cooling the CCD sensor. Schematically, this image intensifier is comprised of the photo-cathode, the multi-channel plate (MCP) and a phosphor screen. The camera has an input window made of quartz, which limits its use to the UV spectral range, below 165 nm. The photocathode, which defines the spectral response and sensitivity, is an S20-type which is especially efficient in the UV, with a quantum efficiency over 10% between 200 and 400 nm according to the manufacturer. This intensified image is then guided to the CCD sensor
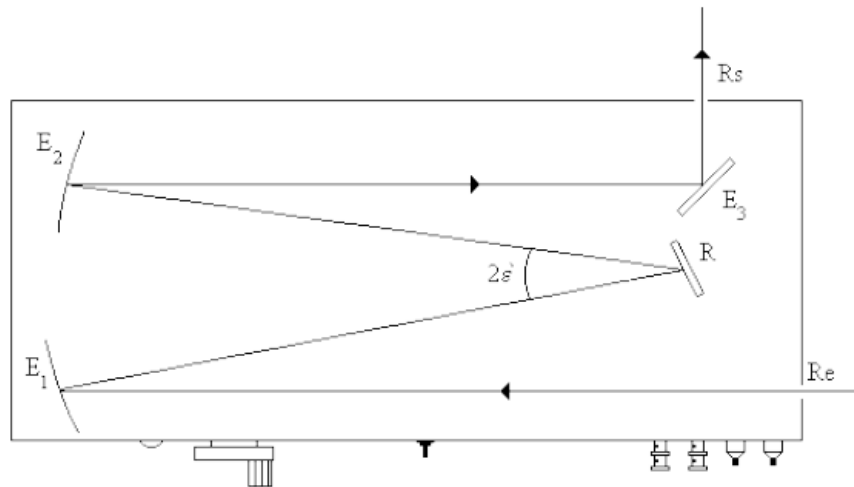
Figure 2.8: Monochromator configuration scheme.

through a lens coupling system, which provides high signal-to-noise ratio even at low light environment and reduces the stray light with the anti-reflex coatings of the lenses.

The CCD sensor consists of a 752 horizontal x 582 vertical pixel matrix, each pixel of which is 7.9 x 7.7 μm in size according to the manufacturer. The sensor is cleaned automatically before triggering at frequencies below 4 Hz. This considerably reduces the CCD sensor background noise. The camera's spatial resolution is primarily determined by the size and spacing of the microchannels in the MPC and by the CCD pixel size.

The video unit of the camera quantifies the charge of each of the CCDs pixel and transmits it through the video signal by using the CCIR protocol. The camera is controlled by a RS232 interface by using different commands. An in-house designed casing positions the camera at the plane in which the image of the monochromator's entrance slit is formed. This casing allows the camera to be rotated and moved in height and depth, which is extremely useful for alignment purposes. The alignment is also assisted by a program developed to display the quality of the alignment in each of the three axes. This enables us to position the photocathode's surface where the monochromator forms the image of the entrance slit.

The ICCD camera has two operating modes: pulsed and continuous. The pulsed mode is normally used to record the spectra emitted by the plasma. The continuous mode is used to calibrate our experimental device. A response function is obtained by recording the continuous spectra of different, accurately calibrated intensity standards, such us incandescent, deuterium or xenon lamps.

The spectroscopic channel is also used to obtain the necessary information for the reconstruction of the self-absorbed profiles. Self-absorption is checked by means of a mirror M3 placed behind the discharge lamp. Two sets of data are registered in every experiment. Firstly, we record the radiation coming directly from the plasma column with the mirror M3 covered. After that, the mirror M3 is uncovered and we record both the radiation coming directly from the plasma plus the radiation which passes through the plasma after having been reflected by M3. By comparing these two sets of data, it is possible to check if any of the spectral lines is self-absorbed. A computer-controlled shutter is used to cover or uncover the M3 mirror. This shutter is controlled by a unit of digital ports, which provides a voltage difference between the logic values of 24 V, sufficient voltage to drive the motor that controls the shutter.

The pressure of the gas is always adjusted to obtain maximum intensity with minimum self-absorption, which allows a very precise reconstruction of the line profile if necessary. This is especially important for the measurement of atomic parameters, since a self-absorbed profile results in higher Stark widths and lower areas (intensities), which leads to lower values of the transition probabilities. To avoid these problems, we dismissed all the lines with a self-absorption higher than 20%.

Finally, a photodiode P3 (Fig. 2.5) is placed transversely to the discharge lamp to collect the overall brightness of the plasma pulse. This signal is collected and displayed by an oscilloscope, which enables us to check if the spectra have been acquired at the correct time.

2.2 Spectra acquisition: description of a measurement.

Once the plasma generation and diagnostics systems have been described, it is important to explain in some detail how to carry out our experiment, paying attention to all those more delicate aspects of the measurements. To take high quality measurements, it is essential to prepare the laboratory several days in advance. The steps to execute when carrying out the experiment are as follows:

1) **Ensuring a good vacuum**: in order to avoid the presence of spectral lines of unwanted elements, we turn on the vacuum pump several days in advance. This

ensures a complete elimination of gases such us water vapor, which would only complicate the identification of the spectral lines later.

2) **Optical alignment**: before proceeding with the measurements, it is extremely important to align both the interferometric and the spectroscopic channel, defining the optical axis of the experiment. Thus we ensure that all the radiation emitted by the plasma is properly guided to the spectrometer and recorded.

Once the experimental set-up is tuned, it is time to establish the most appropriate measurement conditions, depending on the kind of experiment we want to carry out. The critical aspects when measuring transition probabilities are the plasma repeatability and how clean the windows are, since we are interested in the line intensity. If we are measuring either Stark widths or Stark shifts, it will be desirable to obtain wide and well-defined spectral profiles and information about the spectral lines for different plasma conditions, respectively. This is also a vital point of the experiment, since the quantity and the quality of the spectral lines recorded will depend completely on these conditions. The parameters to adjust are:

3) **Establishing gas flux and pressure**: in order to clean the waste generated after each discharge, it is not advisable to establish a flux of the gas which is too low. The pressure of the gas is controlled by means of the needle valve and it is always adjusted to obtain minimum self-absorption and maximum intensity. By increasing the gas pressure, the number of particles inside the discharge lamp increases, too. This entails a rise in the plasma global emission and electron density, but also a faster window soiling.

4) **Establishing the capacitors' charging voltage**: once the gas flux and pressure are stabilized, it is necessary to adjust the voltage up to which the capacitor bank will be charged. This voltage determines the quantity of energy that is supplied to the plasma. Increasing it causes, again, a rise in the plasma global emission and electron density, which obscures the windows more quickly. It has been experimentally noted how a rise in the voltage causes an increase of both the plasma degree of ionization and the temperature of each of the species present in the gas.

5) **Preionization of the discharge lamp**: to ensure high plasma repeatability, voltages ranging from 500 to 800 V are applied between the anode and the cathode, with currents of the order of mA. As a result of this preionization, the time between the master trigger and the discharge of the capacitor bank is constant.

After tuning-up the experimental set-up and establishing the optimum conditions, it is very important to consider the synchronisation of the experiment. This synchronism must be really precise due to the short lifetime of the plasma, the duration of which is one of the most challenging stages of the measurement. The integration of the ICCD camera and the development of the synchronization circuit have already been described in Peláez (2008); Peláez et al. (2012). Here, only a very general idea will be given for completeness.

6) **Experiment synchronisation**: the experiment starts when the control program sends a trigger signal that works as an input for the synchronism circuit. This circuit is in charge of producing the master trigger signal which causes the generation of the plasma and triggers both the oscilloscope and the ICCD camera. Fig. 2.9 shows the time evolution of the synchronisation circuit inputs and output and the video signal in a pulsed experiment.
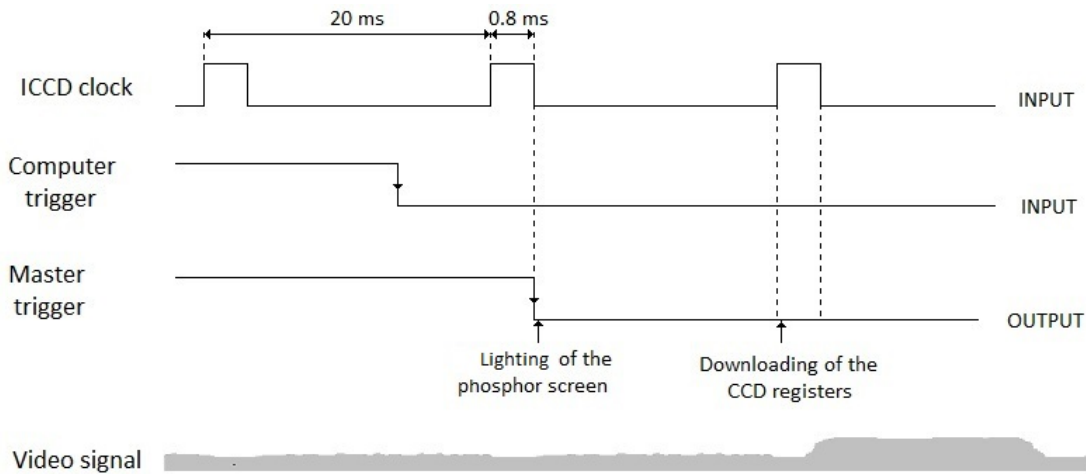
Figure 2.9: Time evolution of the synchronisation circuit inputs and output and the video signal in a pulsed experiment.

7) **Recording of measurements**: the image captured by the ICCD camera is transferred to the data acquisition card, where it is digitalized. Subsequently, a program developed in-house obtains the spectrum from the digital image. In addition to the ICCD camera image, three more signals shown in Fig. 2.10 are registered and displayed by the oscilloscope in each discharge: two interferometric signals and the global plasma emission one.
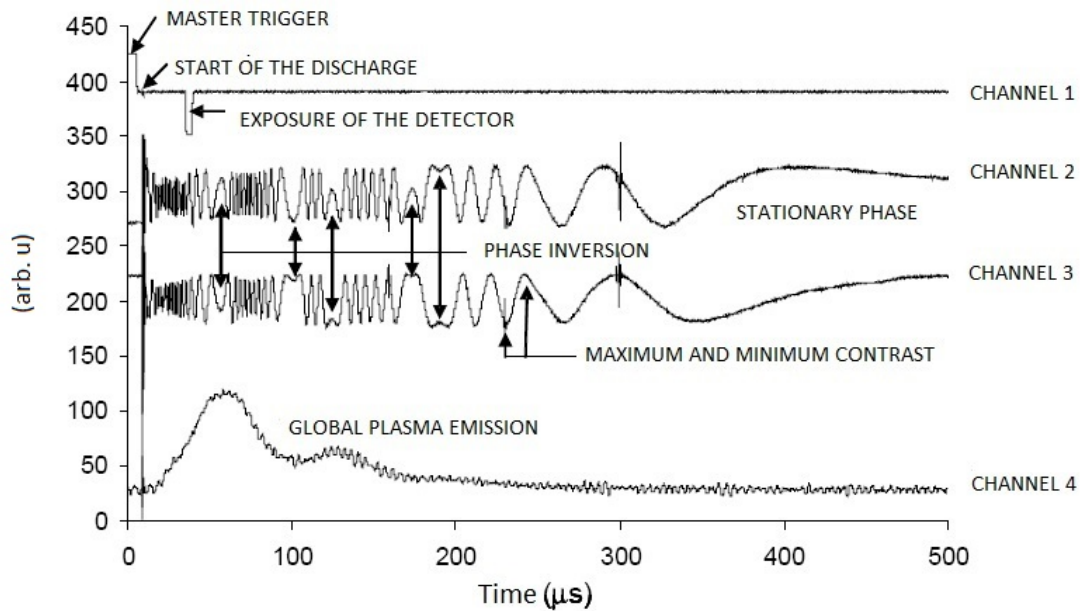
Figure 2.10: Signals recorded by the oscilloscope in each of its channels.

While all the signals are stored on the main computer, the gas continues to flow through the lamp, which is still preionized. Simultaneously, the capacitor bank is recharged in around 9 seconds. Once the voltage reaches the established value, the entire system is ready for another discharge. All the information related to the measurement conditions (wavelength tuning, the gas flux and pressure, pinhole diameter, etc) is kept in the data files.

2.3 Calibration of the spectroscopic channel.

In order to get very precise atomic data, it is essential to carry out a very thorough calibration of the spectroscopic channel. Obtaining a high quality response curve to calibrate our measurements in intensity has been one of the most important parts of this PhD, so a detailed description will be given.

2.3.1 Dispersion calibration and spectral resolution.

As with every dispersive system, the spectroscopic channel needs to be characterized in each of the diffraction orders used during the measurements. We will restrict our

observations to the first diffraction order, since it is the only one used in these experiments. The reciprocal linear dispersion $D(m, \lambda)$ for a Jobin-Yvon HR1500 monochromator is given by the analytical expression:

$$D(m, \lambda) \equiv \frac{d\lambda}{d(channel} = \frac{\lambda c}{2Bf} \frac{-BE + \sqrt{1 + E^2 - B^2}}{1 + E^2} \tag{2.1}$$

where m is the diffraction order (1 in our case), λ is the wavelength, c is the width of the detector channel, f the focal length of the collector mirror within the monochromator and B and E have been defined as:

$$B \equiv B(m, \lambda) = \frac{\frac{m\lambda}{2d}}{1 + cos2\varepsilon'} \tag{2.2}$$

$$E = \frac{sen2\varepsilon'}{1 + cos2\varepsilon'} \tag{2.3}$$

$2d$ being the spacial period of the grating and ε' the half-deviation angle. The dispersion is expressed in units of wavelength per channel of the detector, since these are the units normally used. The rest of the parameters refer to the different characteristics of the spectrometer and can be obtained from the manufacturer's specifications. Previous calibrations made with a 2400 lines/mm grating optimized for the UV (Peláez, 2008) show that the reciprocal linear dispersion of our monochromator is described properly by the equations 2.1, 2.2 and 2.3. However, the manufacturer's parameters have to be slightly modified, the parameters to use being the ones given in Table 2.1.

Table 2.1: Parameters that characterize the reciprocal linear dispersion in our experiment.

Parameter	Value	Description
ε'	0,0551 rad	Half deviation angle
2d	1/2400 mm	Spatial period of the grating
F	1500 mm	Focal of the collector mirror
c	13,9 μm	Width of the detector channel

The determination of the reciprocal linear dispersion of the spectrometer used in this thesis had already been done and described in detail in Peláez et al. (2012). Lamps of Na,

Ne and Hg were used to provide 7 narrow spectral double lines from 250 to 800 nm in the first diffraction order. Fig. 2.11 shows the reciprocal linear dispersion measured with the ICCD camera.
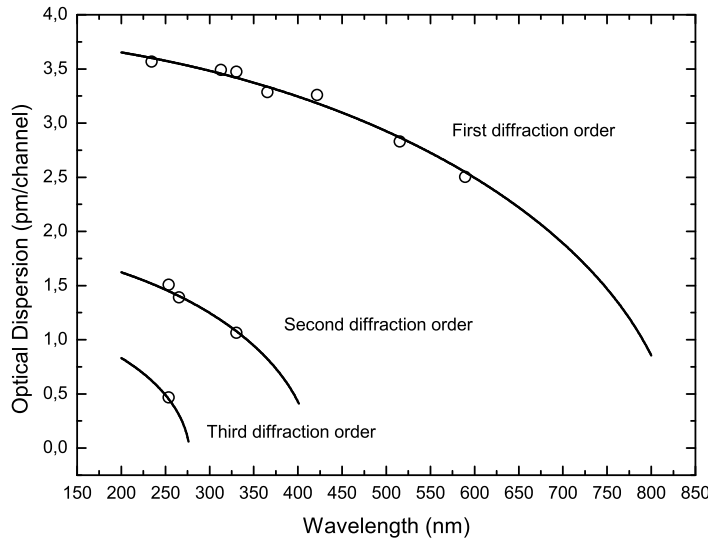
Figure 2.11: Reciprocal linear dispersion of the spectrometer.

2.3.2   Intensity calibration

In an emission experiment, the measurement of both the plasma electron temperature and the transition probabilities of spectral lines requires that we know the intensity of these spectral lines. In order to obtain this intensity from the accumulations registered by the ICCD camera, we need to know the overall response of both the optical and the detection systems to the incident radiation.

2.3.2.1   The Spectrometer response function: definition and initial considerations.

The ratio between the signal provided by the detector and the signal emitted by the radiation source is known as the response function. The response function is determined by recording the radiation emitted by a standard light source of accurately calibrated

intensity. Since the spectral irradiance emitted by this standard lamp is well known, it is possible to calibrate the intensity of the spectral lines and place these intensities on a consistent relative scale. This means that, even if we know the absolute intensity emitted by the standard lamp ($I_s^{emitted}$), we have obviated the problem of calculating the effective solid angle under which this radiation is detected. Therefore, if we calculate the ratio between the intensity detected ($I_s^{detected}$) and the intensity emitted ($I_s^{emitted}$), the dimensional analysis of the transmittance will be as follows:

$$[T] = \frac{[I_s^{detected}]}{[I_s^{emitted}]} = \frac{\frac{counts}{s \cdot nm}}{\frac{J}{s \cdot nm \cdot str}} = \frac{counts \cdot str}{J} \tag{2.4}$$

It is important to notice that once we calibrate all our spectra, the physical quantity that we obtain after fitting each line to a mathematical function is a quantity that differs from the intensity of the spectral line in a constant geometric factor. This factor is related to the solid angle that we mentioned previously.

Before describing the measurements carried out to determine the response function, it is interesting to consider the different physical phenomena that have an influence on how the radiation is detected:

1) **Wavelength**: both the sensitivity of the detector and the efficiency of the diffraction grating depend strongly on the wavelength. The refraction index of the remaining optical elements (mirrors and lenses) varies smoothly with lambda, being their contribution to the response function almost independent of this parameter.

2) **Diffraction order**: the functional dependency of the diffraction grating varies for each of the diffraction orders. Besides, it is important to bear in mind that different wavelength radiations coming from several diffraction orders could overlap, since the grating is efficient in the first three diffraction orders.

3) **Light polarization**: due to the internal structure of the diffraction grating, its response depends strongly on the orientation of the incident light's polarization. It has already been checked in our laboratory (González, 1999; Peláez et al., 2012) that the radiation emitted by the lamps is either not polarized (discharge lamp) or just slightly polarized (standard lamps). Furthermore, the different optical elements which guide the radiation to the detector introduce a very smooth polarization effect which, moreover, is the same for the radiation from both the standard and the

discharge lamp. Therefore, this effect is already taken into account in the response function.

4) **Temperature**: it is always very important to check for thermal drift for either the detector system or for the standard light source. The latter would alter the lamp emission over time and it is avoided by powering the lamps with highly stabilized current sources.

5) **Linearity of the detection system**: the range of linear response of the detector used in our laboratory has previously been studied in Peláez et al. (2012). That work shows how the response of our detector is mostly linear over 80% of its dynamic range. A saturation effect appears for the highest energies and irradiances.

6) **Response of the detector channels**: it has already been studied in Peláez (2008) how the response of the detector depends considerably on the selected channel. This dependency is due to different factors, such as the lens coupling between the phosphor screen and the detector or the photocathode coating which produces wavelength dependent interference fringes. Both effects produce spatial illumination inhomogeneities across the CCD sensor.

2.3.2.2   Measurement and analysis of the response function.

As explained before, the radiation registered by the detector depends both on its wavelength and on the channel upon which this radiation falls. Therefore, it is necessary to obtain a response curve with which we can calibrate the intensity recorded by the ICCD camera versus wavelength and channel. The result is a set of 2-dimensional curves with which we correct each of the spectra recorded during our experiments.

To cover the widest possible spectral range, the response curve is obtained by using 4 accurately calibrated intensity standard lamps whose emission, shown in Fig. 2.12, is well known: two incandescent lamps and two discharge lamps (a deuterium and a xenon one). Table 2.2 shows the model of the standard light sources used and their power supply, as well as the spectral range in which they were used.

The standard lamp is placed between the discharge lamp and the pinhole D1 (see Fig. 2.5) and carefully aligned. In this way, its light passes through all the optical elements crossed by the plasma radiation, but the windows closing the discharge lamp. All the spectra are recorded by using the continuous mode of the ICCD camera. The
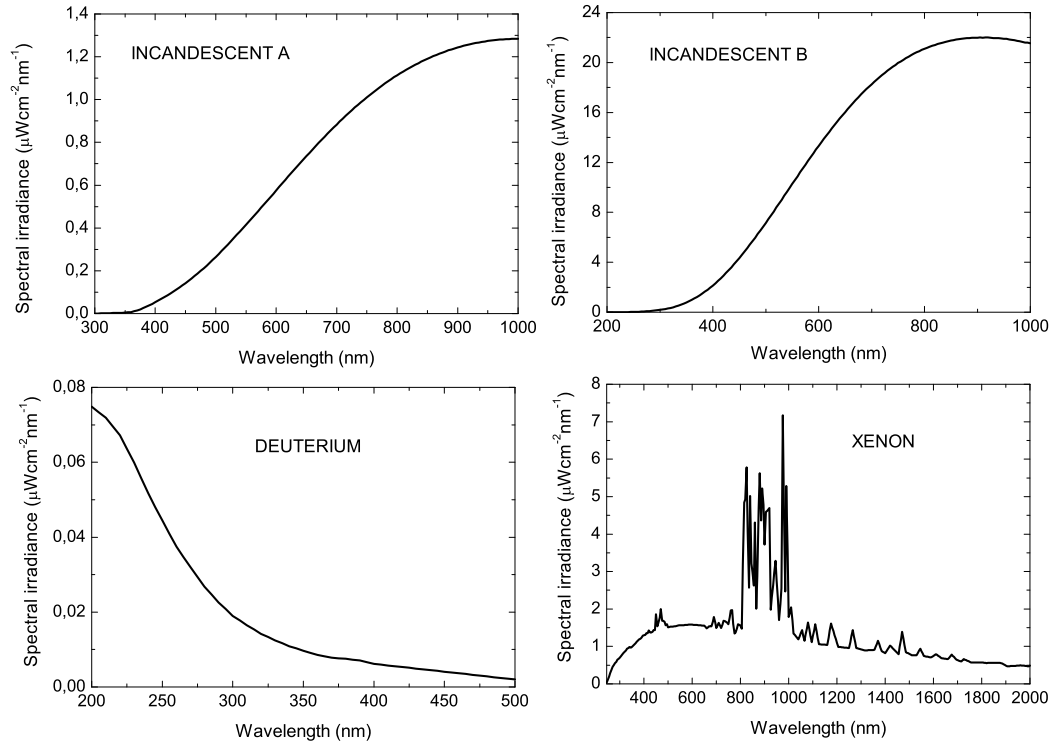
Figure 2.12: Spectral irradiance of the standard lamps used for calibration.

Table 2.2: Standard lamps used to get the response curve in the different spectral ranges.

Lamp	Model	Power Supply	Spectral range(nm)
Deuterium	L202 Hamamatsu	C7860 Hamamatsu	200 - 370
Xenon	L2274 Hamamatsu	C8849 Hamamatsu	350 - 700
Incandescent A	LAES 12V, 50W	6286A Hewlett Packard	400 - 700
Incandescent B	FEL QHT Osram	69935 Newport	350 - 700

monochromator is tuned between 200 and 700 at 5 nm intervals. Depending on the intensity emitted by each of the lamps, a quantity of 10, 20 or 100 spectra are accumulated for each tuning to reduce the noise. A background spectrum is recorded at the beginning and the end of every set of calibration measurements. This spectrum is then subtracted from each of the calibration spectra in order to remove the electrical noise and the background light.

The files used to get the response curve are shown in Table 2.3. The first two columns contain the file name and the name of irradiance file used in each case. The last four columns contain the minimum and maximum wavelengths of the spectral intervals in which those files were used to get the final response curve. In total, more than 40 000 spectra were used to obtain the final response curve, which gives an idea of the quality of this function.

The response function $T(\lambda, channel)$ is given by the following equation:

$$T(\lambda, channel) = C \cdot \frac{I^{detected}}{I^{emitted}} \tag{2.5}$$

where C is a constant. In order to get the response function for every wavelength and channel, all the measurements made with the different standard lamps are fitted to an analytic function described in (2.6), taking into account not only the tuning wavelength, but also the previous and following ones:

$$T(\lambda, channel) = \sum_{i=0}^{n_i} a_i \cdot \lambda^i + \sum_{j=1}^{n_j} b_j \cdot channel^j + \sum_{k_1+k_2=2}^{n_k} c_{k_1 k_2} \cdot channel^{k^1} \cdot \lambda^{k_2} \tag{2.6}$$

where the parameters $a_i, b_i, c_{k_1 k_2}$ are real numbers and k_1 and k_2 are natural numbers. The values of n_i, n_j and n_k are normally 2, 6 and 2, respectively.

Once this mathematical fitting is done, we obtain the values of the parameters a_i, b_i and $c_{k_1 k_2}$, which allows us to obtain a 2-dimensional response function for every wavelength and channel. Fig 2.13 shows this function. The z-axis shows the transmittance normalized to 100. The x and y-axis correspond to the wavelength and channel, respectively.

Table 2.3: Calibration files used to get the response curve.

Calibration file	Lamp emission file	λ_{min1}	λ_{max1}	λ_{min2}	λ_{max2}
DEU-11OCT10.002	LampDeuterio2014.dat	200	340		
DEU-11OCT10.011	LampDeuterio2014.dat	200	340		
DEU-10AGO02.001	LampDeuterio2014.dat	250	340		
DEU-11NOV21.003	LampDeuterio2014.dat	200	345		
DEU-11NOV21.001	LampDeuterio2014.dat	200	345		
DEU-11MAY02.001	LampDeuterio2014.dat	200	345	355	355
DEU-11OCT10.010	LampDeuterio2014.dat	200	345	355	355
DEU-11OCT10.004	LampDeuterio2014.dat	200	345	355	355
DEU-11OCT10.009	LampDeuterio2014.dat	200	345	355	355
DEU-11OCT10.008	LampDeuterio2014.dat	200	345	355	360
DEU-11OCT10.012	LampDeuterio2014.dat	200	345	355	360
DEU-11OCT10.001	LampDeuterio2014.dat	200	345	355	365
DEU-11OCT10.007	LampDeuterio2014.dat	200	345	355	365
DEU-13DIC11.002	LampDeuterio2014.dat	250	345	355	370
DEU-13DIC11.001	LampDeuterio2014.dat	250	345	355	370
BLA-09JUL14.001	IRR-BLA-09JUL14.001	420	700		
BLA-10AGO02.001	IRR-BLA-10AGO02.001	420	700		
BLA-11MAY02.001	IRR-BLA-11MAY02.001	415	700		
BLA-11OCT10.001	IRR-BLA-11OCT10.001	415	700		
BLA-11OCT10.005	IRR-BLA-11OCT10.005	410	700		
BLA-11OCT10.008	IRR-BLA-11OCT10.008	410	700		
BLA-11NOV21.006	IRR-BLA-11NOV21.006	405	700		
BLA-11NOV21.007	IRR-BLA-11NOV21.007	405	700		
BLA-13DIC11.001	LampBlanca4ACal5.dat	400	700		
BLA-13DIC11.002	LampBlanca4ACal5.dat	400	700		
XEN-09JUL14.002	LampXenon2014.dat	355	445	455	700
XEN-11MAY02.001	LampXenon2014.dat	350	445	455	700
XEN-09JUL14.000	LampXenon2014.dat	350	445	455	700
XEN-13DIC11.002	LampXenon2014.dat	355	445	455	700
XEN-13DIC11.003	LampXenon2014.dat	355	445	455	700
XEN-10JUN17.001	LampXenon2014.dat	350	400		
XEN-10JUN17.003	LampXenon2014.dat	350	400		
NG-13DIC11.003	LampNist-GoaCal5.dat	350	700		
NG-13DIC11.004	LampNist-GoaCal5.dat	350	700		
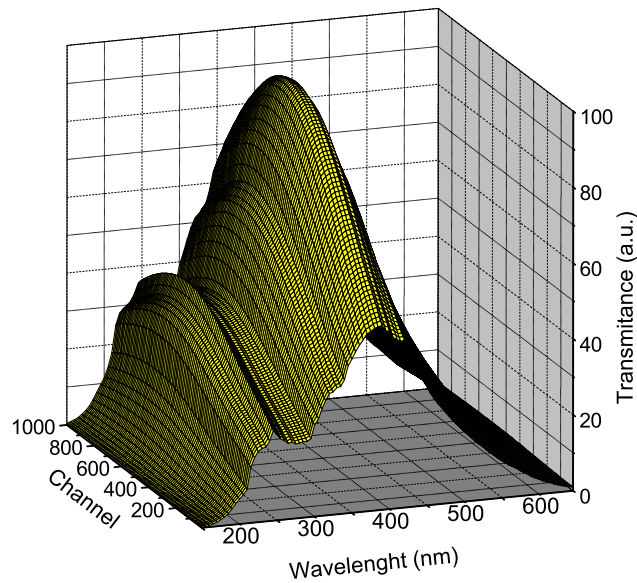
Figure 2.13: Response curve as a function of the channel and wavelength.

It is very interesting to analyze separately how the response curve varies with either the wavelength or the channel. The dependence of the normalised to unity response function on the wavelength for the 500 channel is shown in Fig 2.14 with the standard deviation. The error is under 2% for almost all the curve. It is possible to notice two peaks of intensity at 295 nm and 430 nm, the second one being 2.1 times higher. Even if the diffraction grating is optimized to work on the UV, the fact that the detector has a higher efficiency in the visible region gives a higher transmittance in the region over 400 nm as a result.

Fig 2.15 represents the normalised response of the different channels to a radiation of 500 nm. The error of this curve is around 1%. It is possible to notice how the response of the first channels is almost half of the response at channel 650.

It is interesting to finish this section by mentioning all the factors that have been carefully considered to get the response curve of our spectroscopic channel. It is highly advisable to take all of them into account if we want to obtain a precise calibration function.

1) **Lamp performance over time**: some of the standard light sources have a warm-up period which makes the output signal unreliable until the lamp is completely
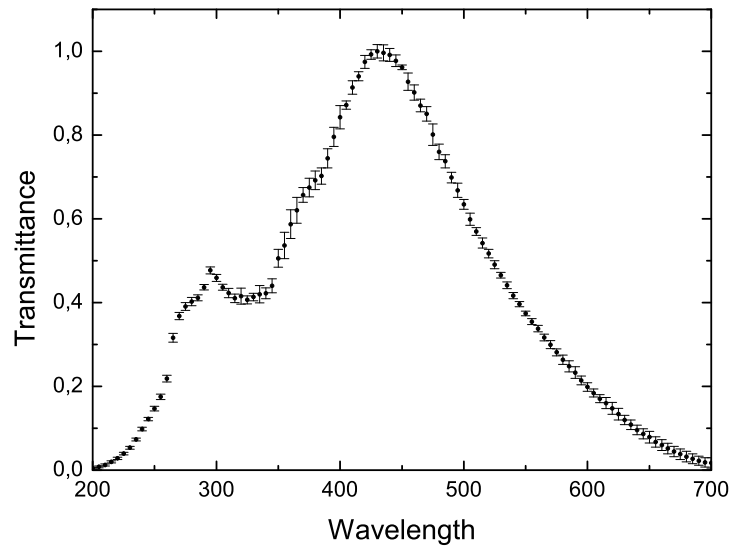
Figure 2.14: Normalised response curve as a function of the wavelength for the channel 500.
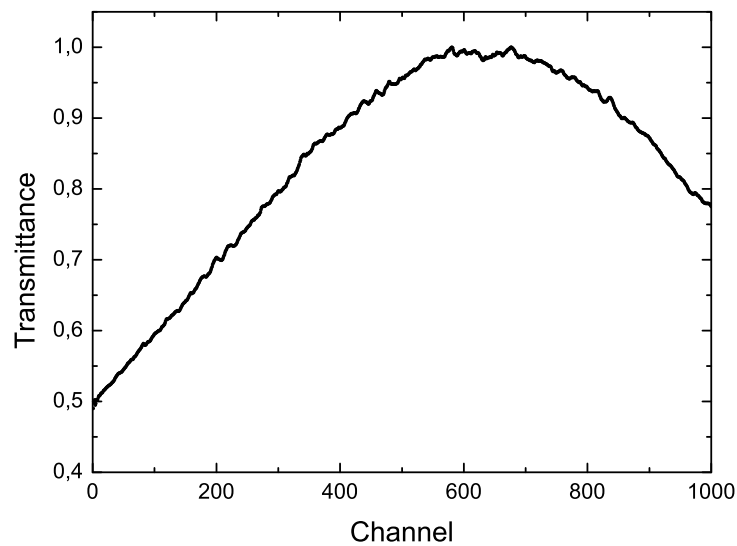
Figure 2.15: Normalised response curve as a function of the channel for the wavelength 500 nm.

stabilized. It is important to know this stabilization time so that the illumination of the lamp can be restricted to the shortest possible time to extend its lifespan. After a certain number of working hours, the emission of the lamp does not correspond with the spectral irradiance provided by the institution responsible for the calibration.

2) **Lamp power supply**: it is very important that the power supply supplies the same electric current with which the lamps spectral irradiance was measured. This current must also be very stable over time.

3) **Checking for higher diffraction orders**: there is the possibility that radiation of a higher diffraction order can enter our detector, distorting the measurements of the transmittance. For this reason, it is always important to check by using an appropriate filter.

4) **Using several standard light sources** to reduce the errors of the response curve, especially in the overlapping regions.

Chapter 3

Data processing and uncertainty determination.

> *"To err is human;*
> *to describe the error properly is sublime."*

> - Cliff Swart -

Once the experimental set-up as well as the way in which the measurements are carried out have been described in some detail, it is important to focus on the methods used to process all the spectra recorded. This chapter provides a detailed explanation of the different stages followed from the raw data to the final values of the transition probabilities and Stark parameters of a spectral line and their associated uncertainties.

The first section gives a general idea of all the process followed to identify, correct and fit each of the spectral lines under study, as well as a schematic vision of the different programs used in each of these stages. The next section focuses on the diagnostics of the plasma and how we have calculated the temperature and the electron density from the experimental data. The plasma diagnostics play a very important role, since these two magnitudes are of vital importance for the calculation of the transition probabilities and the Stark parameters, respectively. The third section deals with the calculation of the transition probabilities and their uncertainties and constitutes the bulk of this thesis. Most of the work done during this PhD has focused on the measurement of accurate

values of transition probabilities in different noble gases. Depending on the quantity and especially the quality of the data present in the literature, we have used two different ways of obtaining these A_{ki}-values. Both methods, as well as the context in which they are used, are explained in this section.

In addition to this measurement of accurate transition probabilities, one of the main aims of this thesis has been to develop a mathematical expression with which to calculate the value of the uncertainties in a systematic way by taking into account all the different aspects that introduce some error into our measurements. Each of these sources of uncertainty is described in this chapter, along with the way in which all of them have been weighted to obtain the final value of the relative uncertainty introduced by our measuring method. This value always accompanies the A_{ki}-values published in the articles that constitute this thesis.

Finally, the last section of this chapter focuses on the measurement of the Stark parameters. It contains a description of the method followed to obtain the Stark widths and shifts of spectral lines from the information obtained from the processing of the different spectra. The uncertainties of these parameters have also been carefully analyzed, obtaining an expression that takes into account all the different sources of error.

3.1 Data processing.

The first thing we have to do once we have our recorded spectra is to perform certain corrections. First of all, we have to identify the spectral lines.

1) **Line identification**: this is a very important stage, since a bad identification might lead to incorrect values of atomic parameters. Identification is performed using the GENERAL program with which we can overlap our spectra with the spectral lines taken from the bibliography of all the different species and stages of ionization that we suspect could be present in our plasma. Sometimes, especially in spectra where singly and doubly ionized atoms appear (as happened in our Krypton experiment), the presence of two very close spectral lines coming from singly and doubly ionized emitters of the same species could lead to two possible identifications of a given spectral line. In these situations, it is helpful to check the relative intensities of the two spectral lines on the literature. Even if these intensities depend on the kind of experiment, they tend to give a helpful approximate idea. It is also useful to

use the fact that lines coming from doubly ionized atoms will disappear from our plasma sooner than the singly ionized ones. If a misidentified line goes through the next stage of data processing, it will normally show some additional problem later, alerting us to the situation.
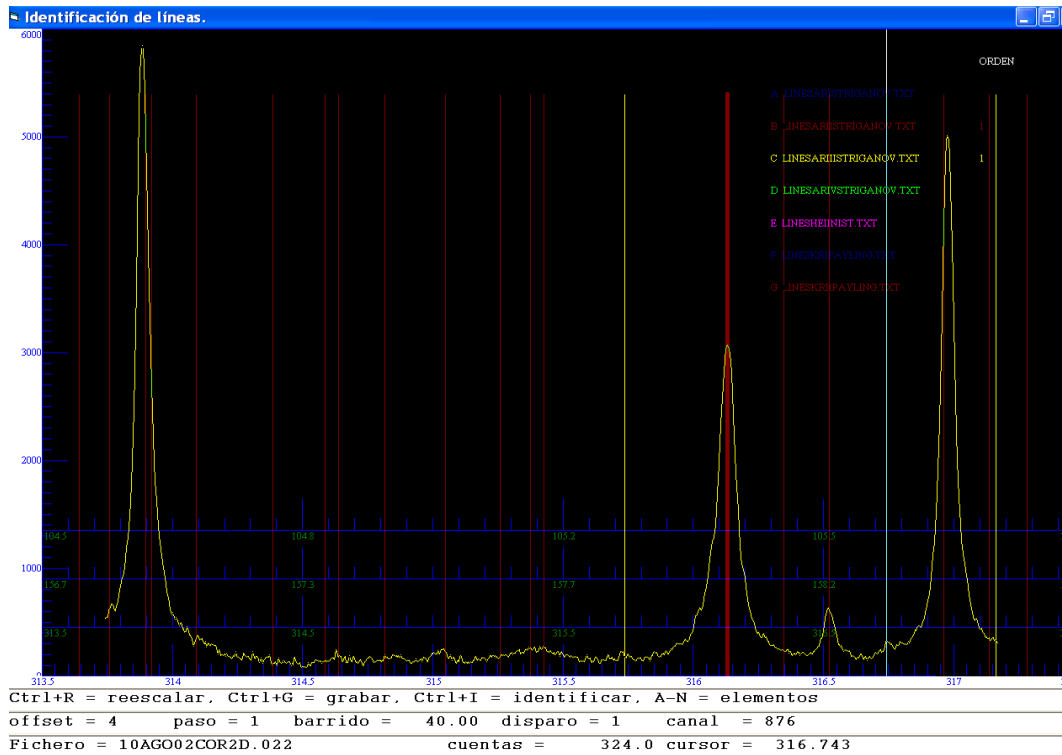
Figure 3.1: Example of the identification of an Argon spectrum.

2) **Intensity calibration**: once the lines have been identified, spectra are intensity calibrated using the response function, as explained in Chapter 2. By performing this calibration, we are taking into account different phenomena such us the different sensitivity of the detector channels and the different transmittance of our spectroscopic channel depending on the wavelength of the radiation.

3) **Self-absorption correction**: self-absorption is the phenomenon in which part of the radiation emitted by the plasma is reabsorbed by itself. This phenomenon is especially important for very intense and resonant lines (transitions connecting a given energy level with the fundamental one). As explained in Chapter 2, we check for self-absorption by placing a mirror behind the discharge lamp (with *behind* we are referring to the direction opposite the spectrometer). If the mirror is working, part of the radiation emitted by the plasma will leave the lamp in the direction of

the spectrometer and part of it will travel in the opposite direction. This radiation will be reflected by the mirror, passing then along the entire plasma column also to be recorded by the detector. The trajectory of these beams has been outlined in Fig. 3.2, where L represents the plasma length, R the mirror reflectivity, x a given position within the plasma column and I_D and I_R the direct and reflected intensity, respectively.
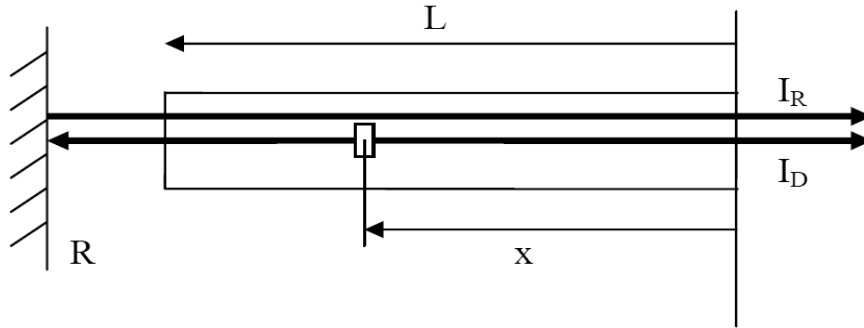
Figure 3.2: Schematic idea of the self-absorption correction.

Several spectra are recorded throughout the experiment, some of them with and some without the mirror. By comparing these two kinds of spectra it is possible to obtain a reconstructed spectrum, as explained in Appendix B. Only those spectral lines the self-absorption of which is lower than 20% are included in our results. Experience has shown that the uncertainty introduced by reconstructing lines whose self-absorption is higher than 20% might lead to values of transition probabilities the uncertainties of which are far higher than desired. However, some spectral lines the self-absorption of which is higher than 20% have occasionally been analyzed if there was a reason to do so. In this situation, a comment is always made to warn the reader against possible problems that might appear with that line in particular. Fig. 3.3 shows an example of the self-absorption correction process for an Ar II spectrum. The original (solid squares) and reconstructed (dotted line) spectra are plotted, together with the reflection coefficient R, which is explained in Appendix B.
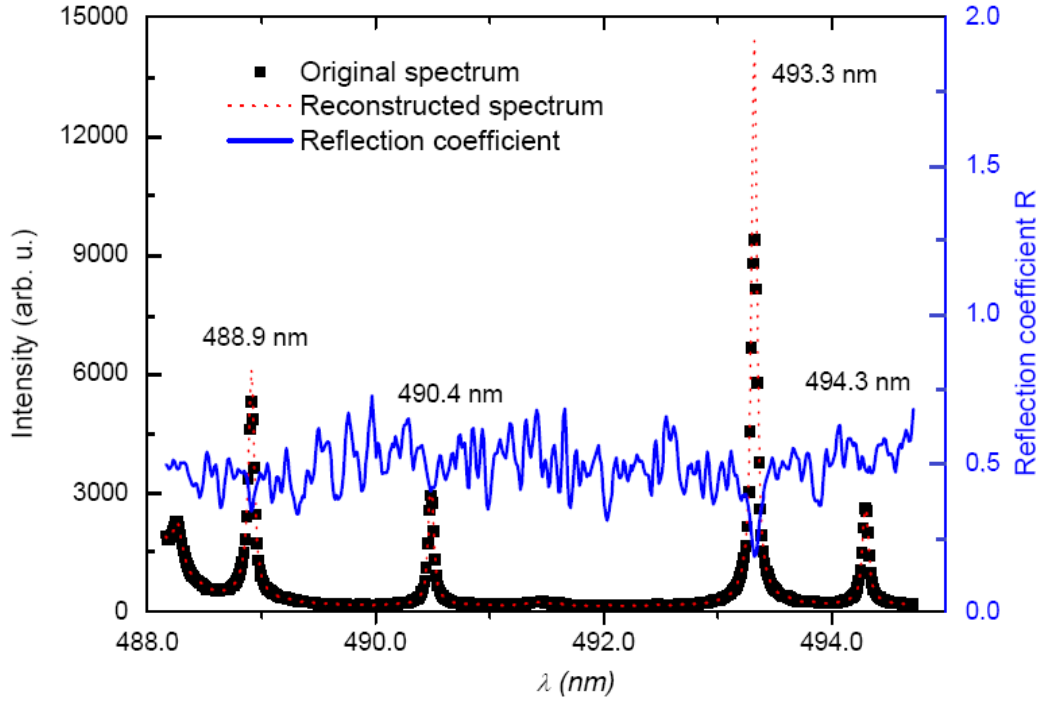
Figure 3.3: Example of the self-absorption correction of an Ar II spectrum.

4) **Spectra fitting**: once our spectra have been corrected using GENERAL, it is possible to fit them to mathematical functions. This fitting is performed using the program B5. This program has been improved during this PhD so that the output file includes some information that will be useful for the calculation of the A_{ki}-values uncertainty, which has been one of the main goals of this thesis. Depending on the broadening mechanisms which appear in the plasmas generated, as seen in Chapter 1, we can fit the recorded spectral lines to Lorentzian or Gaussian functions or to Voigh profiles. In our case, given that the dominant broadening mechanism is the quadratic Stark broadening, we normally use Lorenztian functions. In the case of lines emitted by multielectronic singly ionized atoms, as happens with all the research presented in this thesis, the asymmetry of these Lorenztian functions is close to zero. A continuum luminous background coming from other processes (recombination and Bremsstrahlung radiation) is fitted to a linear polynomial function, which in normal circumstances will have a slope close to zero. The global fit function can be expressed as a sum of the linear background and n Lorentzians:

$$I(\lambda) = F_0 + F_1\lambda + \sum_{l=1}^{n} \frac{I_l + \frac{A_l(\lambda-\lambda_l)}{\gamma_l}}{\left(\frac{\lambda-\lambda_l}{\gamma_l}\right)^2 + 1} \tag{3.1}$$

where F_0 and F_1 are the parameters defining the luminous background, I_l is the peak intensity, λ_l is the wavelength of the centre of the line and A_l and γ_l are the parameters related to the asymmetry and the width of each line, respectively. The algorithm used for this fitting is explained in Gigosos et al. (1994). The B5 program fits the multivariable expression (3.1) trying to minimize the standard deviation of the fitted spectrum to the experimental one. The deviations between both profiles are in most cases around 1% and they will be taken into account when calculating the transition probability uncertainty.

However, it is essential to bear in mind the fact that the best mathematical solution is not necessarily the best fitting of our spectrum. Sometimes, especially when dealing with particularly complicated spectra, the program might suggest a fitting with no physical meaning at all. This is one of the reasons why this kind of task is very time consuming, since it is not possible to carry out a purely automatic processing of the measurements. In order to avoid this problem as far as possible, the user is advised to introduce a first approximation of the centres, peak intensities and widths of the Lorentzian functions. These first values will guide the program and delimit its search, which reduces the computing time and offers a higher possibility of arriving at a solution with physical meaning.

Fig. 3.4 shows an example of an Ar II spectrum fitted with the B5 program. The blue line corresponds to the experimental spectrum and the green line to the fitted one. Each of the mathematical functions used to fit the spectrum are displayed in red. The bottom panel includes the standard deviation of the fitting. It is possible to appreciate some oscillations in the position of the very intense spectral line, which suggests the presence of self-absorption.

Once each of the spectra for the different instants have been fitted, B5 produces an output file with all data necessary to calculate atomic parameters and their uncertainties. From the adjustment parameters A_l and γ_l, it is possible to obtain information about the asymmetry (S_l), total width (ω_l) and area under each of the fitting curves (a_l) of each spectral line. We will refer to this last quantity as the *intensity* of the spectral line. These magnitudes can be calculated even in the case of overlapping lines through the expressions:
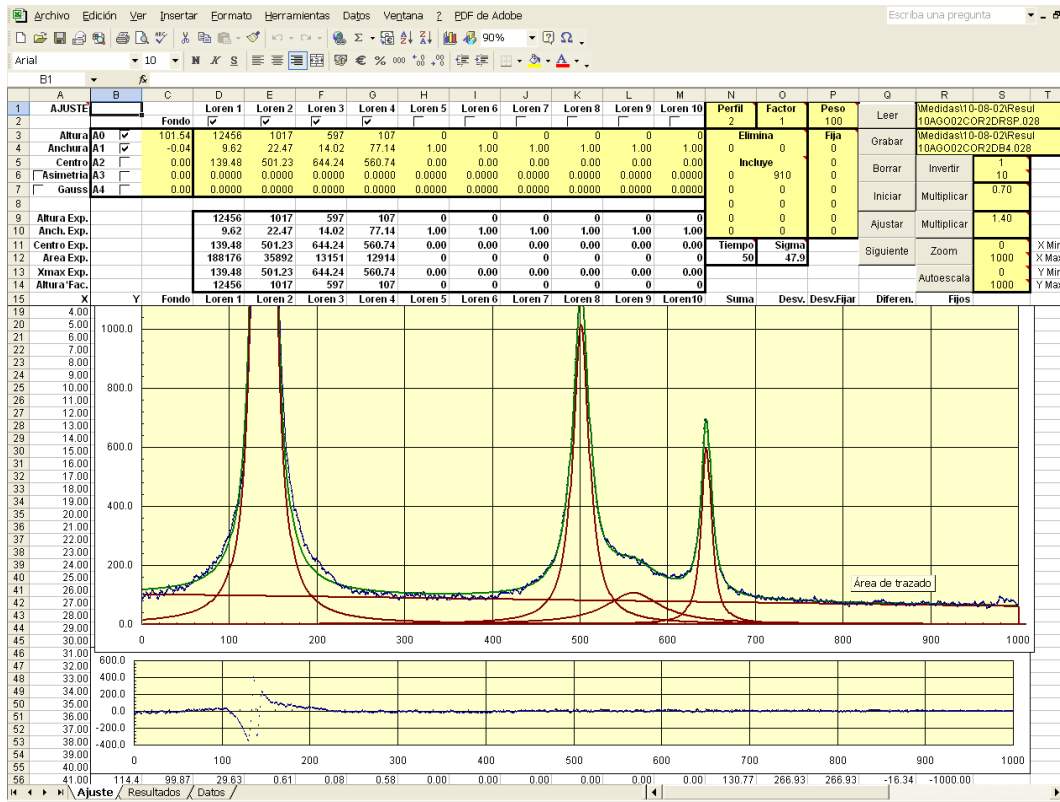
Figure 3.4: Example of a fitted Ar II spectrum.

$$S_l = \frac{A_l}{I_l} \tag{3.2}$$

$$\omega_l = 2\gamma_l\sqrt{S_l^2 + 1} \tag{3.3}$$

$$a_l = \frac{1}{2}\pi I_l \omega_l \tag{3.4}$$

In addition to the previous magnitudes, the output file created by B5 contains information about the standard deviation of this fitting and the distance between each line and the adjacent ones. This data will be used in the calculation of the uncertainty attributed to the intensity of each line.

3.2 Plasma diagnostics.

After processing the spectra, we have all the information necessary for carrying out the plasma diagnostics. Two quantities are essential to characterize our plasma: temperature and electron density. Each of these magnitudes has already been explained in Chapter 1. In this section, we will focus on the experimental methods used to calculate these parameters during our experiments. The generation of homogeneous plasma columns by the geometry of our discharge lamp has been proven already in del Val (1993). Further work has also been carried out to study the possible presence of cold plasma layers (González, 1999; del Val, 1997). These investigations arrived at the conclusion that, should they exist, it is not possible to detect their effect.

3.2.1 Plasma temperature.

Calculation of plasma temperature is one of the most important stages during our experiments, since it is a necessary parameter for determining the transition probability of the lines of interest. According to Van der Mullen (1990), the excitation temperature shows similar values to the kinetic temperature in collision-dominated plasmas, such as the plasma produced in this experiment.

3.2.1.1   Determination of plasma temperature.

We can encounter two possible situations when trying to calculate the excitation temperature of some species. On the one hand, we can find situations (as happened with the Ar II experiment) where it is possible to find in the literature a set of reliable lines the transition probabilities of which are known with a good level of accuracy. We will refer to these spectral lines as the *temperature lines*. In this case, we will use the Boltzmann-Plot technique (already explained in Chapter 1) to obtain a unique value of the excitation temperature for each of the instants of measurement. The Boltzmann-Plot is made by plotting the equation (3.5) as a function of the upper energy level E_k for a carefully selected set of lines lying within the spectral range of interest and the transition probabilities of which can be found in the bibliography:

$$\ln\left(\frac{I_{ki}\lambda}{g_k A_{ki}}\right) = \ln\left(\frac{\hbar c M N(T)}{2Z(T)}\right) - \frac{E_k}{kT} \tag{3.5}$$

By fitting the equation (3.5) to $y = a + bx$, it is possible to obtain the plasma temperature from the slope b as:

$$T = \frac{-1}{kb} \tag{3.6}$$

Fig. 3.5 shows an example of a Boltmann-Plot for Ar II lines. A careful selection of this set of temperature lines is one of the critical parts of this experiment, since the values of all the transition probabilities will depend on the temperature obtained from these lines. For this reason, it is important to select a set of lines the transition probabilities of which are as accurate as possible, preferably those classified as A or B by the National Institute of Standards and technology (NIST) (Kramida et al., 2015).

Nevertheless, even if we are obliged to select a set of lines with transition probabilities the uncertainties of which are relatively high, there are some ways of figuring out how reliable this set of temperature lines is as a whole by looking closely at the Boltzmann-Plot and the R^2 value of the fitting. This test is especially meaningful if our set of temperature lines contains lines measured by different authors. Since the temperature is obtained from the slope of the linear fitting, an error of a constant factor (i.e., some systematic error) would not change the value of the temperature. It is also important to remark that the
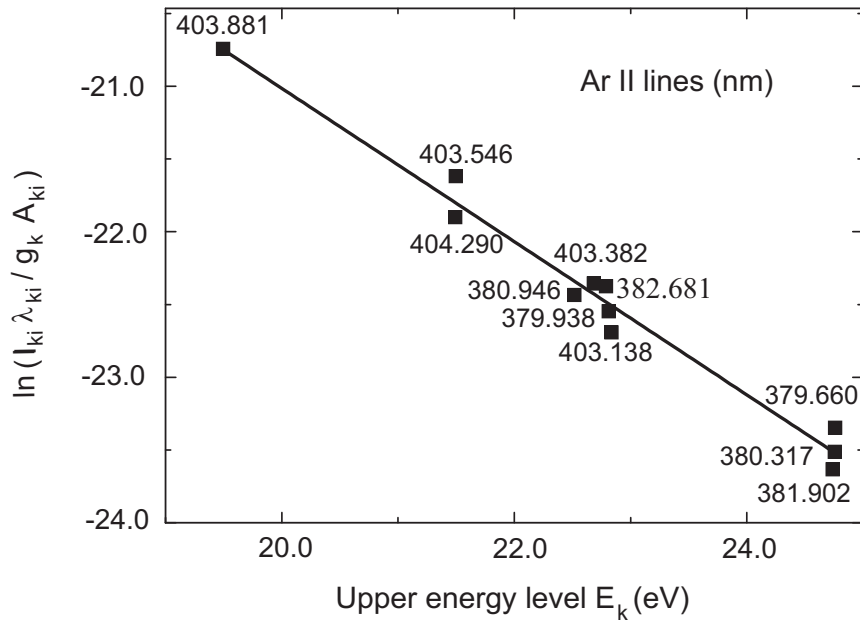
Figure 3.5: Example of a Boltzmann-Plot for Ar II.

temperature and its uncertainty have been calculated in this thesis by a non-weighted linear fit of the Boltzmann-plot. If we include the uncertainties of the reference A_{ki}-values by performing a weighted linear fit, the uncertainties in the temperature will rise, but they will always be lower than the individual uncertainties of each A_{ki}-value. As an example, uncertainties of around 50% in the transition probabilities used as a reference in Kr II led to an uncertainty of around 25% in the temperature.

As the example given in Fig. 3.5 shows, the linearity of the Boltzmann-plots from this work (with R^2 values ranging from 0.90 to 0.99, depending on the gas) supports the assumption that our plasmas are well described by a partial local thermodynamic equilibrium (pLTE) model, at least within the interval of the upper energy levels considered. It is also very important to note that the excitation temperature obtained from the Boltmann-Plot is only valid within the range of higher levels of energy covered by the temperature lines. For this reason, it is advisable to choose a set of lines whose upper energy interval is wide enough for all the spectral lines of interest to lie within it.

On the other hand, there are other situations in which it is not possible to find a set of temperature lines to make this Boltzmann-Plot. This was the case in the measurement of the transition probabilities for Kr III spectral lines in the UV region (into which, though the results have no bearing on this thesis, investigation commenced last year). In this case, the temperature was obtained by using different methods (such as the ratio of spectral lines

of singly and doubly ionized atoms) and calculating an average value of the temperature obtained from each of them. This approach aims to reduce the temperature uncertainty, which is sometimes the only possible way of calculating transition probabilities when using the technique applied in our laboratory. A different approach, such as the *'branching ratio-lifetime'* method, would be an alternative for solving these problems. However, this is a completely different way of facing this kind of experiment and it does not lie within the scope of this thesis. The method in which we obtain the excitation temperature will determine the way in which we will calculate transition probabilities, as will be explained in section 3.3.

3.2.1.2   Temperature uncertainty.

We will now study how to obtain the error associated with the plasma temperature when this magnitude has been calculated from a Boltzmann-Plot, since it is the method that we normally use. We will obtain the uncertainty by using the expression:

$$(\Delta T)^2 = \left(\frac{\partial T}{\partial b}\right)^2 (\Delta b)^2 \tag{3.7}$$

In order to obtain the partial derivative, we derive with respect to the coefficient b in equation (3.6), being able to rewrite the previous expression as:

$$\Delta T = \frac{1}{kb^2}\Delta b \tag{3.8}$$

where Δb is the uncertainty of the b fitting parameter and can be calculated as:

$$(\Delta b)^2 = \frac{\sum_n (y_i - bx_i - a)^2}{(n-2)} \frac{n}{n\sum_n x_i^2 - (\sum_n x_i)^2} \tag{3.9}$$

The uncertainty in the temperature has been calculated from a non-weighted linear fit of the Boltzmann-plot. If we include the uncertainties in the transition probabilities of each of the temperature lines by performing a weighted linear fit, the uncertainty associated with the temperature will be determined by these weights. However, it will always be lower than the individual A_{ki}-value uncertainties of the temperature lines.

3.2.2 Plasma electron density.

A two-wavelength interferometric technique was applied by passing two laser beams of 543.5 and 632.8 nm through the discharge tube in the axial direction. This two-wavelength interferometric method permits the dismissal of the contribution of heavy particles to changes in the refractivity (Aparicio et al., 1998; de la Rosa et al., 1990). The high-axial homogeneity of the electron density and the temperature in this lamp (Val et al., 1998) allow this.

3.2.2.1 Determination of plasma electron density.

In order to determine the plasma electron density, we will use the information contained in all the interferograms recorded throughout the experiment. As shown in Fig. 3.6, it is possible to obtain the evolution of the changes in the phase $(\Delta\Psi(t))$ from these interferograms, to calculate then the changes in the plasma refractivity $\Delta(n-1)(t)$ and finally, to obtain the electron density N_e. Each of these stages is briefly explained below.

1) **Extraction of the temporal evolution of the phase**: a very detailed description of this stage can be found in Aparicio (1996); González (1999); Peláez (2008). The phase changes $\Delta\Psi$ are directly related to the changes in the electron density. The end of the interferogram, where the phase is stationary because the plasma has already expired, is easy to identify and is therefore chosen as a phase origin. The $\Delta\Psi$ is calculated with respect to that phase. Those instants where the interferogram fringes are very close correspond to instants of fast variation in the electron density. The process of extracting the phase variation can be described as:

   * **Determination of the positions of phase inversion in the interferogram (see Fig. 3.6)**: these points correspond to changes in the sign of the slope in the plot electron density against time. It is important to note that there are as many inversion points in the interferograms as relative maxima and minima in the electron density curve, as can be observed in Fig. 3.6.

   * **Selection of the positions of maximum and minimum contrast (see Fig. 3.6)**: the program will add π to the phase variation between each of these consecutive positions until a phase inversion point appears. At this stage, the addition changes into substraction until arriving at another inversion point.
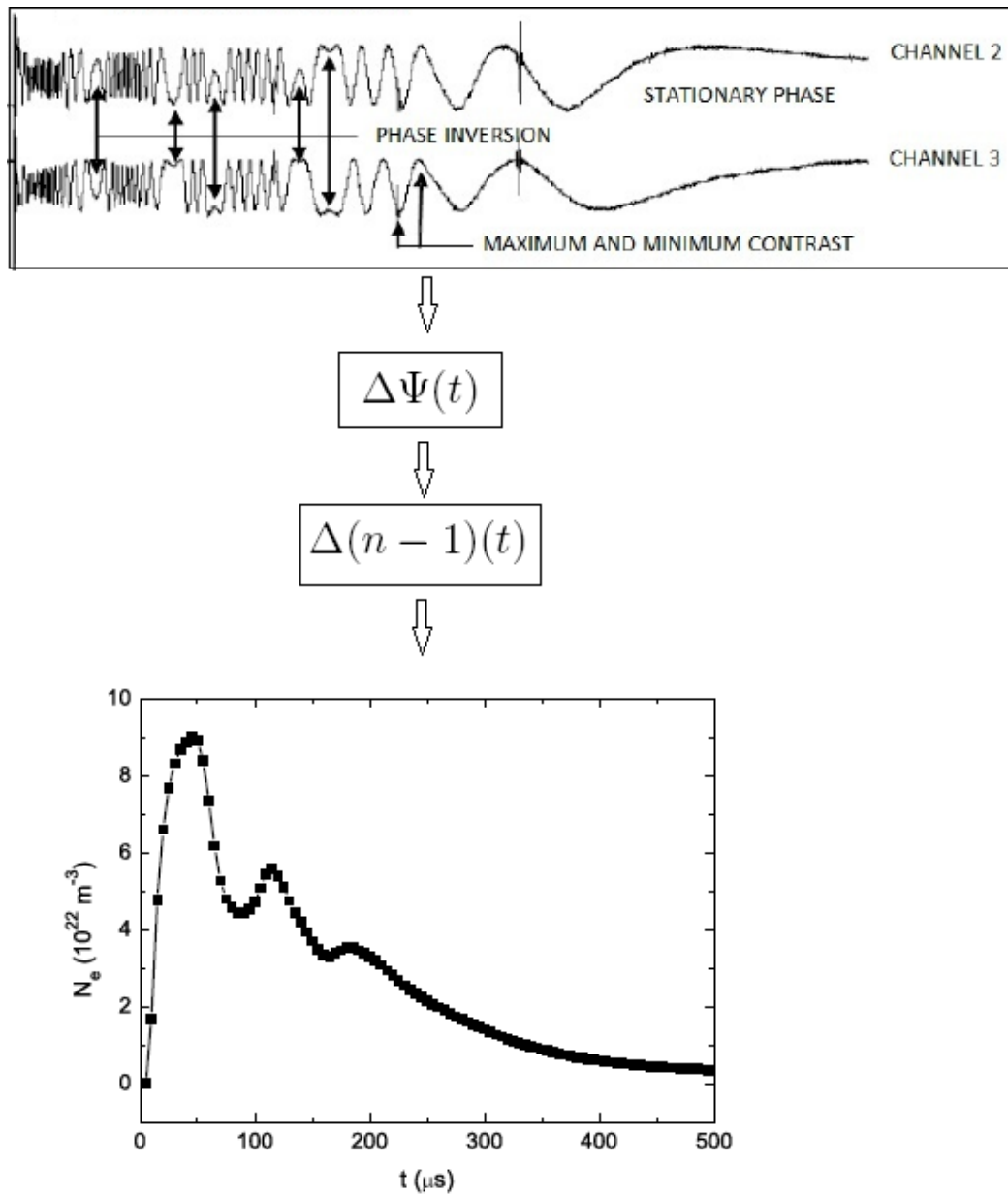
Figure 3.6: Different stages for the calculation of electron density.

  * **Calculation of the phase variation with time**: the program calculates it for each of the recorded interferograms using all the previous information provided by the user.

  * **Averaging the different phase curves**: in this way, a final phase curve is obtained. It is important to bear in mind that two interferograms were registered simultaneously using the wavelengths $\lambda_1 = 632.8$ nm and $\lambda_1 = 543.5$ nm in all our experiments. Both interferograms have been recorded several times in identical conditions, thus making it possible to obtain two curves of the average temporal evolution of the phase: $\Delta\Psi_1(t)$ and $\Delta\Psi_2(t)$.

2) **Calculation of plasma refractivity**: once the temporal evolution of the phase has been obtained, it is possible to calculate the variation of plasma refractivity changes $\Delta(n-1)$ by using equation (3.10) for each of the wavelengths employed:

$$\Delta\Psi(t) = \frac{2\pi}{\lambda} 2L \ \Delta(n-1) \tag{3.10}$$

where L is the length of the plasma column (175 mm) and λ is the wavelength of the radiation.
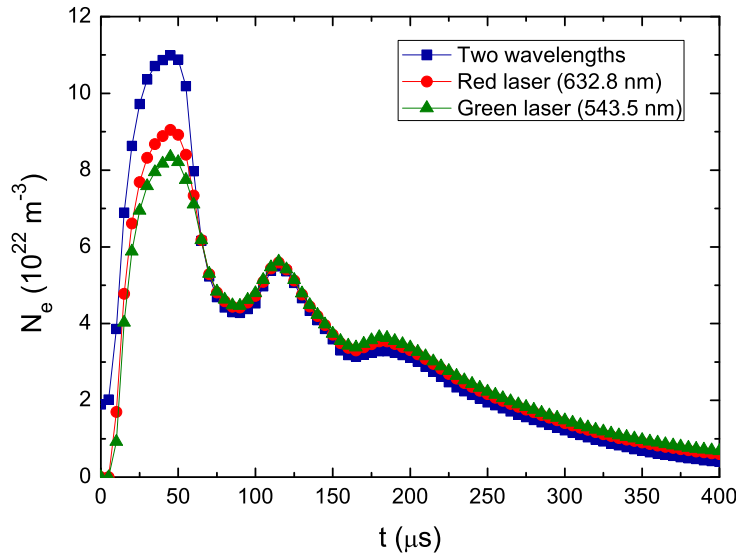
Figure 3.7: Electron densities in the Ar II experiment obtained in three different ways.

3) **Calculation of electron density**: as explained in Chapter 1, it is possible to

evaluate the electron density N_e from the refractivity of the plasma $\Delta(n-1)(t)$ by using the equation (3.11):

$$N_e(t) = -\frac{2\pi}{r_e(\lambda_2^2 - \lambda_1^2)}[\Delta(n-1)_{\lambda_2}(t) - \Delta(n-1)_{\lambda_1}(t)] \tag{3.11}$$

where r_e is the classical radio of the electron, defined as:

$$r_e = \frac{e^2}{4\pi\epsilon_0 m_e c^2} \tag{3.12}$$

e being the electron charge, ϵ_0 the vacuum permittivity, m_e the electron mass and c the speed of light in a vacuum.

Fig. 3.7 shows the evolution of plasma electron density over time in the Ar II experiment. The red and green data correspond to the N_e obtained from the interferograms recorded with the red and green lasers, respectively. The blue curve represents the electron density calculated from equation (3.11), that is to say by using the two-wavelength interferometric method.

3.2.2.2   Electron density uncertainty.

Electron density uncertainties have been estimated considering different relevant physical aspects as well as the statistical errors of our measurements. It is important to remark that these statistical uncertainties are very small due to the large amount of data used to obtain the electron density.

The physical aspects considered have already been described in Aparicio (1996) and are as follows:

∗ **Length of the plasma column**: the length of the plasma column was assigned a value of 175 mm in equation (3.10). However, the value that should be introduced in this equation is not the length of the discharge lamp, but the length of the positive plasma column. This magnitude is very difficult to measure accurately and it has been proven that considering the entire length of the lamp is not an inadequate approximation.

∗ **Inhomogeneities during the discharge**: which tend to be more important during the instants of higher electric current, where the electron density is also higher. This is probably the largest source of uncertainty for the determination of N_e.

∗ **Mechanical instabilities**: there are two different kinds of mechanical instability that can potentially have an effect on the phase variation of the interferograms. On the one hand, the vibrations transmitted through the building structure which have not been absorbed by the anti-vibration table. On the other hand, the instabilities generated by the discharge itself, which causes stress in the lamp structure. A previous work carried out in this laboratory (de la Rosa et al., 1990) found that this last form of instability does not affect axial measurements.

3.3   Calculation of transition probabilities and their uncertainties.

This section describes the measurement of transition probabilities of different noble gases and their uncertainties and constitutes the main part of this thesis. A considerable effort has been made not only to obtain accurate A_{ki}-values, but also to determine the relative uncertainties introduced by our method of measuring, a very important aspect that is neglected on many occasions.

As mentioned before, the technique employed to calculate the plasma temperature determines the mathematical procedure used to obtain transition probabilities. Two different methods have been used during this thesis, depending on the particularities of each experiment. On the one hand, the approach we have called the **'slope-intercept'** method, which is based on the Boltzmann-plot technique for the calculation of the temperature. On the other hand, a method based on **'ratios with reference lines'**, used when the temperature is obtained without using Boltzmann-Plots.

Regarding the uncertainties associated with transition probabilities, it is advisable to bear in mind the recommendations made by Vujnović & Wiese (1992) in their critical compilation of atomic transition probabilities for singly ionized Argon. In this article, the authors explain all the different aspects that they considered when assessing the data available for their compilation in the literature. We have followed their advice closely, taken into account all the possible sources of uncertainty and studied them and their

effect on the final value of transition probabilities in a consistent manner.

3.3.1 The *'slope-intercept'* method.

The method we refer to as the *'slope-intercept'* method can only be used if the plasma temperature has been obtained exclusively by means of a Boltzmann-Plot, since it is based on it.

3.3.1.1 Calculation of transition probabilities.

This method relies on a group of selected spectral lines recorded in our experiment and the transition probability values of which can be taken from the bibliography. As seen in Chapter 1, the intensity of a spectral line corresponding to a transition from the upper energy level k to the lower energy level i, assuming that the plasma is in partial local thermodynamic equilibrium (pLTE), can be expressed as 1.45:

$$I_{ki} = M \frac{A_{ki}g_k}{2\lambda_{ki}} \frac{\hbar c}{Z(T)} \frac{N(T)}{Z(T)} e^{-\frac{E_k}{kT}} \qquad (3.13)$$

where:

$I_{ki}\rightarrow$ intensity of the spectral line already corrected by the response function.

$M\rightarrow$ purely geometrical factor (assuming a relative calibration).

$A_{ki}\rightarrow$ transition probability between the energy states k and i.

$g_k\rightarrow$ statistical weight of the k level ($g = 2J + 1$).

$\lambda_{ki}\rightarrow$ wavelength corresponding to the transition.

$N(T)\rightarrow$ total density of the ion under study.

$Z(T)\rightarrow$ partition function of the ion under study.

$E_k\rightarrow$ upper energy level (eV).

k$\rightarrow$ Boltzmann constant (k $= 8.6217 \times 10^{-5} eV\ K^{-1}$).

For convenience in this calculation, we will make a small change in the notation. Given that once we are studying a particular spectral line we already know that we are referring to that transition in particular, we will replace the subscripts k and i for t. This subscript indicates that we are referring to the measurement of the transition probability carried out in the t-th instant of the plasma life. This subscript ranges from 1 to n_t, the latter quantity being the total number of instants of measurement. With this new notation, reorganizing (3.13) and taking logarithms of both sides, it is possible to write:

$$\ln \left(\frac{I_t \lambda}{g_k A_t} \right) = \ln \left(\frac{\hbar c M N(T_t)}{2 Z(T_t)} \right) - \frac{E_k}{k T_t} \tag{3.14}$$

The previous expression can be plotted as a function of E_k for each of the reference lines, given that all the magnitudes are known. As explained before, this method is known as the **Boltzmann-Plot technique**. The value of the intensity of the line I_t is taken from the fitted spectra, whereas the transition probability is taken from the bibliography. Plotting (3.14) for all the reference lines at a given instant, we obtain a point cloud that can be linearly fitted. Since this representation is made for each of the instants of measurement, we will obtain n_t lines of the best fit:

$$y_t = a_t + b_t x \tag{3.15}$$

where the values of the intercept and slope for each of the instants can be expressed as:

$$a_t = \ln \left(\frac{\hbar c M N(T_t)}{2 Z(T_t)} \right) \tag{3.16}$$

$$b_t = \frac{-1}{k T_t} \tag{3.17}$$

Rewriting (3.14) in terms of (3.16) and (3.17):

$$\ln \left(\frac{I_t \lambda}{g_k A_t} \right) = a_t + b_t E_k \tag{3.18}$$

and rearranging (3.18), it is possible to isolate the value of the transition probability

we want to calculate, expressing it as:

$$A_t = \frac{I_t \lambda}{g_k} e^{-a_t - b_t E_k} \tag{3.19}$$

By using the previous equation for each of the times of measurement throughout the plasma life, we obtain a set of n_t values of transition probabilities. The final A_{ki} value associated to each spectral line is calculated from a weighted average following the next expression taken from statistics:

$$\bar{A} = \frac{\sum_{t=1}^{n_t} \omega_t A_t}{\sum_{t=1}^{n_t} \omega_t} \tag{3.20}$$

where ω_t is the weight attributed to each of the points and it has been defined as:

$$\omega_t = \frac{1}{(\Delta A_t)^2} \tag{3.21}$$

where ΔA_t is the uncertainty associated with the A_t value. This way of weighing each of the points allows us to assign less importance to those data points that for different reasons have higher uncertainties. The expression used to calculate the uncertainty associated with the weighted average is:

$$\Delta \bar{A} = Z \sqrt{\frac{1}{\sum_{t=1}^{n_t} \omega_t}} \tag{3.22}$$

Assuming that our data is normally distributed, the Z factor refers to the z-score and we have assigned it a value of 2.6, which corresponds with a confidence interval of 99%. Therefore, the final value of the uncertainty associated with each of the transition probability values is calculated as follows:

$$\Delta \bar{A} = 2.6 \sqrt{\frac{1}{\sum_{t=1}^{n_t} \omega_t}} \tag{3.23}$$

We will now focus on the calculation of the uncertainty associated with each of the A_t values, since it is necessary to obtain each of the weights, ω_t.

3.3.1.2 Calculation of transition probability uncertainty.

In order to determine the uncertainty associated with each of the A_t-values obtained in the previous section, we start from the equation (3.19), which shows that the transition probability of a line can be expressed as a function of the intensity of that line, I_t, and the intercept a_t and slope b_t of the linear fit performed with the temperature lines:

$$A_t = \frac{I_t \lambda}{g_k} e^{-a_t} e^{-b_t E_k} = f(I_t, a_t, b_t) \tag{3.24}$$

As explained in Sikström et al. (2002), if we assume that the uncertainties associated with the different magnitudes I_t, a_t and b_t are not correlated, we can apply the law of the propagation of the uncertainty in the form:

$$(\Delta A_t)^2 = \left(\frac{\partial A_t}{\partial I_t}\right)^2 (\Delta I_t)^2 + \left(\frac{\partial A_t}{\partial a_t}\right)^2 (\Delta a_t)^2 + \left(\frac{\partial A_t}{\partial b_t}\right)^2 (\Delta b_t)^2 \tag{3.25}$$

As can be seen from the previous equation, in order to calculate the total uncertainty ΔA_t associated with every A_t-value, we need the partial derivatives with respect to the three variables and the uncertainties associated with each of them. Firstly, evaluating each of the partial derivatives in (3.25) we obtain:

$$\frac{\partial A_t}{\partial I_t} = \frac{\lambda}{g_k} e^{-a_t - b_t E_k} \tag{3.26}$$

$$\frac{\partial A_t}{\partial a_t} = \frac{-I_t \lambda}{g_k} e^{-a_t - b_t E_k} \tag{3.27}$$

$$\frac{\partial A_t}{\partial b_t} = \frac{-I_t \lambda E_k}{g_k} e^{-a_t - b_t E_k} \tag{3.28}$$

We now need to calculate the uncertainties attributed to the intensity of the spectral line the A_{ki}-value of which we want to obtain and those related to the slope and y-intercept of the linear fitting of the Boltzmann-Plots.

a) **Uncertainty attributed to spectral line intensity.**

During the fitting of the spectra explained before, an error which affects the inten-

sity (area under the function) of the spectral lines and therefore the value of the transition probability is introduced. To measure accurate transition probabilities, it is necessary to know the sources contributing to this error. By being aware of the weaknesses of our experiment, we will be able to quantify those errors as well as to eliminate, as far as possible, all those aspects that are reducing the quality of our measurements.

It is important to remark that our analysis of the uncertainties has not been restricted to well-defined and separated spectral lines, as in studies carried out by other authors (Sikström et al., 2002), but has also been extended to more complicated situations where two or more lines with similar or even very different intensities are overlapping. Fig. 3.8 defines all the different parameters that will be used for the calculation of the uncertainties.
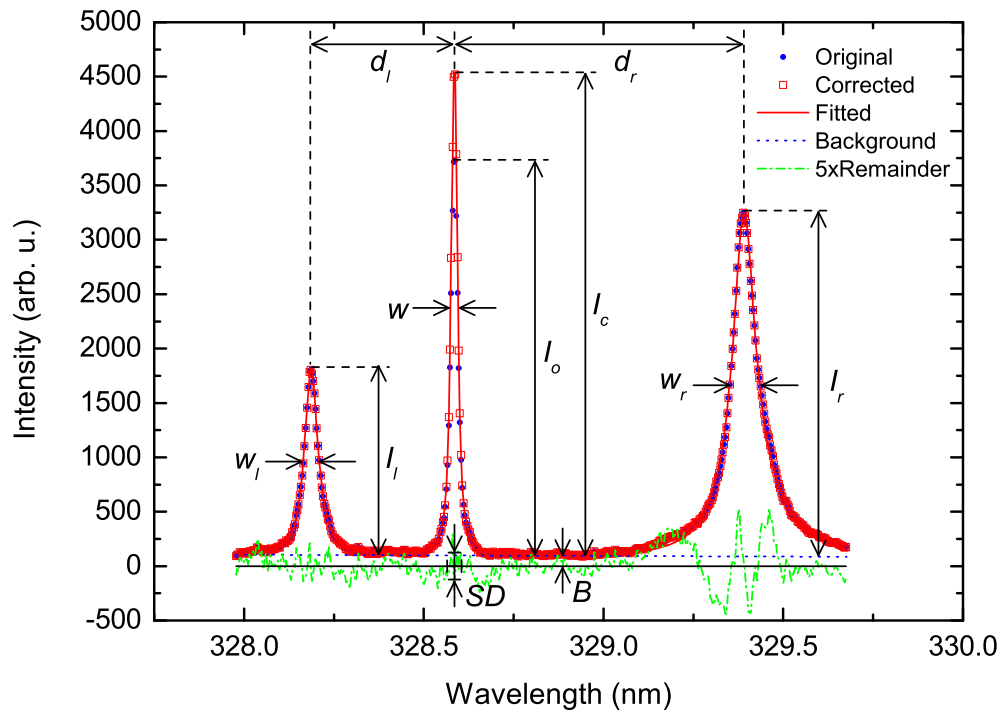
Figure 3.8: Parameters used in the calculation of the intensity uncertainty.

The sources of error that we have considered to be the most important when calculating the intensity of a spectral line are:

* **Calibration error** (σ_{calib}): as shown in Chapter 2, the uncertainty of the response curve as a function of either the wavelength or the detector channel was estimated to be lower than 3%. This error has an effect on the final value of the spectral line intensity and is added in quadrature to the other sources of uncertainty.

* **Fitting accuracy** (σ): ratio between the standard deviation of the residuals (SD) on an interval $2w$ ($w=$ width) and the maximum height of the line (I_c) .

$$\sigma = \frac{SD}{I_c} \tag{3.29}$$

* **Self-absorption coefficient of the spectral lines** (SA): this is the fraction of the original profile that is necessary to add in order to reconstruct the spectral line of interest. We will refer to the measured peak intensity as I_o (original value) and to the reconstructed one as I_c (corrected value). The self-absorption coefficient is obtained from the ratio between the increase in the peak intensity due to the reconstruction procedure, $I_c - I_o$ and the peak intensity of the reconstructed profile (I_c) (Aparicio, 1996; González, 1999). When there are no self-absorption effects, the increase is null and consequently the SA coefficient is also null. We have excluded from our results all the lines for which SA is greater than 0.2.

$$SA = \frac{I_c - I_o}{I_c} \tag{3.30}$$

* **Background-peak** (BP): ratio between the background intensity (B) and the maximum height of the line (I_c).

$$BP = \frac{B}{I_c} \tag{3.31}$$

* **Overlapping with the adjacent left** (O_l) **or right** (O_r) **line**: this quantity is given by the next expression:

$$O_i = \frac{w + w_i}{d_i} \frac{I_i}{I_c} \tag{3.32}$$

where i represents left (l) or right (r), w and w_i are the half-widths of the line under study and the adjacent lines, respectively, and d_i is the distance between the peaks of the line under study and the adjacent one. The second

factor contains the ratio between the intensity of the adjacent line (I_i) and the intensity of the studied line (I_c).

All the previous factors contribute to the final uncertainty in the intensity on different ways and with different weights. After analyzing hundreds of spectra in which it was possible to appreciate the influence of each of these sources of error separately, we arrived at the expression:

$$\frac{\Delta I_t}{I_t} = \sqrt{\sigma^2 + (2(SA)^2)^2 + \left(\frac{BP}{2}\right)^2 + \left(\frac{O_L}{20}\right)^2 + \left(\frac{O_R}{20}\right)^2 + \sigma_{calib}^2} \qquad (3.33)$$

The above equation is the result of the experience acquired after many hours of work and it has been tested with a wide range of situations (overlapping lines with similar and different intensities, self-absorbed lines, spectra with a very high number of lines of singly and doubly ionized atoms, etc.). This has enabled us to improve it during this thesis, obtaining an expression that provides very reasonable values of the uncertainties in the majority of the situations.

b) **Uncertainty attributed to the a_t and b_t parameters.**

As seen in equation (3.25), the other two sources of uncertainty that should be considered are attributed to the linear regression performed with the temperature lines. Therefore, it is necessary to calculate the errors of the fitting parameters Δa_t and Δb_t. The expressions used are:

$$(\Delta a_t)^2 = \frac{\sum_n (y_i - b x_i - a)^2}{n - 2} \frac{\sum_n x_i^2}{n \sum_n x_i^2 - (\sum_n x_i)^2} \qquad (3.34)$$

$$(\Delta b_t)^2 = \frac{\sum_n (y_i - b x_i - a)^2}{n - 2} \frac{n}{n \sum_n x_i^2 - (\sum_n x_i)^2} \qquad (3.35)$$

where n is the number of temperature lines used for the linear regression and the values y_i and x_i are:

$$y_i = \ln \left(\frac{I_i \lambda}{g_k A_t}\right) \qquad (3.36)$$

$$x_i = E_k \tag{3.37}$$

k being the upper energy level. In those cases where the uncertainties of the A_{ki}-values are known, it is possible to carry out a weighted linear regression. In that situation, it would be necessary to modify equations (3.34) and (3.35) in order to include the weight of each point.

3.3.2 The *'ratios with reference lines'* method.

If we have calculated the excitation temperature by using a technique different from the Boltzmann-plot or as an average of the temperatures obtained by different methods, we are obliged to use what we call the *"ratios with reference lines"* method. In this case, we use a set of reference lines the A_{ki}-values of which are known and we avoid the problem of having unknown magnitudes by calculating ratios between the lines we want to study and the reference lines. This method can also been used on those occasions when the temperature is calculated purely from a Boltzmann-Plot.

3.3.2.1 Calculation of transition probabilities.

As was done with the previous method, we start our mathematical analysis from the expression (3.13), which provides the intensity of a spectral line corresponding with a transition from the upper energy level k to the lower energy level i. On this occasion, we will make a different change of notation, replacing the subscripts ki with three different ones: s, r, t. The subscript s indicates that we are referring to the spectral line under study (s from 'studied line'), the subscript t is used to refer to the measurement of a spectral line in the t-th instant and the subscript r to refer to the r-th 'reference' line. For a given spectral line under study the 's' subscript is constant, whereas the subscripts t and r range from 1 to n_t or n_r, respectively. The parameters n_t and n_r represent the 'total number of instants of measurement' and the 'total number of reference lines used'.

From the ratio between the intensity of two spectral lines of the same species and stage of ionization (the line under study and a reference line) and considering the equilibrium assumption, it is possible to obtain the equation 34 in Konjević (1999):

$$\frac{I_{st}}{I_{rt}} = \frac{A_{srt}g_s\lambda_r}{A_rg_r\lambda_s}e^{\frac{-E_s+E_r}{kT_t}} \tag{3.38}$$

where the magnitudes only accompanied by the subscript 's' refer to the studied line and do not change over time and A_{srt} refers to the transition probability of the line under study calculated from the ratio with the $r-th$ reference line for the instant t. Rearranging this equation, we can isolate the unknown transition probability and express it as a function of known quantities:

$$A_{srt} = \underbrace{\frac{I_{st}\lambda_s}{g_s}e^{\frac{E_s}{kT}}}_{studied\ line}\underbrace{\frac{A_{rt}g_r}{I_{rt}\lambda_r}e^{\frac{-E_r}{kT_t}}}_{reference\ line} \tag{3.39}$$

As can be seen, the previous equation can be expressed as a product of two quantities, one of them depending exclusively on magnitudes related to the studied line and the other on magnitudes related to the reference line. Using equation (3.39) for a particular transition, we can calculate a value of the transition probability for each instant and reference line, obtaining a point cloud of $n_t n_r$ data points. Fig. 3.9 shows an example of one of these point clouds for the line 214.508 nm in Kr II. Each of the points correspond with a value of A_{srt}. All the points represented with the same symbol have been calculated from ratios with the same reference line.

The point cloud shown in Fig. 3.9 is then cleaned using the 2σ **criterion**, by which all data points that differ from the average value by more than two times the standard deviation (σ) are removed from the point cloud. To accomplish this task, we calculate the arithmetic mean and its standard deviation for the entire set of data points. After that, all the points that differ more than 2σ from the average value are selected. The furthest of these selected points is then removed and the average and standard deviation are recalculated. Then the criterion is applied again as many times as necessary until all the points of the cloud lie within the $\pm 2\sigma$ region. Fig. 3.10 shows how this criterion cleans the point cloud shown in Fig. 3.9. This method has proven very effective in eliminating all those problematic points that had not been identified previously. It is very helpful in detecting all those situations in which a more careful analysis is needed, such as overlapping lines or when there are problems in the identification of the line.

Once the point cloud has been cleaned, the final value of the transition probability for
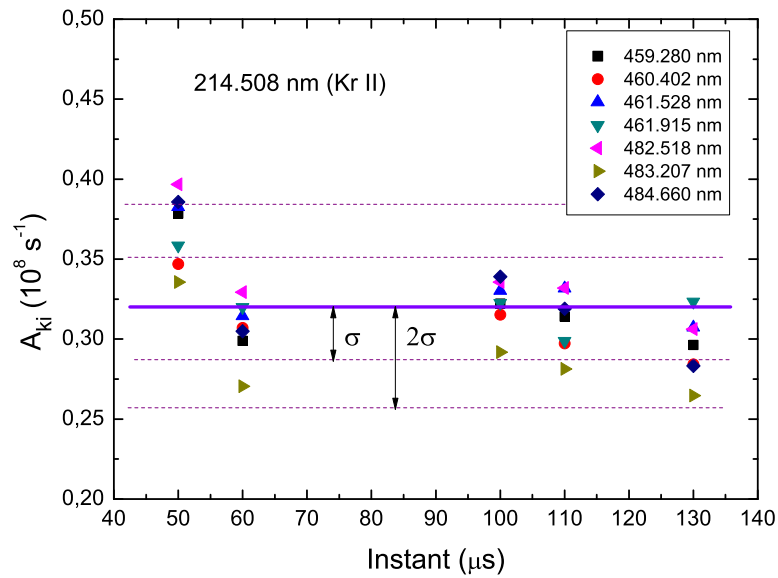
Figure 3.9: Point cloud with the A_{ki}-values of a Kr II spectral line.
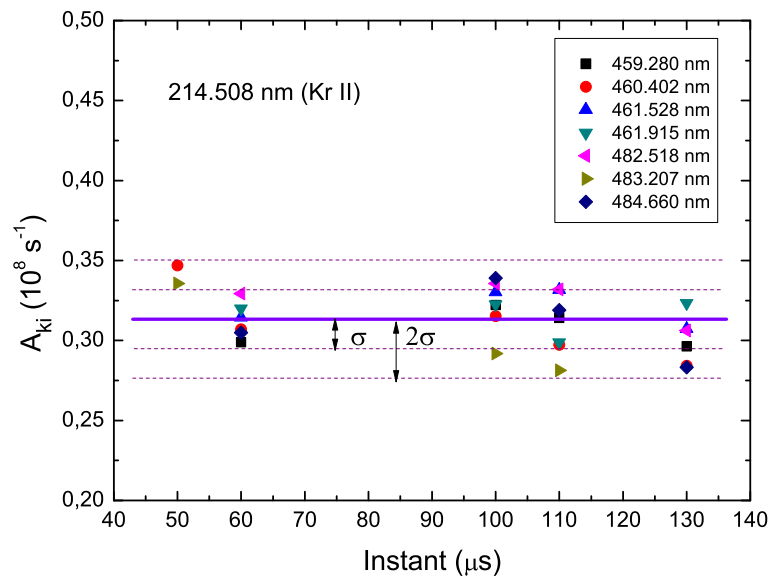
Figure 3.10: Cleaned point cloud of A_{ki}-values after using the 2σ criterion.

the line under study is calculated by means of a weighted arithmetic mean. By weighing each of the data points, those A_{ki}-values showing less reliable behaviour will have less influence in the final $\bar{A}$-value. The expression used to calculate this weighted arithmetic mean is:

$$\bar{A} = \frac{\sum_{r=1}^{n_r} \sum_{t=1}^{n_t} \omega_{rt} A_{srt}}{\sum_{r=1}^{n_r} \sum_{t=1}^{n_t} \omega_{rt}} \tag{3.40}$$

where ω_{rt} is the weight associated to the value A_{srt} and it has been defined as:

$$\omega_{rt} = \frac{1}{(\Delta A_{srt})^2} \tag{3.41}$$

The quantity ΔA_{srt} is the uncertainty associated with each of the data in the point cloud and its calculation will be explained in detail in section 3.3.2.2. The uncertainty associated to the final value of the transition probability, $\bar{A}$, is given by the equation:

$$\Delta \bar{A} = Z \sqrt{\frac{1}{\sum_{r=1}^{n_r} \sum_{t=1}^{n_t} \omega_{rt}} R} \tag{3.42}$$

where Z and R are two factors. Assuming that our data are normally distributed, the Z factor refers to the z-score. We have assigned it a value of 2.6, which corresponds with a tolerance interval of 99%. Regarding the R factor, it has been included to correct the number of degrees of freedom. Even if the point cloud has $n_r n_t$ values, we have not carried out that number of measurements. The real number of degrees of freedom will be n_t^2, since we have recorded n_t spectra for each line. Introducing all these corrections, the final expression of the uncertainty will be:

$$\Delta \bar{A} = 2.6 \sqrt{\frac{1}{\sum_{r=1}^{n_r} \sum_{t=1}^{n_t} \omega_{rt}}} \sqrt{\frac{n_r n_t}{n_t^2 - 1}} \tag{3.43}$$

It is now necessary to evaluate the uncertainty of each of the values in the point cloud,ΔA_{srt}, in order to calculate each of the weights.

3.3.2.2 Calculation of transition probability uncertainty.

In order to determine the uncertainty associated with each of the transition probabilities, we start from the expression used in the previous section, which depends on the intensity of the spectral line under study and the reference line for each instant, the plasma temperature and the A_{ki}-value of the reference line:

$$A_{srt} = \frac{I_{st}\lambda_s}{g_s} e^{\frac{E_s}{kT}} \frac{A_{rt}g_r}{I_{rt}\lambda_r} e^{\frac{-E_r}{kT_t}} = f(I_{st}, I_{rt}, T_t, A_r) \tag{3.44}$$

Our measurement procedure introduces uncertainty on the intensities and temperatures, so we should take into account these sources of error. Taking equation (3.44) and assuming that the uncertainties of I_{st}, I_{rt}, T_t and A_r are not correlated (Sikström et al., 2002), we are able apply the law of the propagation of uncertainty as:

$$(\Delta A_{srt})^2 = \left(\frac{\partial A_{srt}}{\partial I_{st}}\right)^2 (\Delta I_{st})^2 + \left(\frac{\partial A_{srt}}{\partial I_{rt}}\right)^2 (\Delta I_{rt})^2 + \left(\frac{\partial A_{srt}}{\partial T_t}\right)^2 (\Delta T_t)^2 + \left(\frac{\partial A_{srt}}{\partial A_r}\right)^2 (\Delta A_r)^2$$

$$\tag{3.45}$$

where ΔA_{srt} is the uncertainty associated with the transition probability we are calculating, ΔI_{st}, ΔI_{rt} and ΔT_t are the standard uncertainties of the measured quantities and ΔA_r is the standard uncertainty of the transition probabilities taken from the bibliography. As mentioned in Sikström et al. (2002), we are using the term standard uncertainty according to the definition given in Taylor & Kuyatt (1994), i.e. equal to the positive square root of the estimated variance u^2. We need then to evaluate the derivatives in (3.45), for which it is useful to rewrite (3.44) as follows:

$$A_{srt} = C_{sr} \frac{A_r I_{st}}{I_{rt}} e^{\frac{E_s - E_r}{kT_t}} \tag{3.46}$$

where C is a parameter that is constant for each studied line and it is defined as:

$$C_{sr} = \frac{\lambda_s g_r}{\lambda_r g_s} \tag{3.47}$$

Deriving in (3.45) with respect to the different dependent variables, it is possible to obtain the next expressions for each of the magnitudes accompanying the different uncertainties:

$$\frac{\partial A_{srt}}{\partial I_{st}} = C_{sr} \frac{A_r}{I_{rt}} e^{\frac{E_s - E_r}{kT_t}} \tag{3.48}$$

$$\frac{\partial A_{srt}}{\partial I_{rt}} = -C_{sr}\frac{A_r I_{st}}{I_{rt}^2}e^{\frac{E_s - E_r}{kT_t}} \tag{3.49}$$

$$\frac{\partial A_{srt}}{\partial T_t} = C_{sr}\frac{A_r I_{st}}{I_{rt}}\frac{(-E_s + E_r)}{kT_t^2}e^{\frac{E_s - E_r}{kT_t}} \tag{3.50}$$

$$\frac{\partial A_{srt}}{\partial A_r} = -C_{sr}\frac{I_{st}}{I_{rt}}e^{\frac{E_s - E_r}{kT_t}} \tag{3.51}$$

Regarding the standard uncertainty of the transition probabilities taken from the literature, ΔA_r, there are many instances of these values not being given by the authors. Sometimes, even if the authors did not provide any error, some estimation can be found in critical compilations or atomic databases. However, since these uncertainties tend to be higher than the ones introduced by our measurements, they would mask them, preventing the reader from seeing the errors introduced by our method of measuring. For this reason, we think that it is more interesting to provide a relative value of these uncertainties without including ΔA_r. In this way, if some of the reference lines are measured in the future with higher accuracy, the absolute uncertainty of our A_{ki}-values could be recalculated. For this reason, the expression used in this thesis to obtain ΔA_{srt} is:

$$(\Delta A_{srt})^2 = \left(\frac{\partial A_{srt}}{\partial I_{st}}\right)^2(\Delta I_{st})^2 + \left(\frac{\partial A_{srt}}{\partial I_{rt}}\right)^2(\Delta I_{rt})^2 + \left(\frac{\partial A_{srt}}{\partial T_t}\right)^2(\Delta T_t)^2 \tag{3.52}$$

In order to obtain the value of this previous equation, it is necessary to calculate the uncertainty associated with the intensity of the spectral lines and the temperature.

$a)$ **Uncertainty attributed to spectral line intensity.**

The uncertainty in the intensity of the spectra lines for each instant is calculated by taking into account the same factors described in 3.3.1.2, being described by the equation:

$$\frac{\Delta I_t}{I_t} = \sqrt{\sigma^2 + (2SA^2)^2 + \left(\frac{BP}{2}\right)^2 + \left(\frac{O_L}{20}\right)^2 + \left(\frac{O_R}{20}\right)^2 + \sigma_{calib}^2} \tag{3.53}$$

$b)$ **Uncertainty attributed to temperature.**

If the plasma temperature has been calculated from a Boltzmann-plot, the uncertainty attributed to this temperature will be calculated as explained in section

3.2.1.2. If a different method is used, it would be necessary to evaluate the error introduced by it, considering all the possible sources of error that contribute to the final uncertainty.

3.4 Calculation of Stark parameters and their uncertainties.

As explained in Chapter 1, the Stark effect is the main broadening mechanism on those plasmas where the electron density is high enough. Being able to know the functional dependency of the Stark width and shift as a function of the electron density is a really interesting subject, since it provides us with a powerful calibration tool with which it will possible to use these parameters to obtain values of electron densities.

This section contains an explanation of the methods used to calculate the Stark widths w_S and shifts d_S. Before proceeding with these methods, it is important to consider the factors that we should bear in mind when carrying out this kind of experiment. The most appropriate experimental conditions for this kind of experiment are those for which the spectral profiles fulfill these criteria:

1) **Significant Stark width**: since there are different mechanisms that produce the broadening of a spectral line (Stark and Doppler effect, apparatus broadening), it is very important to select some experimental conditions under which the broadening comes primarily from the Stark effect. In these circumstances, our measurements of the Stark parameters will have a higher accuracy.

2) **Low self-absorption**: as explained before, self-absorption tends to deform the profile of the spectral lines leading to a width of line higher than the real one. Therefore, it is important to look for a set of experimental conditions that minimize this effect in order to get accurate values of the Stark parameters.

2) **Well isolated lines**: this allows us to extract a reliable Stark component from the total width of the spectral line.

2) **Good signal-to-noise ratio**: so that it is possible to measure the total width of the spectral line precisely.

3.4.1 Determination of Stark widths and their uncertainties.

The experimental data treatment is explained in detail in Djurović et al. (2006). As explained before, the conditions of our experiment were defined to make sure that the Stark effect was the dominant broadening mechanism. Two other pressure broadening mechanisms, resonance and Van der Waals, are found to be negligible. Therefore, only Gaussian (coming from instrumental and Doppler) and Stark broadening were taken into account in the deconvolution procedure. The expression used to calculate the gaussian width is:

$$w_G = \sqrt{w_D^2 + w_{app}^2} \tag{3.54}$$

w_D and w_{app} being the Doppler and instrumental widths, respectively. Given that a Voigt profile is a non analytically solvable function, we have used an alternative deconvolution method proposed by Davis et al. (1963) to extract the Stark width w_S from the total width w of each line. The expression developed in our laboratory to obtain w_S is:

$$w_S = w(r_0 + r_1 z + r_2 z^2 + r_3 z^3 + r_4 z^4) \tag{3.55}$$

where z is defined as:

$$z = \frac{w_G}{w} \tag{3.56}$$

and $r_0 = 0.9999705$, $r_1 = 0.0029296$, $r_2 = -1.1026020$, $r_3 = 0.0701624$ and $r_4 = 0.0296077$.

Even if the Stark width of non-hydrogenic atoms is inversely dependent on the square root of the electron kinetic temperature, as explained in Chapter 1, the Stark width shows good linear behaviour when expressed as a function of the electron density N_e. Therefore, it is possible to fit the experimental Stark width data to the expression (3.57) :

$$w_S = a_w + b_w \ N_e \tag{3.57}$$

a_w and b_w being the fitting coefficients. Ideally, $a_w \simeq 0$, which means that the Stark width is zero for $N_e = 0$. Even if it is known that there is a functional dependency of w_S

on the temperature, it is not possible to appreciate any temperature dependency within the margin of accuracy, at least within the temperature and electron density working range. This is due to the fact that, even if the electron densities vary by a factor 10 in our experiment, the temperatures only vary by a factor 1.5. In order to compare our values with those from other authors, the w_S data are usually normalized to an appropriate value of the electron density.

The evaluation of the uncertainty associated with the calculated values of the Stark width, Δw_S is carried out by using the expression:

$$\Delta w_S = \sqrt{\sigma_{b_w}^2 + 0.25\ a_w^2 + \left(\frac{w_o^4}{b_w^2}\right)} \tag{3.58}$$

where σ_{b_w} represents the uncertainty associated with the coefficient b_w from the fitting in (3.57) and w_o has defined as:

$$w_o = \frac{w_{app}}{2} \tag{3.59}$$

w_{app} being the width due to the apparatus broadening. Equation (3.58) provides a value of the accuracy that coincides in most cases with the uncertainty that would be assigned by an experience experimentalist after analyzing all the particularities of a given spectral line.

3.4.2 Determination of the Stark shifts and their uncertainties.

Since we do not have an absolute position for the wavelength λ in our spectrometer, we are only able to measure relative Stark shifts. In order to carry out these measurements we used the method explained below (Aparicio et al., 1998):

1) **Plotting the centre of the line against the electron density**: since we already know the central position (channel) of the line under study from the spectra fitting, we can plot that position (y-axis) as a function of the electron density N_e, obtaining as a result a plot centre of the line against electron density.

2) **Calculating the shift (in channels)**: by performing a linear fit in the previous point cloud, it is possible to extrapolate the position of the line centre to zero electron

density. This value, expressed in channels, is then subtracted from the measured centre of the line at each instant, obtaining the Stark shift in channels.

3) **Converting the shift in channels into a shift in a wavelength scale**: each of the shifts expressed in channels are multiplied by the value of the linear inverse dispersion of our spectrometer at the wavelength assigned to the centre of that spectral line by the bibliography. We can now plot this shift in nanometres as a function of the electron density.

4) **Obtaining the Stark shift**: as happens with the Stark width, the Stark shift also shows good behaviour when linearly-fitted. Therefore, we can use the expression:

$$d_S = a_d + b_d \ N_e \tag{3.60}$$

where d_S is the Stark shift and $a_d = 0$ due to the procedure used and b_d are the two parameters of the linear fitting. We normally assume that there is no shift when the electron density is zero, so the y-intercept is normally zero too. Fig. 3.11 shows an example of this linear fit for two Ar II lines. In order to make the comparison with other authors easier, our tables normally include the d_S data for a given value of the electron density.
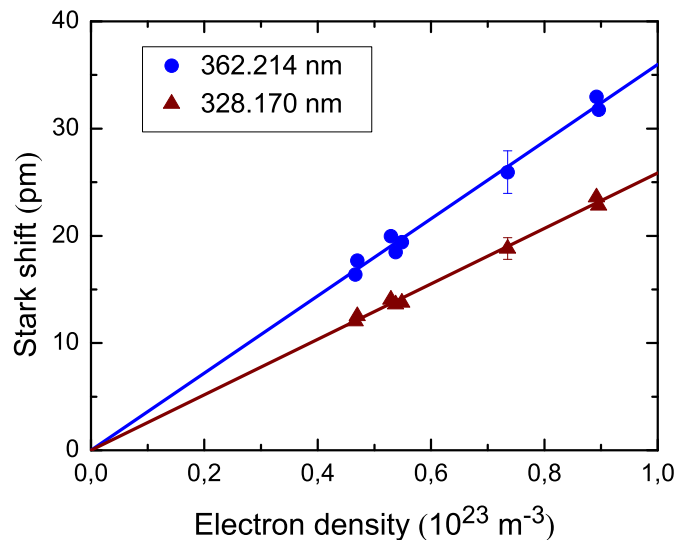
Figure 3.11: Example of shift versus electron density for two Ar II lines.

As happened with transition probabilities and Stark widths, an expression has been established in order to obtain an estimation of Stark shift uncertainty. The possible sources of error are combined giving as a result the expression:

$$\Delta d_S = \sqrt{\sigma_b^2 + 4\sigma_a^2 + \left(\frac{d_o^4}{b^2}\right)} \tag{3.61}$$

where σ_b and σ_a are the error in the slope's coefficient and that in the y-intercept respectively and where d_o is defined as:

$$d_o = \frac{w_{app}}{10} \tag{3.62}$$

w_{app} being the width due to the apparatus broadening. The coefficients chosen in (3.61) are once more the result of experience acquired after many ours analyzing a wide variety of different spectra.

Chapter 4

Measurement of Stark parameters in Ar II UV spectral lines.

"Experiment escorts us last-
His pungent company
Will not allow an Axiom
An Opportunity"

- Emily Dickinson -

Stark broadening data of spectral lines emitted by non-hydrogenic ionized atoms is of great interest within different fields of physics. The dependence of these data on electron density makes these parameters a very useful tool for the analysis of laboratory plasmas. Furthermore, the evaluation of the physical conditions in stellar atmospheres where argon is found requires knowledge of the Stark parameters of these ionic spectral lines, the broadening and asymmetry of which are also of use in the analysis of hydrodynamic models of the solar atmosphere.

A great number of experimental studies have been devoted to the measurement of Ar II Stark parameters. However, there is still a lot of missing data, particularly in the UV region. The goal of this work is to upgrade the Ar II atomic spectra database with new Stark width and shift values in the UV, opening new possibilities of laboratory and remote plasma diagnostics, electron density predictions and chemical abundance calculations. All

the references, as well as a detailed description of the latest developments in the field can be found in the accompanying article.

4.1 Experimental details.

A low-pressure pulsed arc with high-reproducibility features was used as a plasma source. As the experimental set-up has already been described in Chapter 2, only a brief summary of the measurement conditions will be included here. A more complete description of the experiment can be found in the accompanying article. The plasma was produced inside a cylindrical tube of Pyrex, 175 mm in length and 19 mm in internal diameter. Pure argon at a pressure of 500 Pa flowed continuously through the discharge tube at a rate of 1.0 sccm. The pressure of the argon was adjusted to obtain minimal self-absorption and maximum intensity.

Table 4.1: Experimental measurement conditions.

Lamp running conditions	
Ar pressure	500 Pa
Ar flow	1.0 sccm
Discharge voltage	7.7 kV
Optical parameters	
Spectroscopic channel pinholes	$\phi = 2.5$ mm (D1 and D2 in Fig. 2.5)
Width of the entrance slit	35 μm
Diffraction order	1
Acquisition parameters	
Camera	ICCD 4 Quick E S20
Measurement instants	40, 50, 60, 70, 100, 110, 120, 130, 180 μs
Exposure time	2.5-5 μs
Spectral interval	265-405 nm

A capacitor bank of 20 μF charged up to 7.7 kV was discharged through the lamp to create the plasma pulses. The emission of the plasma lasted for 400 μs. All the Ar II spectral lines were recorded in the first order of diffraction at nine different instants from 40 to 180 μs after the beginning of the discharge, with exposure times ranging between 2.5 and 5 μs. Ten spectra were recorded for each instant, three of them with the self-absorption control mirror and seven without it. A continuous current of several mA was

applied through the gas in the tube to ensure the plasma reproducibility. Table 4.1 shows the experimental conditions used in this experiment.
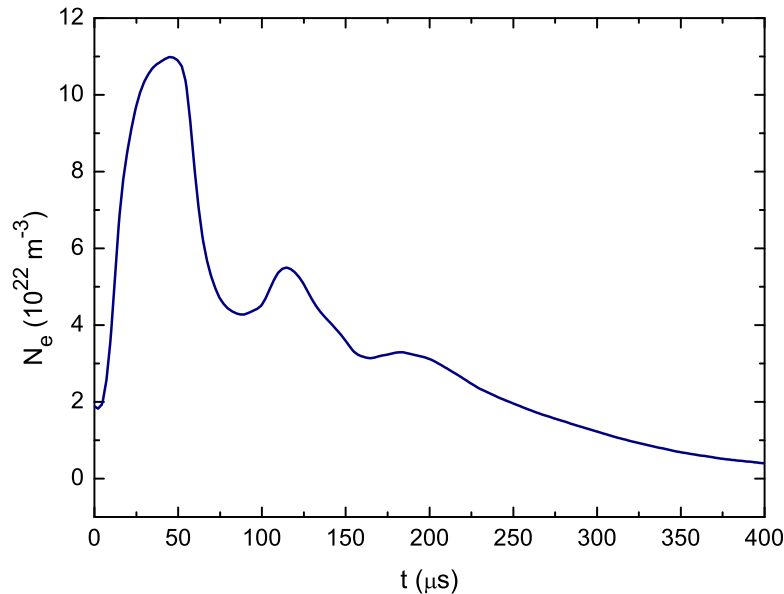
Figure 4.1: Temporal evolution of electron density in this experiment.

The electron temperature, in the range $16000 - 26000$ K with an estimated uncertainty of around 15%, was obtained from the Boltzmann-plots of a set of 13 Ar II lines belonging to the spectral interval $379 - 404$ nm and whose transition probabilities have uncertainties lower than 15%. The interval of the upper energy levels considered varies between 19.49 and 24.76 eV. The electron density, in the range of $(0.20 - 1.15) \times 10^{23}$ m^{-3} as shown in Fig. 4.1, was determined by a two-wavelength interferometric method. The experimental errors were estimated to be lower than 10%.

Under these experimental conditions, the Stark effect was the dominant broadening mechanism. In order to extract the Stark half-width from the total experimental linewidth, a standard deconvolution procedure was employed. As the resonance and Van der Waals broadening were found to be negligible, only Gaussian (instrumental+Doppler) and Stark broadening were taken into account in this deconvolution procedure.

4.2   Results and conclusions.

This work reports 126 Stark half-widths and 111 shifts of ultraviolet singly ionized argon lines belonging to 57 multiplets in the spectral interval ranging from 265 to 405 nm. From them, 53 half-widths and 44 shifts are new data presented in this paper for the first time. All the data has been normalized to an electron density of 10^{23} m^{-3} and an electron temperature of 22000 K, so that they can be compared with other measurements carried out in different plasma conditions. Special attention was paid to the experimental conditions, plasma diagnostics and experimental data treatment.

Our Stark parameters have been compared with the available experimental results from other authors, showing reasonable agreement within 30% in the majority of the cases. In addition, they have also been contrasted with theoretical values when possible. These analyses have allowed us to check the regular behaviour inside multiplets, supermultiplets and transition arrays in detail. The majority of the deviations have been explained by analysing the complex structure of the Ar II energy levels. All the measured Stark widths and shifts show a clear linear dependence on the electron density.

Stark parameter measurement of Ar II UV spectral lines

S. Djurović,[1]* M. T. Belmonte,[2] R. J. Peláez,[3] J. A. Aparicio[2]* and S. Mar[2]

[1]*Department of Physics, Faculty of Sciences, University of Novi Sad, Trg Dositeja Obradovića 4, 21000 Novi Sad, Serbia*
[2]*Departamento de Física Teórica Atómica y Óptica, Facultad de Ciencias, Universidad de Valladolid, E-47071 Valladolid, Spain*
[3]*Laser Processing Group, Instituto de Óptica, CSIC, C/ Serrano 121, E-28006 Madrid, Spain*

ABSTRACT

In this paper, we present results of experimental determination of Stark parameters of Ar II spectral lines. We report 126 half-width and 111 shift results, 53 half-widths and 44 shifts of which are presented here for the first time. The obtained data may be of astrophysical interest. The results were compared with available experimental results of other authors and with calculated ones in the cases where it was possible. A low-pressure pulsed arc, filled with pure argon, was used as a plasma source. All measurements were done under electron density which ranges from 0.20×10^{23} to 1.15×10^{23} m^{-3} and electron temperature from 16 000 to 26 000 K.

Key words: atomic data – line: profiles – plasmas.

1 INTRODUCTION

Stark broadening data of non-hydrogenic lines emitted by ionized atoms are always of interest in laboratory and astrophysical physics research. The relationship between these data and electron density is very useful in laboratory plasma diagnostics. The evaluation of the physical conditions in stellar atmospheres and abundance determinations requires some knowledge of the broadening parameters for a large number of ionic spectral lines, also of Ar II lines. Broadening and asymmetries of the spectral lines are used for the analysis of the hydrodynamic models of the solar atmosphere (Asplund et al. 2009). The optical spectra of early B-type stars contain a number of unblended Ar II lines (Keenan et al. 1990; Lanz et al. 2008; Fossati et al. 2009). Lanz et al. also analysed Ar II lines in the blue spectrum of B main-sequence stars in the Orion association. They also derived the mean argon abundance by using the observed Ar II spectra in star HD 35299. Singly ionized argon lines were also observed in the Orion nebula (Esteban et al. 2004; Lanz et al. 2008). Furthermore, Peimbert (2003) observed ultraviolet Ar II lines in the 30 Doradus nebula.

In this paper, we present measured Stark parameters data for 126 Ar II spectral lines in the spectral region between 265 and 405 nm. Measurements were performed by using a very well-characterized low-pressure pulsed plasma source. Electron density, determined by the two-wavelength interferometric method, was in the range of 0.20–1.15 × 10^{23} m^{-3}. Electron temperature, obtained by the Boltzmann plot technique, was between 16 000 and 26 000 K.

A number of experimental studies have been devoted to Ar II spectral line Stark parameter measurement (Jalufka, Oertel & Ofelt 1966; Roberts 1966, 1968; Blandin et al. 1968; Chapelle et al. 1968

a,b; Konjević et al. 1970; Morris & Morris 1970; Labat et al. 1974; Behinger & Thoma 1978; Nick & Helbig 1986; Pitman & Konjević 1986; Djeniže et al. 1989; Dzierzega & Musiol 1994; Pellerin, Musiol & Chapelle 1997; Aparicio et al. 1998a; Iglesias et al. 2006). However, there are still a lot of data missing, particularly in the UV region. We report 126 half-width and 111 shift results, 53 half-widths and 44 shifts of which have not been previously measured. The new data belong mostly to the 4p–4d and 3d–4f transition arrays. The obtained Stark parameters were compared with available experimental results of other authors, those mentioned above, and with calculated ones in the cases where it was possible (Griem 1974; Dimitrijević & Konjević 1980, 1987; Dimitrijević & Kršljanin 1986). The analysis of the measured Stark parameters has allowed us to check regular behaviours inside multiplets, supermultiplets and transition arrays in detail. Most of the existing irregularities have been explained from the study of the complex structure of energy levels of the singly ionized argon.

2 EXPERIMENT, PLASMA DIAGNOSTICS AND DATA TREATMENT

The experimental arrangement is described in detail in our previous works (Aparicio et al. 1998a; Djurović et al. 2006). Here, for completeness, only a short description of experiment, plasma diagnostics and data treatment will be given.

Measurements were performed in a low-pressure pulsed arc plasma. Pulses were created by discharging a capacitor bank, charged up to 7.7 kV, through a cylindrical Pyrex tube, 175 mm long and 19 mm in internal diameter. Pure argon was continuously flowing through the tube at a pressure of 0.5 kPa. Argon pressure was adjusted in order to get sufficiently high spectral line intensities and, at the same time, achieve minimal or null self-absorption effect for the lines in consideration. Self-absorption check was

*E-mail: djurovic@uns.ac.rs (SD); apa@opt.uva.es (JAA)
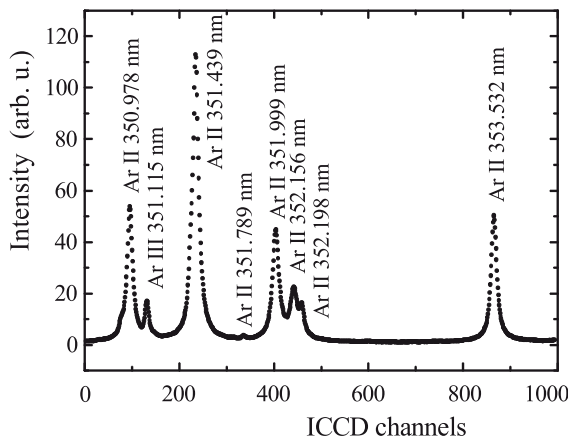
Figure 1. Example of a part of the spectrum.

performed by means of a mirror placed behind the discharge tube. The spectra were recorded using a spectrometer equipped with an intensified charge-coupled device (ICCD). All spectra were registered in first order of diffraction at 10 different instants of the plasma life. A part of the recorded argon spectrum is shown in Fig. 1. This illustrates the quality of the performed measurements. It is important to remark that two consecutive spectra registered in identical experimental conditions differ in less than 3 per cent. The spectrometer's instrumental function was estimated by introducing a laser beam (632.8 nm) on to the entrance slit. A high-performance HeNe laser, typically employed for interferometry purposes, was used. Its bandwidth is lower than 1.4 pm. The convolved effect of its bandwidth, the monochromator's entrance slit width (35 μm), the grating diffraction and other diffusion effects into the ICCD camera yielded a measured instrumental broadening of approximately 7 pm (3.0 ICCD channels at an inverse linear dispersion of 2.3 pm channel^{-1} for 632.8 nm). A detailed analysis of all these effects is extensively explained in Peláez et al. (2012, 2013). An incandescent calibrated lamp and a deuterium lamp were used to obtain the spectrometer's transmittance.

A two-wavelength interferometric method was used for electron density N_e determination. The electron density was in the range 0.20–1.15×10^{23} m^{-3} with an estimated experimental uncertainty around 10 per cent. Electron temperature T_e was determined by a Boltzmann plot of 13 Ar II lines. All of them belong to the spectral interval 379–404 nm, and their transition probabilities have uncertainties lower than 15 per cent (Aparicio, Gigosos & Mar 1997). The interval of the considered upper energy levels is 19.49–24.76 eV. The temperature in this experiment is in the range 16 000–26 000 K, while its estimated uncertainty is about 15 per cent.

The experimental data treatment is explained in detail in Djurović et al. (2006). A fitting procedure was applied to the experimentally obtained spectra in order to determine the total half-widths of the investigated spectral lines. In order to extract the Stark half-width from the total experimental linewidth, a standard deconvolution procedure was employed (Davies & Vaughan 1963). Under these experimental conditions, the Stark effect was the dominant broadening mechanism. Two other pressure broadening mechanisms, resonance and van der Waals, were found to be negligible. Therefore, only Gaussian (instrumental + Doppler) and Stark broadening were taken into account in the deconvolution procedure.

Stark shifts were obtained as follows (Aparicio et al. 1998b). First, it is assumed that there is no shift when the electron density

is zero. Since the exact position of an observed spectral line on the detector at zero electron density is unknown, this position was obtained by extrapolating to null electron density the linear fit of the line centre positions versus N_e plot. Once this value is subtracted from the measured line centres, the desired Stark shift values in picometres are obtained by multiplying the calculated differences by the linear inverse dispersion.

3 RESULTS AND DISCUSSION

Measured Ar II Stark parameters are shown in Table 1. In the first four columns multiplet number, configurations, terms and wavelengths of the lines are given. The multiplets are arranged in the same way as it was done in NIST Atomic Spectra Database. The fifth and sixth columns contain measured Stark half-widths w_m in picometres and in angular frequency units, respectively, those obtained in this work (TW) and the values measured by other authors (Jalufka et al. 1966; Roberts 1966, 1968; Chapelle et al. 1968a,b; Konjević et al. 1970; Labat et al. 1974; Behinger & Thoma 1978; Nick & Helbig 1986; Pittman & Konjević 1986; Djeniže et al. 1989; Dzierzega & Musiol 1994; Pellerin et al. 1997; Aparicio et al. 1998a; Iglesias et al. 2006). Reference numbers are indicated in the next column. The next three columns contain comparison with the theoretical half-width data. The experimental half-widths were compared with calculated ones by using the modified semi-empirical (MSE) formula from Dimitrijević & Konjević (1980) w_{MSE} and the simplified modified semi-empirical (SMSE) formula from Dimitrijević & Konjević (1987) w_{SMSE}. An additional comparison was made with the theoretical data tabulated in Griem (1974) w_G. The last six columns contain the shift results d_m, which are organized in the same way as the half-width data. In this case, only a smaller quantity of experimental values of other authors was available for comparison (Blandin et al. 1968; Morris & Morris 1970; Labat et al. 1974; Djeniže et al. 1989; Dzierzega & Musiol 1994; Aparicio et al. 1998a). For the calculation of d_{MSE} data, we used the formula from Dimitrijević & Kršljanin (1986).

Both w_m and d_m experimental results in Table 1 are followed by the letter A, B or C, which correspond to estimated accuracy: A means errors up to 15 per cent, B errors between 15 and 30 per cent and C means errors between 30 and 50 per cent. This classification was done in the same way as in the critical review paper of Konjević & Wiese (1976) and later critical reviews. Possible errors in the line shape recording, transmittance correction, line overlapping, as well as fitting and deconvolution procedure were all included in our data accuracy estimation. For instance, a simple analysis of the relevance of the Gaussian component of the linewidth on the final obtained Lorentzian width reveals that, in the most unfavourable situation (e.g. multiplet 1), the average Gaussian to Lorentzian width ratio is around 1.0. This is the case of less than 15 per cent of measured profiles. This ratio reduces below 0.5 for Lorentzian widths greater than 30 pm, which represent more than 85 per cent of measured Ar II lines. In the scarce cases where these ratios were greater than 1.0, the obtained Stark half-widths were rejected for further considerations. This analysis has been incorporated in the final estimated accuracy.

We provided results of 126 spectral lines belonging to 57 multiplets in the wavelength region of 265–405 nm. Among them, there are 53 half-width and 44 shift new data which are presented in this paper for the first time. Since different authors performed their measurements at different plasma conditions, all data were normalized for comparison to an electron density of 10^{23} m^{-3} and electron temperature of 22 000 K by following the $T_e^{-1/2}$ dependence.

Table 1. Experimental Stark half-widths w_m and shifts d_m of Ar II spectral lines (TW). Estimated accuracy of the experimental data is denoted by letters A (<±15 per cent), B (<±30 per cent) and C (<±50 per cent). For the comparison, available experimental results of other authors [1: Jalufka et al. (1966); 2: Roberts (1966); 3: Chapelle et al. (1968a); 4: Blandin et al. (1968); 5: Roberts (1968); 6: Chapelle et al. (1968b); 7: Morris & Morris (1970); 8: Konjević et al. (1970); 9: Labat et al. (1974); 10: Behinger & Thoma (1978); 11: Nick & Helbig (1986); 12: Pittman & Konjević (1986); 13: Djeniže et al. (1989); 14: Dzierzega & Musiol (1994); 15: Pellerin et al. (1997); 16: Aparicio et al. (1998a); 17: Iglesias et al. (2006) are given. The experimental Stark parameters are compared with theoretical data (Griem 1974; Dimitrijević & Konjević, MSE 1980; Dimitrijević & Kršljanin, MSE 1986; Dimitrijević & Konjević, SMSE 1987) as well. All the data are normalized to an electron density of 10^{23} m^{-3} and electron temperature of 22 000 K.

No	Transition	Term	Wavelength (nm)	w_m (pm)	w_m (10^{11} s^{-1})	Ref.	w_m/w_{MSE}	w_m/w_{SMSE}	w_m/w_G	d_m (pm)	d_m (10^{10} s^{-1})	Ref.	d_m/d_{MSE}	d_m/d_{SMSE}	d_m/d_G
1	$(^3P)3d$–$(^3P)4p$	$^4D_{3/2}$–$^4D^o_{1/2}$	387.526	17.62 B	2.210	TW		1.35	0.95						
										2.65	3.324	7			
				19.20	2.409	15									
				27.81	3.489	16				2.12	2.660	16			
		$^4D_{3/2}$–$^4D^o_{3/2}$	391.477	18.39 B	2.261	TW		1.41	0.97	$d < 2.5$		TW			
										3.18	3.909	7			
				20.70	2.545	15									
				21.14	2.599	16				<2.0		16			
		$^4D_{7/2}$–$^4D^o_{5/2}$	394.427	23.25 A	2.816	TW		1.83	1.21	$d < 2.5$		TW			
										4.77	5.776	7			
				22.00	2.664	15									
				24.27	2.939	16				4.55	5.510	16			
		$^4D_{5/2}$–$^4D^o_{5/2}$	396.836	20.36 B	2.436	TW		1.82	1.05	$d < 2.5$		TW			
										7.84	9.379	4			
										4.24	5.073	7			
				23.60	2.823	15									
				29.73	3.557	16				<2.0		16			
				24.85	2.973	17									
				19.42	2.323	17									
				24.85	2.973	17									
		$^4D_{7/2}$–$^4D^o_{7/2}$	401.386	23.34 B	2.729	TW		1.83	1.17	$d < 2.5$		TW			
				26.40	3.087	3									
										7.76	9.074	4			
				37.51	4.386	5									
										2.33	2.725	7			
				20.78	2.430	9				7.79	9.109	9			
				15.64	1.829	11									
				21.00	2.456	13				7.17	8.384	13			
				16.18	1.892	14				3.12	3.648	14			
				14.27	1.669	14				2.95	3.450	14			
				22.54	2.636	14									
				17.91	2.094	14									
				15.26	1.785	14				3.20	3.742	14			
				25.20	2.947	15									
				21.74	2.542	16				1.92	2.245	16			
				24.85	2.906	17									
				31.07	3.633	17									
		$^4D_{5/2}$–$^4D^o_{7/2}$	403.880	24.05 C	2.778	TW		1.86	1.19	3.12 B	3.604	TW		1.01	0.43
										4.24	4.897	7			
				24.10	2.784	15									
				30.24	3.493	16				<6.0		16			
2		$^4D_{7/2}$–$^2D^o_{5/2}$	378.638	23.49 A	3.087	TW		1.85							
				20.30	2.668	15									
				23.97	3.150	16				3.44	4.521	16			
		$^4D_{5/2}$–$^2D^o_{5/2}$	380.857	22.53 C	2.926	TW		1.76		4.80 B	6.234	TW		1.71	
				18.70	2.429	15									
3		$^4D_{5/2}$–$^4S^o_{3/2}$	349.948	29.03 C	4.466	TW		2.27							
										5.30	8.154	7			
4	$(^3P)4s$–$(^3P)4p$	$^4P_{5/2}$–$^2D^o_{3/2}$	397.476	22.91 C	2.732	TW	1.09	0.54		−6.89 C	−8.216	TW	1.08	1.51	
5		$^4P_{5/2}$–$^2P^o_{3/2}$	384.540	21.53 B	2.743	TW	1.13	0.53		−5.95 C	−7.581	TW	0.94	1.41	
		$^4P_{3/2}$–$^2P^o_{3/2}$	397.448	22.42 B	2.674	TW	1.09	0.51		−6.24 C	7.442	TW	0.91	1.36	
6		$^4P_{5/2}$–$^4S^o_{3/2}$	372.931	16.62 C	2.251	TW	0.87	0.43		−6.96 B	−0.9428	TW	1.39	1.78	
				99.50	13.479	1									
										−3.18	−4.308	7			
				16.16	2.189	8									
				20.78	2.815	8									
				22.52	3.051	9				6.93	9.388	9			

Table 1 – *continued*

No	Transition	Term	Wavelength (nm)	w_m (pm)	w_m (10^{11} s^{-1})	Ref.	w_m/w_{MSE}	w_m/w_{SMSE}	w_m/w_G	d_m (pm)	d_m (10^{10} s^{-1})	Ref.	d_m/d_{MSE}	d_m/d_{SMSE}	d_m/d_G
				13.20	1.788	14									
				12.53	1.697	14									
				16.70	2.262	14									
				13.29	1.800	14									
				12.69	1.719	14									
				22.90	3.102	15									
										<−2.0		16			
		$^4P_{3/2}-^4S^o_{3/2}$	385.058	17.12 C	2.175	TW	0.83	0.41		−5.86 C	−7.446	TW	1.07	1.37	
				21.78	2.767	3									
										−0.08	−0.102	4			
				37.99	4.827	5									
				19.99	2.540	6									
										−4.77	−6.061	7			
				16.84	2.140	14				−1.63	−2.071	14			
				13.26	1.685	14				−1.86	−2.363	14			
				18.72	2.379	14									
				14.13	1.795	14									
				15.31	1.945	14									
				23.50	2.986	15									
				25.99	3.302	16				−1.62	−2.058	16			
		$^4P_{1/2}-^4S^o_{3/2}$	392.862	17.82 C	2.175	TW	0.83	0.41		−6.79 B	−8.288	TW	1.19	1.51	
				21.78	2.659	3									
										−0.08	0.098	4			
				19.99	2.440	6									
				12.51	1.527	11									
				21.00	2.563	13									
				17.46	2.131	14									
				12.86	1.570	14									
				18.11	2.211	14									
				17.07	2.084	14									
				23.30	2.844	15									
				33.98	4.148	16				<2.0		16			
7	(³P)4s–(¹D)4p	$^2P_{3/2}-^2P^o_{1/2}$	289.161	54.24 A	12.221	TW				22.48 A	50.065	TW			
				31.08	7.003	10									
				23.60	5.318	15									
		$^2P_{3/2}-^2P^o_{3/2}$	294.289	33.48 B	7.283	TW				3.97 C	8.636	TW			
										11.12	24.190	7			
				19.26	4.190	10									
				21.25	4.623	13				−2.29	−4.982	13			
				20.20	4.394	15									
		$^2P_{1/2}-^2P^o_{1/2}$	297.905	59.17 A	12.561	TW				22.75 A	48.296	TW			
				28.79	6.112	10									
				24.03	5.101	15									
		$^2P_{1/2}-^2P^o_{3/2}$	303.351	35.18 A	7.203	TW				5.59 B	11.445	TW			
				21.17	4.334	10									
				19.77	4.048	13									
				21.20	4.340	15									
8		$^2P_{3/2}-^2D^o_{5/2}$	284.413	16.73 C	3.897	TW	1.49			−4.70 C	−10.947	TW	1.53		
										−2.12	−4.938	7			
				15.94	3.713	13				−2.29	−5.334	13			
		$^2P_{1/2}-^2D^o_{3/2}$	293.259	20.67 C	4.528	TW	1.71			−7.79 B	−17.065	TW	2.35		
9	(³P)3d–(¹D)4p	$^2P_{1/2}-^2P^o_{3/2}$	363.481	49.09 C	7.000	TW				22.15 C	3.159	TW			
10		$^2P_{3/2}-^2D^o_{5/2}$	360.588	25.50 B	3.695	TW				d < 2.5		TW			
										3.71	5.376	7			
11	(¹D)4s–(¹D)4p	$^2D_{3/2}-^2D^o_{5/2}$	403.546	31.73 B	3.671	TW	1.46			−4.75 B	−5.495	TW	0.80		
				29.10	3.367	15									
				37.11	4.293	16				<−5.0		16			
		$^2D_{3/2}-^2D^o_{3/2}$	404.289	29.27 C	3.374	TW	1.40			−4.29 B	−4.945	TW	0.72		
				19.05	2.196	9									
				27.70	3.193	15									
				41.87	4.826	16				−6.07	−6.997	16			
12	(³P)4p–(³P)5s	$^4P^o_{3/2}-^4P_{1/2}$	362.214	68.40 A	9.822	TW	1.22	0.69	1.15	35.99 A	51.681	TW	1.77	1.74	1.15
										31.25	44.875	7			
				66.20	93.506	15									

Table 1 – *continued*

No	Transition	Term	Wavelength (nm)	w_m (pm)	w_m (10^{11} s^{-1})	Ref.	w_m/w_{MSE}	w_m/w_{SMSE}	w_m/w_G	d_m (pm)	d_m (10^{10} s^{-1})	Ref.	d_m/d_{MSE}	d_m/d_{SMSE}	d_m/d_G
				81.11	11.647	16				30.14	43.281	16			
		$^4P^o_{1/2}$–$^4P_{1/2}$	366.960	62.74 B	8.778	TW	1.09	0.62	1.03	28.99 B	40.559	TW	1.39	1.36	0.90
										40.26	56.327	7			
		$^4P^o_{5/2}$–$^4P_{3/2}$	367.827	67.08 B	9.341	TW	1.24	0.68	1.09	27.04 B	37.653	TW	1.39	1.31	0.84
										33.37	46.468	7			
		$^4P^o_{3/2}$–$^4P_{3/2}$	372.043	63.76 C	8.678	TW	1.15	0.63	1.02	25.68 A	34.953	TW	1.29	1.22	0.78
										31.78	43.256	7			
				61.60	8.384	15									
				85.15	11.590	16				25.18	34.273	16			
		$^4P^o_{5/2}$–$^4P_{5/2}$	376.527	62.63 B	8.323	TW	1.19	0.62	0.98	25.26 B	33.568	TW	1.36	1.21	0.75
				75.04	9.972	16				18.41	24.465	16			
		$^4P^o_{1/2}$–$^4P_{3/2}$	377.052	68.64 B	9.096	TW	1.20	0.66	1.07	26.42 A	35.012	TW	1.29	1.22	0.78
										26.49	35.104	7			
										30.76	40.763	13			
				77.57	10.280	16				28.82	38.192	16			
		$^4P^o_{3/2}$–$^4P_{5/2}$	380.946	68.70 A	8.919	TW	1.27	0.66	1.04	35.10 A	45.568	TW	1.84	1.64	1.01
										30.19	39.194	7			
				74.60	9.685	15									
				76.15	9.886	16				28.22	36.636	16			
13		$^4P^o_{1/2}$–$^2P_{3/2}$	365.089	69.48 A	9.821	TW	1.34	0.68		39.17 A	55.365	TW	2.15	1.85	
										33.90	47.916	7			
14	(^{3}P)4p–(^{3}P)4d	$^4P^o_{5/2}$–$^4D_{3/2}$	345.409	45.90 B	7.248	TW		0.97		18.23 A	28.787	TW			
		$^4P^o_{5/2}$–$^4D_{5/2}$	347.675	46.18 C	7.198	TW		0.98		17.65 A	27.509	TW			
				38.54	6.007	13				12.60	19.638	13			
				35.40	5.517	15									
		$^4P^o_{1/2}$–$^4D_{1/2}$	350.978	46.82 A	7.161	TW		0.94		13.40 A	20.494	TW			
										20.66	31.597	7			
				38.00	5.812	15									
		$^4P^o_{3/2}$–$^4D_{5/2}$	351.439	49.93 B	7.616	TW		1.03		14.26 A	21.752	TW			
										22.78	34.748	7			
				46.00	7.017	15									
		$^4P^o_{1/2}$–$^4D_{3/2}$	353.532	48.52 A	7.314	TW		0.97		17.87 A	26.937	TW			
										23.84	35.353	7			
				48.52	7.314	15									
15	(^{3}P)4p–(^{1}D)3d	$^4P^o_{3/2}$–$^2S_{1/2}$	347.823	32.35 B	5.038	TW		1.37		6.53 B	10.169	TW			
		$^4P^o_{1/2}$–$^2S_{1/2}$	352.198	37.44 B	5.686	TW		1.54							
16	(^{3}P)4p–(^{3}P)4d	$^4P^o_{5/2}$–$^4F_{3/2}$	319.423	48.27 A	8.913	TW		1.02		18.06	33.348	TW			
		$^4P^o_{5/2}$–$^4F_{5/2}$	322.163	39.54 C	7.177	TW		0.84		13.97 C	25.359	TW			
		$^4P^o_{3/2}$–$^4F_{3/2}$	322.597	42.51 B	7.696	TW		0.88		16.57 A	29.997	TW			
		$^4P^o_{1/2}$–$^4F_{3/2}$	326.357	48.80 A	8.632	TW		0.98		17.35 A	30.690	TW			
17		$^4P^o_{5/2}$–$^4P_{5/2}$	313.902	45.27 B	8.656	TW		0.96	1.04	15.85 A	30.306	TW			0.69
				33.94	6.489	10									
				35.60	6.807	15									
		$^4P^o_{3/2}$–$^4P_{5/2}$	316.967	44.25 B	8.298	TW		0.92	0.99	16.80 B	31.504	TW			0.72
				33.18	6.222	10									
				41.01	7.690	13				13.28	24.903	13			
				35.60	6.676	15									
		$^4P^o_{5/2}$–$^4P_{3/2}$	318.104	53.21 A	9.907	TW		1.13	1.18	18.78 A	34.965	TW			0.79
				33.37	6.213	10									
				35.00	6.516	15									
		$^4P^o_{3/2}$–$^4P_{3/2}$	321.252	48.91 A	8.929	TW		1.01	1.07	16.55 A	30.213	TW			0.69
				34.90	6.371	10									
				36.60	6.681	15									
		$^4P^o_{3/2}$–$^4P_{1/2}$	324.369	47.32 B	8.473	TW		0.98	1.02	18.37 A	32.894	TW			0.75
				35.09	6.283	10									
				36.80	6.589	15									
		$^4P^o_{1/2}$–$^4P_{3/2}$	324.980	48.54 B	8.659	TW		0.98	1.04	18.18 A	32.431	TW			0.74
				34.52	6.158	10									
				34.52	6.158	13									
				41.01	7.316	13									
				36.60	6.529	15									
		$^4P^o_{1/2}$–$^4P_{1/2}$	328.170	51.30 A	8.974	TW		1.03	1.08	25.85 A	45.221	TW			1.03
				41.80	7.312	15									

Table 1 – *continued*

No	Transition	Term	Wavelength (nm)	w_m (pm)	w_m (10^{11} s^{-1})	Ref.	w_m/w_{MSE}	w_m/w_{SMSE}	w_m/w_G	d_m (pm)	d_m (10^{10} s^{-1})	Ref.	d_m/d_{MSE}	d_m/d_{SMSE}	d_m/d_G
18	(³P)4p–(³P)5s	⁴D°$_{3/2}$–⁴P$_{1/2}$	403.381	89.75 B	10.392	TW	1.40	0.72		33.42 A	38.695	TW	1.53	1.31	
										36.02	41.706	7			
				83.00	9.610	15									
				89.40	10.351	16				31.96	37.005	16			
19		⁴D°$_{3/2}$–²P$_{3/2}$	401.121	82.16 B	9.620	TW	1.29	0.66		35.99 C	42.142	TW	1.65	1.41	
				91.52	10.716	16				61.18	71.637	16			
20	(³P)4p–(³P)4d	⁴D°$_{7/2}$–⁴D$_{5/2}$	376.350	55.23 A	7.346	TW		0.97	1.05	16.40 B	21.814	TW			0.59
										25.43	33.825	7			
				56.84	7.561	16				16.59	22.067	16			
		⁴D°$_{7/2}$–⁴D$_{7/2}$	378.084	51.12 B	6.737	TW		0.89	0.96	17.80 A	23.460	TW			0.63
										23.84	31.420	7			
				50.40	6.643	13				9.51	12.534	13			
				57.70	7.605	15									
				76.25	10.050	16				19.01	25.054	16			
		⁴D°$_{5/2}$–⁴D$_{3/2}$	379.938	54.97 A	7.174	TW		0.93	1.02	21.51 A	28.074	TW			0.76
										19.60	25.581	7			
				48.50	6.330	15									
				57.54	7.510	16				20.93	27.317	16			
		⁴D°$_{5/2}$–⁴D$_{5/2}$	382.681	53.78 A	6.919	TW		0.90	0.99	20.13 A	25.897	TW			0.70
										20.66	26.579	7			
				67.70	8.710	15									
				65.03	8.366	16				19.01	24.456	16			
		⁴D°$_{3/2}$–⁴D$_{1/2}$	384.152	48.23 A	6.157	TW		0.78	0.88	20.09 B	25.648	TW			0.57
										17.48	22.316	7			
				44.40	5.668	15									
				48.64	6.210	16				20.12	25.686	16			
		⁴D°$_{5/2}$–⁴D$_{7/2}$	384.473	59.14 B	7.538	TW		0.99	1.07	20.55 B	26.192	TW			0.71
				20.00	2.549	15									
		⁴D°$_{1/2}$–⁴D$_{1/2}$	388.033	50.36 B	6.301	TW		0.79	0.90	28.95 B	36.224	TW			0.98
										18.01	22.535	7			
				54.10	6.769	16				11.12	13.914	16			
		⁴D°$_{3/2}$–⁴D$_{5/2}$	390.063	55.47 B	6.869	TW		0.89	0.98	21.29 B	26.363	TW			0.71
										23.84	29.520	7			
				52.84	6.543	16				31.05	38.448	16			
		⁴D°$_{1/2}$–⁴D$_{3/2}$	391.158	51.42 A	6.332	TW		0.81	0.90	24.07 A	29.638	TW			0.80
										23.31	28.702	7			
				48.34	5.952	16				24.88	30.636	16			
21	(³P)4p–(¹D)3d	⁴D°$_{3/2}$–²S$_{1/2}$	385.614	32.77 C	4.152	TW		1.05		4.06 C	5.144	TW			
22	(³P)4p–(³P)4d	⁴D°$_{5/2}$–⁴F$_{5/2}$	351.999	55.67 B	8.465	TW		0.96		19.59 A	29.787	TW			
		⁴D°$_{3/2}$–⁴F$_{3/2}$	354.851	54.27 C	8.120	TW		0.90		19.28 B	28.847	TW			
										26.49	39.634	7			
23		⁴D°$_{7/2}$–⁴P$_{5/2}$	337.091	54.76 A	9.079	TW		0.98		18.99 A	31.485	TW			
										21.72	36.012	7			
		⁴D°$_{5/2}$–⁴P$_{5/2}$	342.161	58.28 A	9.379	TW		1.01		21.30 A	34.277	TW			
										23.84	38.364	7			
24		⁴D°$_{3/2}$–²F$_{5/2}$	339.790	60.57 A	9.884	TW		1.01		21.21 A	34.610	TW			
										26.49	43.226	7			
		⁴D°$_{5/2}$–²F$_{7/2}$	343.042	63.28 A	10.131	TW		1.09		21.14 A	33.845	TW			
										23.31	37.319	7			
25		⁴D°$_{5/2}$–²D$_{5/2}$	286.584	69.64 A	15.975	TW				|d| < 2.5		TW			
26		²D°$_{5/2}$–⁴D$_{3/2}$	395.838	62.43 A	7.507	TW		0.95		17.52 A	21.066	TW			
				12.00	1.443	15									
		²D°$_{5/2}$–⁴D$_{5/2}$	398.816	59.38 B	7.034	TW		0.90		22.25 B	26.355	TW			
										21.19	25.100	7			
				58.00	6.870	15									
				68.97	8.170	16				34.49	40.854	16			
		²D°$_{3/2}$–⁴D$_{1/2}$	403.138	57.66 C	6.684	TW		0.83		21.28 B	24.669	TW			
27	(³P)4p–(¹D)3d	²D°$_{3/2}$–²S$_{1/2}$	404.748	37.93 C	4.362	TW		1.06							
28	(³P)4p–(³P)4d	²D°$_{5/2}$–²F$_{5/2}$	346.413	64.07 B	10.059	TW		1.02	1.05	26.04 A	40.882	TW			0.83
										26.49	41.589	7			
				70.57	11.079	12									
				62.01	9.735	13				22.24	34.916	13			

Table 1 – *continued*

No	Transition	Term	Wavelength (nm)	w_m (pm)	w_m (10^{11} s^{-1})	Ref.	w_m/w_{MSE}	w_m/w_{SMSE}	w_m/w_G	d_m (pm)	d_m (10^{10} s^{-1})	Ref.	d_m/d_{MSE}	d_m/d_{SMSE}	d_m/d_G
				58.50	9.184	15									
		$^2D^o_{3/2}$–$^2F_{5/2}$	354.560	66.67 C	9.992	TW		1.00	1.04	25.08 B	37.586	TW			0.76
29		$^2D^o_{3/2}$–$^2P_{3/2}$	320.432	104.18 A	19.115	TW				17.94 A	32.918	TW			
		$^2D^o_{3/2}$–$^2P_{1/2}$	327.332	90.79 A	15.964	TW				28.50 A	50.113	TW			
				88.78	15.611	12									
				78.00	13.715	15									
30		$^2D^o_{5/2}$–$^2D_{5/2}$	295.539	79.10 A	17.062	TW				3.02 C	6.514	TW			
				57.78	12.463	10									
				102.44	22.096	12									
				69.60	15.013	15									
		$^2D^o_{3/2}$–$^2D_{5/2}$	301.448	83.62 A	17.337	TW									
				66.55	13.798	10									
				69.80	14.471	15									
31		$^2P^o_{3/2}$–$^2F_{5/2}$	365.528	67.72 C	9.549	TW		0.95		22.06 B	31.106	TW			
				71.71	10.112	12									
				63.00	8.883	15									
				86.47	12.193	16				17.60	24.817	16			
32		$^2P^o_{1/2}$–$^2P_{3/2}$	323.681	93.27 A	16.772	TW		0.78		18.88 A	33.951	TW			0.38
				72.08	12.962	10									
				75.60	13.595	15									
		$^2P^o_{1/2}$–$^2P_{1/2}$	330.723	93.07 A	16.031	TW		0.75		35.02 A	60.321	TW			0.67
										35.49	61.131	7			
				73.23	12.614	10									
				95.61	16.469	12									
				81.90	14.107	13				19.02	32.761	13			
		$^2P^o_{3/2}$–$^2P_{1/2}$	336.658	94.78 A	15.755	TW		0.74		27.60 A	45.879	TW			0.51
										27.54	45.779	7			
33		$^2P^o_{1/2}$–$^2D_{3/2}$	302.891	77.92 B	16.001	TW				$|d|<2.5$		TW			
		$^2P^o_{3/2}$–$^2D_{5/2}$	309.340	88.77 A	17.477	TW				$|d|<2.5$		TW			
				111.54	21.960	12									
				69.70	13.723	15									
34	$(^3P)4p$–$(^1D)5s$	$^2P^o_{1/2}$–$^2D_{3/2}$	276.465	34.37 B	8.472	TW	1.18	0.59		13.79 B	33.991	TW	1.29	1.18	
35	$(^3P)4p$–$(^3P)4d$	$^4S^o_{3/2}$–$^4F_{3/2}$	395.273	70.09 A	8.452	TW		0.90		24.73 A	29.820	TW			
				58.90	7.102	15									
				70.59	8.512	16				27.91	33.655	16			
36		$^4S^o_{3/2}$–$^4P_{5/2}$	386.853	69.45 B	8.743	TW		0.90	1.04	36.45 B	45.887	TW			1.08
										31.78	40.008	7			
				71.28	8.973	13				39.03	49.135	13			
				78.70	9.907	15									
				73.42	9.243	16				30.54	38.447	16			
		$^4S^o_{3/2}$–$^4P_{3/2}$	393.255	72.00 B	8.771	TW		0.92	1.04	27.34 A	33.307	TW			0.78
										29.66	36.133	7			
				80.40	9.795	15									
				86.67	10.559	16				26.09	31.784	16			
37		$^2S^o_{1/2}$–$^2D_{3/2}$	316.137	74.66 B	14.074	TW				5.58 C	10.519	TW			
38	$(^1D)3d$–$(^3P_2)4f$	$^2F_{5/2}$–$^2[3]^o_{7/2}$	316.529	47.22 B	8.879	TW		2.23							
		$^2F_{7/2}$–$^2[3]^o_{7/2}$	318.617	44.90 B	8.333	TW		2.09							
39	$(^1D)3d$–$(^3P_1)4f$	$^2F_{5/2}$–$^2[4]^o_{7/2}$	304.608	45.62 A	9.263	TW		2.25		17.21 A	34.945	TW			
										12.71	25.807	7			
		$^2F_{7/2}$–$^2[4]^o_{9/2}$	306.689	49.56 A	9.927	TW		2.41		16.17 B	32.389	TW			
										12.71	25.458	7			
40	$(^1D)4p$–$(^1D)5s$	$^2F^o_{5/2}$–$^2D_{3/2}$	392.572	74.73 B	9.136	TW	1.27	0.65		33.46 A	40.904	TW	1.61	1.41	
										36.02	44.034	7			
				89.81	10.979	13				30.76	37.604	13			
				78.50	9.596	15									
				95.16	11.633	16				31.86	38.948	16			
		$^2F^o_{5/2}$–$^2D_{5/2}$	392.605	68.65 C	8.391	TW	1.16	0.59		33.39 A	40.812	TW	1.61	1.41	
		$^2F^o_{7/2}$–$^2D_{5/2}$	394.610	74.86 B	9.057	TW	1.26	0.64		30.18 A	36.514	TW	1.44	1.26	
										34.96	42.298	7			
				91.80	11.107	15									
				82.02	9.923	16				33.58	40.628	16			
41	$(^1D)4p$–$(^1D)4d$	$^2F^o_{7/2}$–$^2G_{9/2}$	356.103	57.43 C	8.532	TW		1.03		15.00 B	22.285	TW			
				63.90	9.494	15									

Table 1 – *continued*

No	Transition	Term	Wavelength (nm)	w_m (pm)	w_m (10^{11} s^{-1})	Ref.	w_m/w_{MSE}	w_m/w_{SMSE}	w_m/w_G	d_m (pm)	d_m (10^{10} s^{-1})	Ref.	d_m/d_{MSE}	d_m/d_{SMSE}	d_m/d_G
42		$^2F^o_{5/2}-^2D_{5/2}$	341.446	67.05 B	10.835	TW	1.22			27.88 B	45.054	TW			
										41.32	66.772	7			
43		$^2F^o_{5/2}-^2F_{5/2}$	335.092	67.96 A	11.403	TW	1.23			22.65 A	38.003	TW			
				70.14	11.768	2									
				70.27	11.790	5									
										28.07	47.097	7			
				59.10	9.916	15									
		$^2F^o_{7/2}-^2F_{5/2}$	336.552	66.49 A	11.059	TW	1.20			21.87 A	36.377	TW			
										32.84	54.624	7			
		$^2F^o_{7/2}-^2F_{7/2}$	337.644	83.92 A	13.869	TW	1.51			30.88 A	51.032	TW			
										34.96	57.774	7			
				72.52	11.985	13				42.62	70.433	13			
				66.80	11.039	15									
44		$^2P^o_{3/2}-^2P_{3/2}$	366.044	115.78 A	16.280	TW				21.43 B	30.133	TW			
										25.96	36.502	7			
				125.00	17.576	16				15.57	21.893	16			
		$^2P^o_{3/2}-^2P_{1/2}$	367.100	110.39 C	15.433	TW				25.25 C	35.300	TW			
		$^2P^o_{1/2}-^2P_{1/2}$	375.405	122.39 A	16.361	TW				30.24 A	40.426	TW			
45		$^2P^o_{3/2}-^2D_{5/2}$	363.983	110.33 A	15.690	TW				26.20 A	37.258	TW			
										23.84	33.902	7			
				21.60	3.072	15									
		$^2P^o_{1/2}-^2D_{3/2}$	368.006	142.41 B	19.811	TW									
46		$^2P^o_{3/2}-^2S_{1/2}$	302.675	110.85 A	22.796	TW									
		$^2P^o_{1/2}-^2S_{1/2}$	308.298	119.74 B	23.734	TW				−12.61 B	−24.995	TW			
47	$(^1D)3d-(^1D_2)4f$	$^2D_{5/2}-^2[1]^o_{3/2}$	275.730	41.50 C	10.284	TW									
48		$^2D_{3/2}-^2[3]^o_{5/2}$	274.479	59.01 A	14.757	TW				8.92 B	22.306	TW			
										9.53	23.832	7			
49	$(^1D)3d-(^3P_2)6f$	$^2D_{3/2}-^2[1]^o_{3/2}$	264.784	95.05 A	25.542	TW				43.78 A	117.645	TW			
50	$(^1D)4p-(^1D)4d$	$^2D^o_{3/2}-^2P_{3/2}$	381.902	95.29 B	12.309	TW				35.83 B	46.283	TW			
				137.64	17.780	16				<5.0		16			
		$^2D^o_{5/2}-^2P_{3/2}$	382.567	100.13 C	12.889	TW				26.75 C	34.434	TW			
				105.40	13.568	15									
		$^2D^o_{3/2}-^2P_{1/2}$	383.052	113.88 C	14.625	TW									
51		$^2D^o_{3/2}-^2D_{5/2}$	379.659	101.68 B	13.290	TW				30.47 B	39.826	TW			
				101.13	13.218	16				24.37	31.853	16			
		$^2D^o_{5/2}-^2D_{5/2}$	380.317	108.62 B	14.148	TW				37.43 A	48.754	TW			
										32.84	42.775	7			
				42.62	5.551	13				33.23	43.283	13			
				100.70	13.117	15									
				114.68	14.938	16				37.92	49.392	16			
52		$^2D^o_{3/2}-^2F_{5/2}$	371.821	87.72 B	11.954	TW				23.31 B	31.766	TW			
										33.90	46.197	7			
				96.10	13.096	15									
				94.25	12.844	16				23.36	31.834	16			
		$^2D^o_{5/2}-^2F_{7/2}$	373.789	91.44 B	12.330	TW				31.03 B	41.842	TW			
										36.02	48.570	7			
				89.93	12.126	13				35.64	48.058	13			
				101.20	13.646	15									
				113.87	15.355	16				22.45	30.272	16			
53	$(^1D)4p-(^3P)5d$	$^2D^o_{5/2}-^4P_{5/2}$	352.156	61.88 A	9.401	TW				17.57 A	26.692	TW			
54	$(^1D)3d-(^1D_2)4f$	$^2P_{3/2}-^2[1]^o_{3/2}$	292.463	46.00 A	10.132	TW				4.83 C	10.639	TW			
		$^2P_{1/2}-^2[1]^o_{3/2}$	296.024	49.73 A	10.692	TW									
										6.36	13.674	7			
55		$^2P_{1/2}-^2[2]^o_{3/2}$	293.148	48.32 A	10.593	TW				6.96 C	15.288	TW			
										10.59	23.217	7			
56	$(^1S)3d-(^1D_2)4f$	$^2D_{5/2}-^2[2]^o_{5/2}$	340.861	59.12 C	9.587	TW	2.46								
57	$(^3P)5p-(^1S)5s$	$^4D^o_{3/2}-^2S_{1/2}$	400.536	116.79 C	13.715	TW	0.52								

3.1 Half-width results

For each spectral line, the Stark half-width dependence on electron density was checked. This dependence is clearly linear for all the considered lines.

For the analysis of our experimental data, we used the criterion for regular Stark half-width behaviour within multiplets, super-multiplets and transition arrays which was established in Wiese & Konjević (1982). For this analysis, experimental data from Table 1
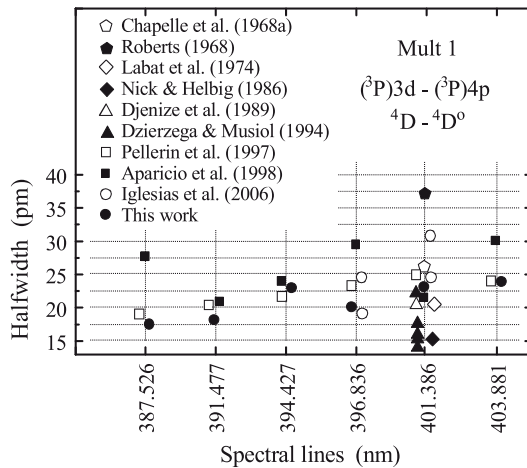
Figure 2. Experimental half-width result comparison for lines in multiplet 1.

were also converted to angular frequency units in order to avoid the wavelength influence. Line half-widths usually agree within a few per cents in multiplets, within ±30 per cent in supermultiplets and within ±40 per cent in transition arrays. Exceptions occur typically in the cases where some perturbing levels are very close to the upper or lower level of the considered transition. We have found both regular and irregular behaviours for Ar II spectral lines.

The most significant result of this work is undoubtedly the good agreement existing between the Stark half-widths of lines belonging to the same multiplet, which vary within ±10 per cent for most cases. An example of this regular behaviour has been shown in Fig. 2, where our data for multiplet 1 have been plotted as solid circles. A typical irregular behaviour due to the existence of perturbing energy levels can be found in multiplet 7. Here, half-widths for lines 289.161 and 297.905 nm are around 55 pm, whereas half-widths for lines 294.289 and 303.351 nm are around 35 pm. This great intramultiplet variation is explained in Fig. 3, where positions of the closest perturbing levels for the upper energy levels are depicted. Perturbing levels are too far from the lower energy level of the transitions and have no significant influence on the broadening or shifting of spectral lines. The difference between upper energy level and the closest perturbing level for the lines 289.161 and 297.905 nm is much smaller than the same difference calculated for the other two lines. This explains not only the observed difference in half-widths of the lines in multiplet 7 but also the difference in the measured positive shifts. There is finally only one exception, not explainable by the presence of perturbing energy levels. This corresponds to the line 337.644 nm in multiplet 43, which has a 15 per cent higher half-width than the average value in that multiplet. It is important to remark that all energy and perturbing energy level data were taken from NIST Atomic Spectra Database.

If we analyse the Stark half-width regularities within supermultiplets, we can see that the maximum deviation is around ±34 per cent. The exceptions correspond to half-widths of lines 349.948 nm [multiplet 3, supermultiplet 3d ^{4}D–4p ^{4}(SD)^o] and 274.479 nm [multiplet 48, supermultiplet 3d ^{2}(PDF)–4f ^{2}[1,2,3,4]^o]. Their values are about 50 per cent higher than the corresponding average half-widths in the supermultiplet. Data from multiplets 44–46 and 50–52 [supermultiplet 4p ^{2}(PD)^o–4d ^{2}(SPDF)] are excluded from this analysis due to the existence of perturbing energy levels very close to the lower level of the transition.
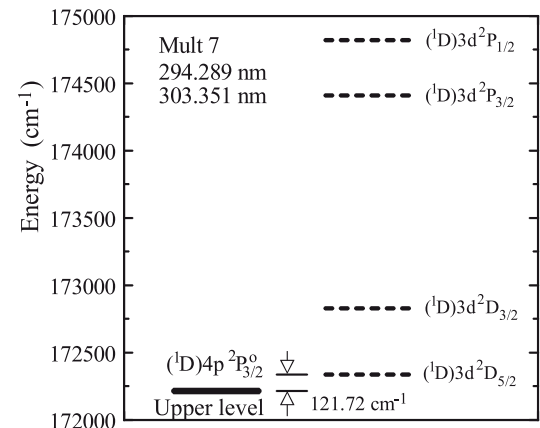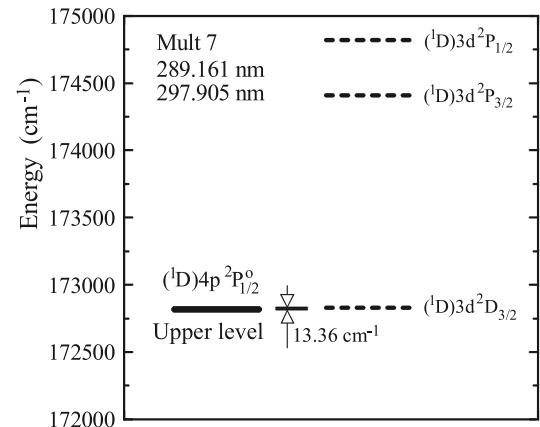
Figure 3. Closest perturbing levels (dashed lines) to the upper energy levels of the lines of multiplet 7.

Concerning Stark half-width regularities, only six transition arrays were available for analysis: 3d–4p, 4s–4p, 4p–3d, 4p–5s, 4p–4d and 3d–4f. The maximum observed individual half-width variation relative to its average value is ±44 per cent. By analysing variations inside each transition array, there are some remarkable findings. If we exclude the line 349.948 nm (multiplet 3) in the 4p–5s transition array from this calculation, variations are lower than ±15 per cent. In the same way, variations decrease below ±24 per cent in the 3d–4p transition by excluding the line 363.481 nm (multiplet 9). In this last case, the high measured half-width of this line is again explainable by the existence of a perturbing level close to the upper level of the transition. It is also interesting that in the 4s–4p transition array half-width variations are lower than ±29 per cent except for the half-width of the line 293.259 nm (multiplet 8). The half-width variations in the 4p–3d and 3d–4f transition arrays are around ±29 and 44 per cent, respectively. Finally, the 4p–4d transition array is a special case since it not only contains more than half of the measured lines but also the greatest number of exceptions. These appear in the half-widths of the lines belonging to multiplets 25, 30, 32, 33 and 37, where results are deviated from 60 to 80 per cent above the average value. In all these cases close perturbing levels to the upper energy level of the transition exist.

Therefore, we can conclude that, after taking into account the estimated experimental accuracy, the regularity in half-width behaviour in most of multiplets, supermultiplets and transition arrays

can be considered to be satisfied in the sense of Wiese & Konjević (1982) criteria.

3.2 Shift results

As can be seen in Table 1, Stark shifts d_m were determined for a lower number of lines than half-widths. In the cases where the shift values were very small, close to the limit of the measurement precision, only estimations (e.g. $d_m < 2.5$ pm) are provided in this table. In those cases where the shift could not be determined with satisfactory precision, the values are omitted.

The criterion for regular Stark shift behaviour was established in Wiese and Konjević (1992). Line shifts in multiplets generally should agree within ±10 per cent. When shifts are a relatively large fraction of half-widths, they should vary within ±25 per cent in supermultiplets and transition arrays. On the other hand, when shifts are significantly smaller than half-widths, the variations might become much larger.

In our measurements, the variation of individual shifts inside most of the considered multiplets is within ±16 per cent. This means reasonably good agreement with the above-mentioned regularity, particularly if one considers the experimental errors. However, there are some exceptions which arise from a detailed analysis of Table 1. The different observed shifts in multiplet 7 have already been justified above. A similar explanation is valid for the low shifts observed in lines 323.681 and 320.432 nm (multiplets 29 and 32, respectively). The Stark shifts of lines 362.214 nm (multiplet 12), 328.170 nm (multiplet 17), 388.033 nm (multiplet 20) and 337.644 nm (multiplet 43) are about 30 per cent higher than the average in their multiplets. In these cases, this irregular behaviour could not be explained by any perturbing level influence. However, an illustration of the quality of the performed shift measurements of two of these lines is shown in Fig. 4 as example. Finally, the disagreement between shifts in multiplet 8 could be easily explained by the large experimental errors.

If we analyse the Stark shift regularities within supermultiplets, regular behaviour exists in most of cases, but again some exceptions are worth to be mentioned. The most significant irregularity appears between shift results of multiplets 9 and 10 inside supermultiplet 3d ^{2}P–4p ^{2}(PD)^o. The positions of perturbing energy levels close to the upper levels of the involved transitions could explain this difference. The positions of perturbing levels can also explain the small values of the shifts of lines with the same upper levels (4d ^{2}D$_{3/2, 5/2}$).
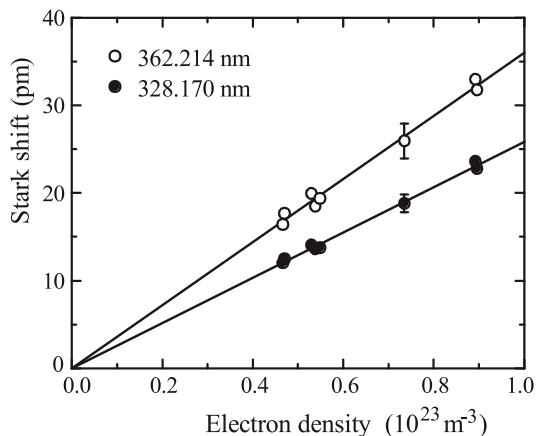
Figure 4. Shift versus electron density calibration for two Ar II lines.

The line 286.584 nm of multiplet 25 [supermultiplet 4p ^{4}D^o–4d ^{2}(DF)] and the lines of multiplets 30, 33 and 37 [supermultiplet 4p ^{2}(SPD)^o–4d ^{2}(PDFG)] have a very low accuracy in their Stark shift or even only an estimation has been possible. Shift data of multiplets 44–46 and 50–52 [supermultiplets 4p ^{2}(PD)^o–4d ^{2}(SPDF)] vary about ±10 per cent. However, there is an interesting exception concerning the result of the line 308.298 nm. In this case, a negative shift (blue shift) appears. It can be seen from the energy level diagram that both, upper and lower energy levels of the transition, have close perturbing levels, which lead to a negative shift. Finally, in supermultiplet 3d ^{2}(PDF)–4f ^{2}[1,2,3,4]^o shift values are divided into two different groups. In multiplet 39 shifts are around 17 pm, whereas in multiplets 48, 54 and 55 shifts are around 7 pm. The energy levels and their perturbing level structure can explain this difference.

If we exclude these exceptions, the variation of shift results in rest of supermultiplets is about ±33 per cent, a conclusion which can also be extended to transition arrays.

3.3 Comparison with other experimental results

Generally speaking, most of our results agree reasonably well (within ±30 per cent) with other authors' data. There are a few exceptions. The greatest differences appear with the extremely large half-widths reported by Jalufka et al. (1966) and by Roberts (1968) for lines 372.931 and 385.058 nm, respectively (multiplet 6). Additionally, there are some published data significantly lower (from 50 to 90 per cent) than our experimental half-widths, e.g. line 380.317 nm in multiplet 51 (Djeniže et al. 1989) and lines 289.161 and 297.905 nm (multiplet 7), 384.473 nm (multiplet 20), 395.838 nm (multiplet 26) and 363.983 nm (multiplet 45), all of them reported by Pellerin et al. (1997). Aparicio et al. (1998a) published higher half-widths for line 387.526 nm (multiplet 1) and for lines 385.058 and 392.862 nm (multiplet 6). In this last case, it is probably due to the presence of some self-absorption effect combined with a too high inverse linear dispersion, around six times greater than that provided by our spectrometer. There are 12 more results (see Table 1) whose differences with our data are within ±50 per cent. The comparison of all the existing half-width data of lines belonging to multiplet 1 is shown in Fig. 2. This illustrates the level of agreement as well as some of the commented discrepancies.

Concerning shifts, the amount of previously published data is much smaller than for half-widths. The agreement of most of our measured results and data given by other authors is within ±50 per cent. There are 10 lines whose shifts differ from ours in percentages between ±50 and ±70 per cent, and there are several larger disagreements. Among them, we can see that the shifts for lines 385.058 and 392.862 nm (multiplet 6), given by Blandin et al. (1968), are 99 per cent smaller than ours, but with the same shift directions. Labat et al. (1974) reported the shift for the line 372.931 nm (multiplet 6) with the same value as ours, but curiously with opposite direction. In these cases, the data from these authors disagree, not only with ours but also with other authors' data. Anyway, it should also be considered that the above-mentioned discrepancies correspond to shifts which are just a few picometres. There is an interesting situation in multiplet 7, for which energy level structure was already commented above. Morris & Morris (1970) reported a shift value of +11.2 pm for the line 294.289 nm (our shift is +3.97 pm), while Djeniže et al. (1989) reported negative shift, −2.29 pm. Unfortunately, there are no other results for this comparison.

3.4 Comparison with theoretical results

For the comparison between our experimental half-widths and theoretical data, we calculated half-widths by using the MSE formula by Dimitrijević & Konjević (1980) and the SMSE formula by Dimitrijević & Konjević (1987). For shift calculations we used the MSE formula by Dimitrijević & Kršljanin (1986) and the SMSE formula by Dimitrijević & Konjević (1987). Furthermore, we also used theoretical data for both half-widths and shifts of Griem (1974).

There are some theoretical requirements which must be satisfied for MSE calculations. Unlike semi-empirical calculations (Griem 1968), transitions with $\Delta n = 0$ are separated in the MSE formula. In this case, the calculation only takes into account the nearest perturbing levels with $l+1$ and $l-1$, for both upper and lower levels of the considered transition. In order to obtain the proper theoretical values, this set of four nearest perturbing levels must be known. In this work, energy levels of the transitions and perturbing levels were taken from NIST Atomic Spectra Database. The condition $3kT/2\Delta E_{jj'} \leq 2$ must also be satisfied. Here, $3kT/2$ is the kinetic energy of the perturbing electrons and $\Delta E_{jj'} = |E_j - E_{j'}|$ is the energy difference between the upper (or lower) level of the considered transition and the nearest perturbing energy levels. Usually, the closest perturbing levels correspond to the same principal quantum number as does the upper (or lower) level of the transition. However, there are situations where a very close level exists with $\Delta n \neq 0$. In these cases, MSE calculations could not provide proper results and they are omitted from Table 1. This happens, for instance, in multiplet 7.

As a general conclusion, our experimental half-widths are in relatively good agreement with those calculated by the MSE formula. All ratios w_m/w_{MSE} lie between 0.83 and 1.46, with the exception of multiplet 8 where they range from 1.49 to 1.71. Discrepancies increase when comparing shift results. Most of the d_m/d_{MSE} values range from 0.72 to 1.40, the largest ratios appearing in multiplets 8, 12, 13, 18, 19 and 40, where they lie between 1.53 and 2.35. Otherwise, it is well known that Stark shift measurements are, in general, less accurate than Stark half-width ones, especially in the cases where shifts are very low.

When employing the SMSE formula for comparisons, the condition $3kT/2\Delta E_{jj'} \leq 2$ should be also satisfied. However, there are no restrictions for the principal quantum number. These conditions are completely satisfied only for multiplets 3, 4, 6, 21 and 57, and almost satisfied for multiplets 1, 2, 5, 12, 13, 15, 18, 19, 27, 34, 40 and 56. These multiplets belong to 3d–4p, 4p–3d, 4s–4p, 4p–5s and 3d–4f transitions. Whereas half-width ratios w_m/w_{SMSE} for the 3d–4p transition range from 1.76 to 2.27, the shift ratios lie between 1.01 and 1.71. Concerning the 4p–3d transition, only three multiplets 15, 21 and 27 exist. In these cases, half-width ratios lie between 1.05 and 1.54. Predicted shifts are small and negative, their sign being opposite to the experimentally measured. In these cases, comparisons are excluded from Table 1. The same situation appears in the 3d–4f transition. Finally, for 4s–4p and 4p–5s transitions, half-width ratios range from 0.41 to 0.72, whereas shift ratios lie between 1.21 and 1.85. It is also important to remark that relatively large discrepancies can be expected in comparisons with predictions obtained from the simplified calculation.

We also tried calculations in the cases where $2 < 3kT/2\Delta E_{jj'} \leq 9$, obtaining reasonably good agreement with our experimental half-widths. This happens for all multiplets which belong to the 4p–4d transition. Half-width ratios range from 0.78 to 1.23. In all these cases, SMSE calculations predict small negative shifts between -2 and -5 pm. However, the experimental ones are positive with values

around a few tens of picometres, in agreement with other authors' results and with Griem (1974) calculations (e.g. shift results in multiplets 17 or 20). These ratios and those obtained in the cases where $3kT/2\Delta E_{jj'} > 9$ were not included in Table 1.

Finally, Griem's calculations (Griem 1974) are available only for multiplets 1, 12, 17, 20, 28, 32 and 36. Generally, the ratio w_m/w_G ranges from 0.74 to 1.19, while d_m/d_G ratio lies between 0.51 and 1.15. There are only two remarkable exceptions, line 403.880 nm (multiplet 1) and line 323.681 nm (multiplet 32), where the shift ratios are 0.43 and 0.38, respectively.

4 CONCLUSIONS

Here we report 126 Stark half-widths and 111 shifts of ultraviolet singly ionized argon lines belonging to 57 multiplets, in the spectral interval from 265 to 405 nm. From them, 53 half-widths and 44 shifts were not previously published. All these data have been obtained in a low-pressure pure argon pulsed arc plasma with high-reproducibility features. Electron density ranged from 0.20 to 1.15×10^{23} m^{-3} and electron temperature from 16 000 to 26 000 K. Special attention was paid to experimental conditions, plasma diagnostics as well as experimental data treatment. Electron densities were determined by two-wavelength interferometry and electron temperature by the Boltzmann plot technique using 13 Ar II lines. Furthermore, a self-absorption check was performed and an appropriate deconvolution procedure was applied.

All measured Stark widths and shifts showed a clear linear dependence on electron density. A very detailed analysis of Stark parameter regularities within multiplets, supermultiplets and transition arrays has been performed. The most significant conclusion is that a very good regular behaviour in half-widths and shifts is generally found according to the predictions performed in Wiese & Konjević (1982), after considering the experimental errors. This means, for instance, that Stark parameters of another non-measured Ar II line belonging to one of the multiplets analysed in this work can be easily predicted at $N_e = 10^{23}$ m^{-3} if the energy levels of this transition are not highly perturbed. From this, the electron density of the plasma emitting the radiation corresponding to that line can be inferred. Most of the observed deviations from the regular behaviours have been explained from the detailed analysis of the Ar II complex energy level structure and the perturbing level positions relative to the transition levels.

The comparison between these experimental results and other authors' results shows, in most cases, reasonable agreement within ± 30 per cent. Some significant exceptions have been detected (e.g. line 401.386 nm, Fig. 2). In the cases like these, some new independent experimental measurements would be useful not only to clarify the large observed discrepancies but also to test theory.

The measured Stark parameters were also compared to the theoretical values in the cases where it was possible. We used calculated data by using the MSE formula from Dimitrijević & Konjević (1980) for half-widths, the MSE formula from Dimitrijević & Kršljanin (1986) for shifts, and for both half-widths and shifts the SMSE formula from Dimitrijević & Konjević (1987) and the theoretical data tabulated in Griem (1974). There are some necessary conditions, commented above, which should be satisfied for applying MSE and SMSE calculations. In the cases where these conditions were not fulfilled, the comparison is omitted. The observed relatively large variations in w_m/w_{MSE} and d_m/d_{MSE} ratios (from 0.7 to 2.3) can be considered as normal in this kind of comparison. Similar level of

agreement between experimental and calculated Stark parameters has already been found by MSE formula authors (Dimitrijević & Konjević 1980; Dimitrijević & Kršljanin 1986; Popović & Dimitrijević 1996). A little higher disagreement is found in the comparison with SMSE calculations. However, we have shown that this formula can provide reasonably good half-width results even when the upper limit of 2 for the ratio $3kT/2\Delta E_{jj'}$ is exceeded and reaches values up to 9. The best agreement between our experimental data and calculations is obtained with Griem's theoretical results (Griem 1974), where complete quantum mechanical calculations were applied.

Finally, it is important to remark the significant enlargement of the Ar II atomic spectra data base provided by this work. In addition to this, the set of new data provided opens new possibilities of laboratory and remote plasma diagnostics, electron density predictions and abundance calculations, as has previously been made with Ar II lines in the astrophysical field.

ACKNOWLEDGEMENTS

REFERENCES

Aparicio M. A., Gigosos M. A., Mar S., 1997, J. Phys. B: At. Mol. Opt. Phys., 30, 3141

Aparicio J. A., Gigosos M. A., Gonzalez V. R., Perez C., de la Rosa M. I., Mar S., 1998a, J. Phys. B: At. Mol. Opt. Phys., 31, 1029

Aparicio J. A., Perez C., del Val J. A., Gigosos M. A., de la Rosa M. I., Mar S., 1998b, J. Phys. B: At. Mol. Opt. Phys., 31, 4909

Asplund M., Grevesse N., Sauval A. J., Scott P., 2009, ARA&A, 47, 481

Behinger K., Thoma P., 1978, J. Quant. Spectrosc. Radiat. Transfer, 20, 615

Blandin J., Sahal-Brechot S., Chapelle J., Sy A., 1968, Phys. Lett., 26A, 487

Chapelle J., Sy A., Cabannes F., Blandin J., 1968a, J. Quant. Spectrosc. Radiat. Transfer, 8, 1201

Chapelle J., Sy A., Cabannes F., Blandin J., 1968b, C. R. Acad. Sci. Paris Ser. B, 266, 1513

Davies J. T., Vaughan J. M., 1963, ApJ, 137, 1302

Dimitrijević M. S., Konjević N., 1980, J. Quant. Spectrosc. Radiat. Transfer, 24, 451

Dimitrijević M. S., Konjević N., 1987, A&A, 172, 345

Dimitrijević M. S., Kršljanin V., 1986, A&A, 165, 269

Djeniže S., Malešević M., Srećković A., Milosavljević M., Purić J., 1989, J. Quant. Spectrosc. Radiat. Transfer, 42, 429

Djurović S., Peláez R. J., irišan M., Aparicio J. A., Mar S., 2006, J. Phys. B: At. Mol. Phys. Opt., 39, 2901

Dzierzega K., Musiol K., 1994, J. Quant. Spectrosc. Radiat. Transfer, 52, 747

Esteban C., Peimbert M., García-Rojas J., Ruiz M. T., Peimbert A., Rodríguez M., 2004, MNRAS, 355, 229

Fossati L., Ryabchikova T., Bagnulo S., Alecian E., Grunhut J., Kochukhov O., Wade G., 2009, A&A, 503, 945

Griem H. R., 1968, Phys. Rev. A, 165, 258

Griem H. R., 1974, Spectral Line Broadening by Plasmas. Academic Press, New York

Iglesias E. J., Ghosh J., Elton R. C., Griem H. R., 2006, J. Quant. Spectrosc. Radiat. Transfer, 98, 101

Jalufka N. W., Oertel G. K., Ofelt G. S., 1966, Phys. Rev. Lett., 16, 1073

Keenan F. P., Bates B., Dufton P. L., Holmgren D. E., Gilheany S., 1990, ApJ, 348, 322

Konjević N., Wiese W. L., 1976, J. Phys. Chem. Ref. Data, 5, 259

Konjević N., Labat J., irković Lj., Purić J., 1970, Z. Phys., 235, 35

Labat J., Djeniže S., irković Lj., Purić J., 1974, J. Phys. B: At. Mol. Phys., 7, 1174

Lanz T., Cunha K., Holtzman J., Hubeny I., 2008, ApJ, 678, 1342

Morris J. C., Morris R. U., 1970, Aerospace Research Laboratories Report No. ARL 70-0038, Aerospace Research Laboratories, Office of Aerospace Research, United States Air Force

Nick K. P., Helbig V., 1986, Phys. Scr., 33, 55

NIST Atomic Spectra Database, 2008, available at: http://www.nist.gov/pml/data/asd.cfm

Peimbert A., 2003, ApJ, 584, 735

Peláez R. J., Mar S., Aparicio J. A., Belmonte M. T., 2012, Appl. Spectrosc., 66, 970; 2013, Appl. Spectrosc., 67(4), 114A (erratum)

Pellerin S., Musiol K., Chapelle J., 1997, J. Quant. Spectrosc. Radiat. Transfer, 57, 377

Pittman T. L., Konjević N., 1986, J. Quant. Spectrosc. Radiat. Transfer, 35, 247

Popović L. È., Dimitrijević M. S., 1996, A&A Suppl. Ser., 116, 359

Roberts D. E., 1966, Phys. Lett., 22, 417

Roberts D. E., 1968, J. Phys. B, 1, 53

Wiese W. L., Konjević N., 1982, J. Quant. Spectrosc. Radiat. Transfer, 28, 185

Wiese W. L., Konjević N., 1992, J. Quant. Spectrosc. Radiat. Transfer, 47, 185

Chapter 5

Measurement of Transition Probabilities in Ar II UV spectral lines.

"But, of course, people who understand life
are not bothered about numbers!
I don't want to become like those grown-ups
who only care about numbers. So I bought
a box of paints and some crayons."

-Antoine de Saint-Exupéry, *The Little Prince* -

Argon plasmas have been extensively studied over the last fifty years due to their desirable characteristics and the suitability of their spectral lines to function as a tool for plasma diagnostics, particularly for the calculation of excitation temperature. The measurement of transition probabilities for argon is of widespread interest in astrophysics, as UV spectral lines of Ar II have been used in the determination of stellar abundances in B-type stars. In the field of astronomical instrumentation, Ar II UV lines have been identified in the ThAr hollow cathode lamps that have become the standard for wavelength calibration of astronomical spectrographs.

Due to this importance, a considerable effort has been invested into the assembling

of an accurate and complete set of Ar II transition probabilities. However, some of the data included in the NIST database still has uncertainties of around 50%. The aim of this experiment is to extend the present database of atomic parameters to the ultraviolet region by measuring accurate transition probabilities of singly ionized argon lines in the spectral interval ranging from 294 to 386 nm. A detailed description of recent developments in the field and the bibliography can be found in the accompanying article.

5.1   Experimental details.

In this experiment, we measured relative intensities of singly ionized argon spectral lines emitted by a low-pressure-pulsed discharge lamp in order to obtain experimental absolute transition probabilities. As reference data, we used a set of 11 A_{ki}-values taken from the bibliography the uncertainties of which are lower than 15%.

As the experimental set-up has already been described in Chapter 2, only a brief summary of the experimental conditions will be given. More complete experimental details are provided in the accompanying article. The discharges were carried out through a cylindrical tube made of Pyrex glass, 175 mm long and 19 mm in internal diameter. Pure argon at a pressure of 500 Pa flowed continuously through the discharge tube at a rate of 1.0 sccm. The pressure of argon was adjusted to obtain minimal self-absorption and maximum intensity.

Plasma pulses were created by discharging a capacitor bank of 20 μF through the discharge tube. The capacitor bank was charged up to 7.5 kV. In these conditions, the plasma emission lasted for 150 μs. All the Ar II lines were recorded in the first order of diffraction and the exposure time ranged from 2.5 to 5 μs, depending on the necessities of the different spectral lines. These lines were recorded at five different instants from 40 to 120 μs after the beginning of the discharge. Ten spectra were recorded for each instant, three of them with the self-absorption control mirror and seven without it. In order to ensure the plasma reproducibility, the gas in the tube was preionized by using a continuous current of several mA. Table 5.1 summarizes the experimental conditions used. In total, 1500 discharges were made.

The singly ionized argon excitation temperature was determined by using the Boltzmann-plot technique for 11 Ar II spectral lines in the wavelength range between 379 and 405 nm

Table 5.1: Experimental measurement conditions.

Lamp running conditions	
Ar pressure	500 Pa
Ar flow	1.0 sccm
Discharge voltage	7.5 kV
Optical parameters	
Spectroscopic channel pinholes	$\phi = 2$ mm (D1 and D2 in Fig. 2.5)
Width of the entrance slit	35 μm
Diffraction order	1
Acquisition parameters	
Camera	ICCD 4 Quick E S20
Measurement instants	40, 50, 60, 110, 120 μs
Exposure time	2.5-5 μs
Spectral interval	294-386 nm

for which the transition probabilities are well known. The temperature obtained ranges from 19 000 to 22 000 K, with statistical uncertainties lower than 15%. The measured electron densities are in the range of $(3.5 - 9.0) \times 10^{22}$ m^{-3}, with experimental errors estimated to be lower than 10%. The influence of heavy particles on the variation of the plasma refractive index was eliminated by using a two-wavelength interferometric method.

For the electron densities and temperatures considered in this work, calculations carried out using Griem's criteria establish that the Ar II energy level scheme is in a partial local thermodynamic equilibrium (pLTE) for the levels whose energies are greater than 19 eV. The pLTE within the energy interval considered in this experiment is also corroborated by the linear behaviour of the Boltzmann-plots, with R^2 coefficients of around 0.97, very close to the unit.

5.2   Results and conclusions.

This article provides a set of 43 atomic transition probabilities for singly ionized argon spectral lines in the ultraviolet region ranging from 294 to 386 nm. Amongst those values, 11 of them are new, at least as far as the authors are aware, and 22 of them correspond to transition probabilities whose existing values had uncertainties of around 50%. We have

paid special attention to the analysis of all the possible sources of error and the calculation of the final value of the uncertainty associated with the transition probabilities.

In addition, the measured A_{ki}-values have been carefully studied and compared with the existing data, presenting very good agreement with the data taken from the Vujnović & Wiese compilation (Vujnović & Wiese, 1992). However, we have found significant disagreement with some of the data taken from the NIST database which is worth analysing. The values presented here extend the present database of measured Ar II transition probabilities to the UV region, providing new values that could be useful in refining new theoretical models.

Improved and expanded measurements of transition probabilities in UV Ar II spectral lines

M. T. Belmonte,[1][*] S. Djurović,[2] R. J. Peláez,[3] J. A. Aparicio[1] and S. Mar[1]

[1]*Departamento de Física Teórica, Atómica y Óptica, Universidad de Valladolid, Paseo de Belén 7, E-47011 Valladolid, Spain*
[2]*Department of Physics, Faculty of Sciences, University of Novi Sad, Trg Dositeja Obradovića 4, 21000 Novi Sad, Serbia*
[3]*Laser Processing Group, Instituto de Óptica, CSIC, Serrano 121, E-28006 Madrid, Spain*

ABSTRACT

Transition probabilities have a significant interest in the astrophysical field. The aim of this experiment is to extend the present data base of measured Ar II transition probabilities to the ultraviolet (UV) region and to improve the quality of some of the already existing data. Despite all the efforts made to assemble an accurate set of transition probabilities (A_{ki}), some of the data recommended by the National Institute of Standards and Technology (NIST) for Ar II spectral lines in the UV region have uncertainties around 50 per cent. We measured relative intensities of spectral lines emitted from a low-pressure-pulsed discharge lamp which generates an argon plasma. Excitation temperatures of 19 000–22 000 K are determined from the Boltzmann-plot of 11 Ar II spectral lines for which accurate A_{ki} data are available from the literature. The transition probabilities of these 11 spectral lines were used for calculating new A_{ki}-values. Electron densities (N_e) of 3.5–9.0×10^{22} m^{-3} are determined by two-wavelength interferometry method. The measurements yield to a collection of 43 atomic transition probabilities of Ar II lines in the spectral region of 294–386 nm, 11 of which are new, at least up to the authors knowledge, and 22 improved A_{ki}-values for which the existing data in the literature have uncertainties around 50 per cent. Comparison with previous data shows how our measurements have good agreement with the most accurate A_{ki}-values from the bibliography, whereas some of the values recommended by NIST present a significant disagreement.

Key words: Atomic data – Line: profiles – Plasmas – methods: laboratory: atomic.

1 INTRODUCTION

Knowledge of atomic parameters such as the transition probability is of great importance, not only in the theoretical field, but also in the diagnostics of any radiation emitting source, as conventional lamps, lasers, industrial plasmas, fusion or in astrophysics. This fact becomes more relevant for the ionized atoms due to the absence of accurate experimental data from the literature, as is clear from the consultation of the National Institute of Standards and Technology (NIST) data base. Argon plasmas have been extensively studied over the last fifty years due to their desirable characteristics (Wiese 1988) and the suitability of their spectral lines to work as a tool for plasma diagnostics, particularly for temperature determination (Behringer & Thoma 1976). However, despite all the efforts made to assemble an accurate set of transition probabilities (Vujnović & Wiese 1992), some of the data recommended by Kramida et al. (2014) for Ar II spectral lines in the (ultraviolet) UV region have uncertainties of around 50 per cent (Rudko & Tang 1967).

The determination of radiative transition probabilities or oscillator strengths on argon is of common interest in astrophysics. The analysis of the high-resolution stellar spectra is now available in order to estimate the stellar abundances. Weak stellar absorption lines lie on the linear part of the curve growth and hence they have line strengths that are very sensitive to the element abundance. Thus, UV spectral lines of Ar II have been used in the determination of these parameters in B-type stars like γ Peg, HR 1350, 8 Cygni, η Lyrae, Orion B stars (Keenan et al. 1990; Adelman 1998; Lanz et al. 2008). Transition probabilities have contributed to the estimation of abundances in the solar atmosphere, which is quite important for modelling the evolution of the terrestrial and Venusian atmospheres (Lodders 2008). In the field of astronomical instrumentation, UV spectral lines of Ar II have been identified in ThAr lamps. These hollow cathode lamps have become the standard for wavelength calibration of astronomical spectrographs. Wavelength accuracy determines the precision of the radial velocity measurements, and currently there is a great interest in optimizing their precision e.g. radial velocity searches of extrasolar planets or the study of the variability of fundamental constants (Lovis & Pepe

[*] E-mail: teruca@opt.uva.es

2007; Murphy et al. 2007). On the other hand, radiometric calibrations of astrophysical instrumentation in the UV and visible range are based on reference Ar I and Ar II branching ratios. In the last decade great effort has been done to provide *f*-values for interpreting the UV and VUV observations made with the *Hubble Space Telescope* (Fedchak & Lawler 2001).

Nowadays, NIST data base (Kramida et al. 2014) is a worldwide reference data base for transition probability data. This work tries to analyse the self-consistency of the A_{ki}-values proposed by NIST for Ar II in the spectral interval 294–386 nm. This paper reports reliable and new transition probabilities for UV Ar II spectral lines, extending much further the experimental work performed by Aparicio, Gigosos & Mar (1997) in our laboratory, where transition probabilities of Ar II lines in the region 360–750 nm were measured. In this experiment, we have measured 43 ionized argon spectral lines in the UV region, yielding 11 new A_{ki}-values for which there are no previous available experimental data, at least up to the authors' knowledge. The method used is based on the measurement of relative intensities of spectral lines emitted from a low-pressure-pulsed discharge lamp which generates an argon plasma with electron densities of 3.5–9.0×10^{22} m^{-3} and temperatures of 19 000–22 000 K. The values of the new transition probabilities are obtained by using 11 spectral lines whose A_{ki}-values are already well established in the literature.

2 EXPERIMENTAL METHOD

2.1 Set-up

The experimental set-up shown in Fig. 1 has been described in detail in previous articles (Gigosos et al. 1994) and therefore, only the most relevant aspects will be summarized here for completeness. Also, more specific details corresponding to the present experiment have been reported by Djurovic et al. (2011). Measurements were carried out using a low-pressure-pulsed plasma source.

The plasma was produced inside a cylindrical tube of Pyrex, 175 mm in length and 19 mm in interior diameter. Argon at a pressure of 500 Pa was continuously flowing at a rate of 1 cm^3 min^{-1}. The pressure of argon was adjusted to obtain minimal self-absorption and maximal intensity. The lamp has been designed to avoid sputtering as much as possible. The plasmas were created by
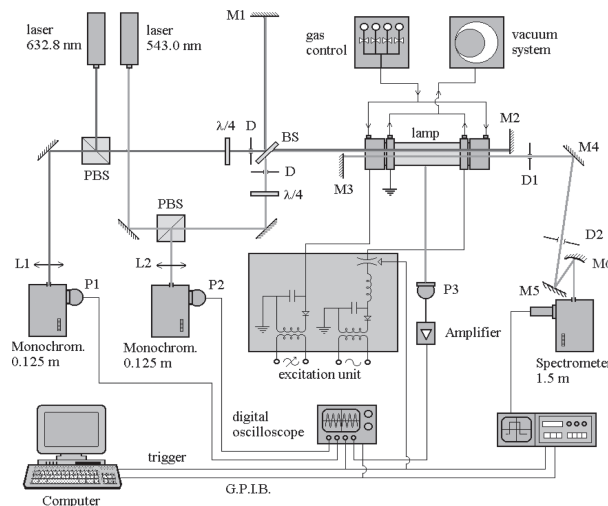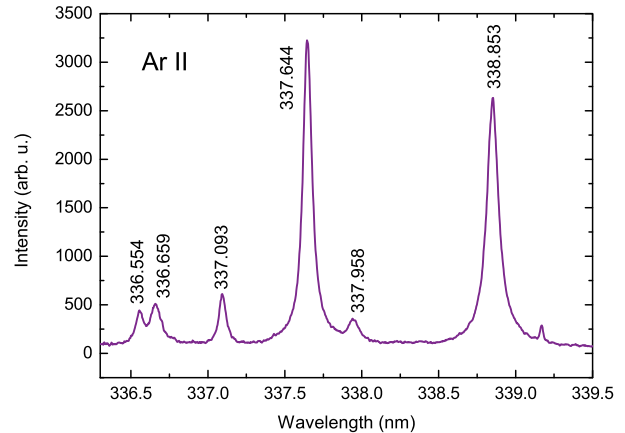
Figure 2. Ar II spectrum at the instant 50 µs of the plasma life.

discharging a capacitor bank of 20 µF charged up to 7.5 kV. The gas in the tube was preionized by a continuous current of several mA in order to ensure plasma reproducibility. In these conditions, the plasma emission lasted for 150 µs. Self-absorption was checked by means of a mirror placed behind the discharge tube (M3 in Fig. 1). Spectroscopic and interferometric end-on measurements have been made simultaneously during the plasma life, and have been taken 2 mm off the lamp axis from symmetrical positions referred to it. The high-axial homogeneity and the very good cylindrical symmetry of electron density and temperature in this lamp (del Val et al. 1998) allow this.

Light emitted from the plasma was limited by two diaphragms and focused by a concave mirror on to the entrance slit of a Jobin–Yvon monochromator (1.5 m focal length, 2400 lines mm^{-1} UV holographic grating). An intensified charge coupled device (ICCD) camera was placed at the exit plane of the monochromator. The slit width of 35 µm was selected in order to obtain the best compromise between the intensity and the resolution. The spectrometer was calibrated in wavelength with uncertainty less than 1 per cent. One of the recorded argon spectrum is shown in Fig. 2. Previous measurements of the spectral transmittance of the windows closing the tube lead us to change them every 800 discharges, in order to reduce the optical transmittance loss to values under 5 per cent at the wavelengths considered in this work. The electrodes were cleaned and polished several times during the experiment. In total 1500 discharges were made.

An incandescent calibrated lamp and a deuterium lamp were used to obtain the spectrometer's transmittance for all wavelengths of interest and for all ICCD channels. The halogen incandescent lamp was calibrated from another incandescent lamp primarily calibrated in NIST with uncertainty around 1.5 per cent. The deuterium lamp (Hamamatsu L6566) was calibrated by the manufacturer who provides a similar uncertainty. The uncertainty of our spectrometer's transmittance function is estimated lower than 4 per cent. The spectral lines were recorded at five different instants from 40 to 120 µs after the beginning of the discharge. All lines were registered in the first order of diffraction. The exposure time was 5 µs. For each instant, 10 different runs were recorded. Three profiles were recorded with and seven without the self-absorption control mirror. The averages and statistical deviations of each group of spectra are calculated in order to increase the signal-to-noise ratio. This statistical deviation is below 5 per cent in more than 95 per cent of the measured spectral intervals. From the comparison of these averaged

Figure 1. Experimental arrangement.

spectra, we can also check and correct the self-absorption effects and reconstruct the profiles when possible.

The reconstructed spectra were fitted to sums of Lorentzian functions which represent the spectral line profiles and a linear function which represents the continuum emission. The fitting procedure used provides the line intensity, centre, position, and line half-width. The deviations between the experimental profiles and the fitted functions are always lower than 1.5 per cent. Asymmetry was negligible for the Ar II lines. The area under the profile is considered as the relative line intensity used to calculate the transition probabilities. A first selection of suitable Ar II spectral lines is made by excluding all those with some of the following problems: unreliable identification, low intensity, very self-absorbed profiles or highly overlapped spectral lines.

2.2 Plasma diagnostics

The electron density was determined by using a two-wavelength interferometry method (de la Rosa García et al. 1990; Aparicio et al. 1998). The lamp is placed in one of the arms of a Twyman–Green interferometer simultaneously illuminated with two He–Ne lasers (543.5 and 632.8 nm). The laser beams used for interferometric measurements were directed along the discharge tube 2 mm off the tube axis symmetrically with respect to the direction of spectroscopic observations. The influence of heavy particles on variations in the plasma refractive index is eliminated by using this technique. Measured electron densities in this work were in the range 3.5–9.0 × 10^{22} m^{-3}. The experimental error in N_e was estimated to be lower than 10 per cent.

The ionized argon excitation temperature was determined by using the Boltzmann-plot technique (Lochte-Holtgreven 1968) for 11 Ar II spectral lines for which the transition probabilities were well known, all of them belonging to the spectral interval 379–405 nm. An example is shown in Fig. 3. The transition probabilities of these lines were taken from the compilation performed by Vujnović & Wiese (1992) and from Aparicio et al. (1997), see Table 1.

The temperatures obtained were in the range of 19 000–22 000 K. Statistical uncertainties for the excitation temperature are estimated to be lower than 15 per cent. For the electron densities and temperatures considered in this work, calculations carried out by using Griem's criteria (Griem 1963, 1964, 1997) establish that the Ar II
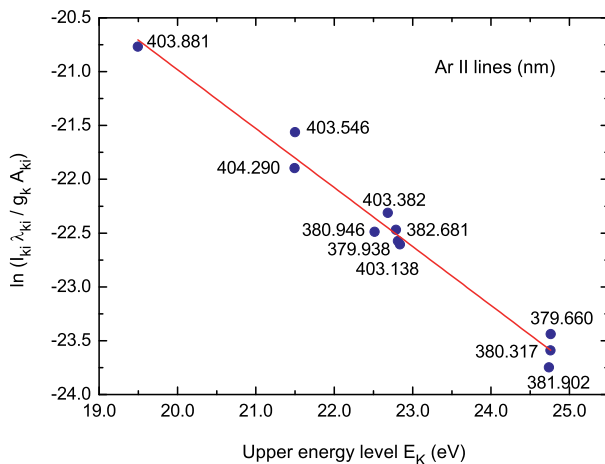
Figure 3. Example of Ar II Boltzmann-plot corresponding to the plasma life instant 50 µs.

energy level scheme is in a partial local thermodynamic equilibrium for levels above 19 eV, which is corroborated by the linear behaviour shown by the Boltzmann-plot (R^2=0.97) within the interval of the energy levels considered (see Fig. 3). Temporal evolution of these plasma parameters is shown in Fig. 4.

## 3 EXPERIMENTAL RESULTS AND DISCUSSION

Once we obtained the values of *y*-intercept and slope from the Boltzmann-plot for each of the five instants of measurement, we calculated the absolute transition probabilities for the studied spectral lines using their upper energy level and the intensity of each of these lines. We obtained five A_{ki}-values for each line, one per each instant of the plasma life. The average is the proposed value (A_{TW}). In order to perform the Boltzmann-plot, we chose lines for which the transition probabilities are well known. The interval of the upper energy levels considered is 19–25 eV. It is important to remark that all the measured spectral lines, except for two, have upper energy levels within this interval. These two Ar II lines have upper energy levels around 25.5 eV. This also guarantees the validity of the procedure employed to calculate the transition probabilities in this work.

Table 1 shows the measured transition probabilities of the Ar II lines used for the determination of the excitation temperature. We considered 11 Ar II lines from 4s–4p, 3d–4p, 4p–5s, and 4p–4d transitions. In the first three columns the transitions, multiplets, and wavelengths (Kramida et al. 2014) are given. The next four columns contain A_{TW}-values in units of 10^8 s^{-1}, experimental uncertainties (U_{TW}) in percentage, the transition probabilities taken from the bibliography (A_{Ref}), and their corresponding uncertainties (U_{Ref}). The last column gives the bibliographic references from which the A_{Ref}-values were taken. The criteria to select the reference data was to use the data from Vujnović & Wiese (1992)-VW when they exist and their uncertainty was qualified as B in Kramida et al. (2014). In the other cases, data from Aparicio et al. (1997)-AGM were taken. The letter B means that the uncertainty takes values in the range 8–10 per cent, whereas the uncertainty given for Aparicio et al. (1997) data is the square root of the different squared statistical errors provided by the author.

Table 2 shows all the measured transitions. The table is organized in the same way as Table 1. The fourth and fifth columns contain the measured A_{TW}-values of Ar II in units of 10^8 s^{-1} and their estimated uncertainty (U_{TW}) For the comparison, available experimental data A_{Ref} from Vujnović & Wiese (1992)-VW, Rudko & Tang (1967)-RT, Behringer & Thoma (1976)-BT, García & Campos (1985)-GC, and Pellerin et al. (1997)-PMDC are given in column sixth. The seventh column gives their uncertainties U_{Ref}. For VW and RT data, two estimations of the uncertainty are shown. The first value corresponds to the one proposed by the authors in percentage, whereas the second one is the qualifying letter assigned by Kramida et al. (2014). This qualifying letter is always B for data compiled by Vujnović & Wiese (1992) and D for those provided by Rudko & Tang (1967) and later compiled by Wiese, Smith & Miles (1969). In this data base, B corresponds to uncertainties between 8 and 10 per cent, C between 19 and 25 per cent, and D between 41 and 50 per cent. Some theoretical data from Statz et al. (1965)-SHKTK and Luyken (1972)-L are also included in the Table 2 and marked with an asterisk. In all cases, Luyken (1972) data contain two different values which correspond to different ways of calculations. The eighth column contains the A_{Ref}/A_{TW} ratios.

Table 1. Transition probabilities of the Ar II lines used for the determination of the excitation temperature. The references Vujnović & Wiese (1992) and Aparicio et al. (1997) are denoted as VW and AGM, respectively.

Transition	Multiplet	Wavelength (nm)	A_{TW} (10^8 s^{-1})	U_{TW} (per cent)	A_{Ref} (10^8 s^{-1})	U_{Ref} (per cent)	Ref
$(^3P)3d$–$(^3P)4p$	$^4D_{5/2}$–$^4D^o_{7/2}$	403.880	0.01	14	0.012	10	VW
$(^1D)4s$–$(^1D)4p$	$^2D_{3/2}$–$^2D^o_{5/2}$	403.546	0.05	16	0.044	10	VW
	$^2D_{3/2}$–$^2D^o_{3/2}$	404.289	0.39	45	0.406	13	VW
$(^3P)4p$–$(^3P)5s$	$^4P^o_{3/2}$–$^4P_{5/2}$	380.946	0.31	12	0.339	11	AGM
$(^3P)4p$–$(^3P)5s$	$^4D^o_{3/2}$–$^4P_{1/2}$	403.381	0.83	14	0.775	11	AGM
$(^3P)4p$–$(^3P)4d$	$^4D^o_{5/2}$–$^4D_{3/2}$	379.938	0.22	13	0.213	11	AGM
	$^4D^o_{5/2}$–$^4D_{5/2}$	382.681	0.30	15	0.281	11	VW
$(^3P)4p$–$(^3P)4d$	$^2D^o_{3/2}$–$^4D_{1/2}$	403.138	0.07	60	0.075	14	VW
$(^1D)4p$–$(^1D)4d$	$^2D^o_{3/2}$–$^2D_{5/2}$	379.659	0.18	23	0.148	11	AGM
	$^2D^o_{5/2}$–$^2D_{5/2}$	380.317	0.89	12	0.876	11	AGM
$(^1D)4p$–$(^1D)4d$	$^2D^o_{3/2}$–$^2P_{3/2}$	381.902	0.15	49	0.166	12	AGM
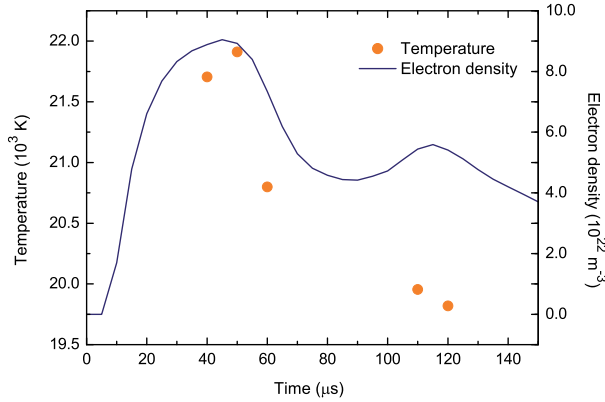
Figure 4. Electron density and temperature evolution in the course of the plasma life.

Following the recommendation made by Vujnović & Wiese (1992), we have paid very careful attention to the estimation of the uncertainty for each of the A_{TW}-values. In order to accomplish this task in a consistent and objective manner, we have estimated the uncertainty of each line by taking into account the following aspects.

(a) Standard deviation (σ): it is the standard deviation of the A_{TW}-value.

(b) Self-absorption coefficient of the spectral lines (SA): it is the fraction that is necessary to add in order to reconstruct the spectral line of interest. For each line, this coefficient is obtained from the ratio between the increment in the peak intensity due to the reconstruction procedure and this peak intensity on the original profile (Aparicio 1996). When there are not self-absorption effects, the increment is null and consequently this SA coefficient is also null. We have excluded from our results all the Ar II lines whose SA is greater than 0.2.

(c) Background-peak (BP): ratio between the background intensity and the maximum height of the line.

(d) Overlap with the adjacent left (O_L) or right (O_R) line: this quantity is given by the next expression:

$$O_i = \frac{w + w_i}{d} \frac{I_i}{I} \qquad (1)$$

where i represents left (L) or right (R), w and w_i are the half-widths of the line under study and the adjacent lines (left or right), respec-

tively, and d is the distance between the peaks of the line under study and the adjacent one. The second factor contains the ratio between the intensity of the adjacent line (I_i) and the intensity of the studied line (I). The uncertainty U_{TW} of each spectral line, in percentage, has been calculated with the next mathematical expression that takes into account each of the aspects discussed previously:

$$U_{TW}(\text{per cent})$$
$$= 100\sqrt{\sigma^2 + (2(SA)^2)^2 + \left(\frac{BP}{2}\right)^2 + \left(\frac{O_L}{20}\right)^2 + \left(\frac{O_R}{20}\right)^2}. \quad (2)$$

In general, the equation (2) tends to overestimate the uncertainty. Only spectral lines whose U_{TW} is lower than 60 per cent have been included in Table 2, except for two, 326.899 nm (84 per cent) and 367.326 nm (70 per cent). In these cases, the new values have been considered relevant due to the absence of previous data. We obtained the lowest uncertainty for the intense and well-isolated lines, whereas the highest uncertainties were obtained in cases where the lines had poor intensities or the profiles, in spite of being well defined, were distorted due to the closeness of the neighbouring lines.

A detailed analysis of the A_{TW} and A_{Ref}-values reveals a systematic inconsistency between some of the data given by Kramida et al. (2014) and ours. Figs 5(a) and (b) compare the transition probability values taken from Vujnović & Wiese (1992) and from Rudko & Tang (1967), respectively, henceforth A_{VW} and A_{RT}, with those measured in this experiment. As can be seen from Fig. 5(a), the A_{VW}-values show very good agreement with A_{TW}. The linear regression fit has a y-intercept of 0.028 ± 0.016 and a slope of 0.999 ± 0.036. It is possible to observe how the A_{ki}-values in Fig. 5(a) are randomly distributed along the unit-slope line, giving a R^2 value of 0.985. As is shown in Fig. 5(b), the linear regression fit for A_{RT}-values has a y-intercept of -0.040 ± 0.087 and a slope of 2.204 ± 0.170 with an R^2 value of 0.848, which shows that the A_{RT}-values are 2.2 times larger than A_{TW} on average.

Some further analysis can be made by upper energy levels. Only the multiplet $^4P^o$–^4P from the transition 4p–4d contains enough spectral lines with transition probabilities measured in this work as well as by other authors. Fig. 6 (a) shows again the good agreement between VW and TW data. It is important to remark that, in case of the comparison with RT data, the linear behaviour is even improved (R^2=0.990) and the y-intercept is null within its error bar. Both A_{TW} and A_{VW} data are related with A_{RT} data simply by a factor. Regarding the multiplets with the upper level $(^3P)4d\,^2P$, Fig. 7 shows

Table 2. Ar II UV transition probabilities measured in this experiment, A_{TW}, and the available data of other authors, A_{Ref}. The experimental references are denoted as: Vujnović & Wiese (1992)-VW, Rudko & Tang (1967)-RT, Behringer & Thoma (1976)-BT, García & Campos (1985)-GC, and Pellerin et al. (1997)-PMDC. Theoretical references are denoted as: Statz et al. (1965)-SHKTK and Luyken (1972)-L. Theoretical data in A_{Ref} column are followed by *. Transitions and multiplets appear in the same order as in Kramida et al. (2014).

Transition	Multiplet	Wavelength (nm)	A_{TW} (10^8 s^{-1})	U_{TW} (per cent)	A_{Ref} (10^8 s^{-1})	U_{Ref} (per cent)	Ref	$A_{\text{Ref}}/A_{\text{TW}}$
(^{3}P)4s–(^{3}P)4p	^{4}P$_{5/2}$–^{2}P$^o_{3/2}$	384.541	0.010	21	0.002*		SHKTK	0.20
					0.016	22, C	VW	1.60
					0.0091	41, D	RT	0.91
					0.0134*		L	1.34
					0.0088*		L	0.88
(^{3}P)4s–(^{1}D)4p	^{2}P$_{3/2}$–^{2}P$^o_{3/2}$	294.289	0.42	33	0.53	11, B	VW	1.26
					0.453	12, D	RT	1.08
					0.252	14	GC	0.60
	^{2}P$_{1/2}$–^{2}P$^o_{3/2}$	303.351	0.073	11	0.099	11, B	VW	1.41
					0.0876	12, D	RT	1.25
					0.0807*		L	1.15
					0.0341*		L	0.49
					0.088	15	BT	1.26
					0.077	12	GC	1.10
(^{3}P)3d–(^{1}D)4p	^{2}P$_{3/2}$–^{2}P$^o_{1/2}$	368.254	0.034	45	0.017	14, B	VW	0.57
					0.00165	8, D	RT	0.06
					0.0395*		L	1.32
					0.0088*		L	0.29
(^{3}P)4p–(^{3}P)5s	^{4}P$^o_{1/2}$–^{4}P$_{1/2}$	366.960	0.09	17	0.126	8, D	RT	1.40
	^{4}P$^o_{5/2}$–^{4}P$_{3/2}$	367.827	0.17	12	0.254	32, D	RT	1.49
(^{3}P)4p–(^{3}P)4d	^{4}P$^o_{5/2}$–^{4}F$_{3/2}$	319.423	0.086	12	0.236	36, D	RT	2.62
	^{4}P$^o_{1/2}$–^{4}F$_{3/2}$	326.357	0.13	11	0.155	15, B	VW	1.19
					0.348	36, D	RT	2.68
					0.127	15	BT	0.98
	^{4}P$^o_{5/2}$–^{4}F$_{7/2}$	326.899	0.002	84				
	^{4}P$^o_{5/2}$–^{4}P$_{5/2}$	313.902	0.49	18	0.52	31, C	VW	1.06
					1.00	27, D	RT	2.04
	^{4}P$^o_{3/2}$–^{4}P$_{5/2}$	316.967	0.43	18	0.49	32, C	VW	1.14
					0.817	27, D	RT	1.90
					0.435	15	BT	1.01
	^{4}P$^o_{5/2}$–^{4}P$_{3/2}$	318.104	0.36	12	0.37	30, C	VW	1.03
					0.627	21, D	RT	1.74
					0.372	15	BT	1.03
(^{3}P)4p–(^{3}P)4d	^{4}P$^o_{3/2}$–^{4}P$_{1/2}$	324.369	1.07	11	1.056	31, C	VW	0.98
					1.99	26, D	RT	1.86
					0.937	15	BT	0.87
	^{4}P$^o_{1/2}$–^{4}P$_{3/2}$	324.980	0.60	14	0.63	31, C	VW	1.05
					1.00	21, D	RT	1.67
					0.621	15	BT	1.04
	^{4}P$^o_{1/2}$–^{4}P$_{1/2}$	328.170	0.41	11	0.42	31, C	VW	1.02
					0.733	26, D	RT	1.79
					0.393	15	BT	0.96
	^{4}D$^o_{3/2}$–^{4}D$_{1/2}$	384.152	0.19	12	0.269	14, B	VW	1.42
					0.267	19, D	RT	1.41
					0.2455	10	PMDC	1.29
	^{4}D$^o_{5/2}$–^{4}D$_{7/2}$	384.473	0.049	17	0.048	15, B	VW	0.96
					0.0474	28, D	RT	0.95
(^{3}P)4p–(^{1}D)3d	^{4}D$^o_{3/2}$–^{2}S$_{1/2}$	385.614	0.066	18				
(^{3}P)4p–(^{3}P)4d	^{2}D$^o_{3/2}$–^{2}P$_{3/2}$	320.432	0.24	12	0.402	53, D	RT	1.68
	^{2}D$^o_{3/2}$–^{2}P$_{1/2}$	327.332	0.20	16	0.371	6, D	RT	1.86
	^{2}D$^o_{5/2}$–^{2}D$_{5/2}$	295.539	0.19	13				
	^{2}D$^o_{3/2}$–^{2}D$_{5/2}$	301.448	0.039	19	0.043	15	BT	1.08
	^{2}P$^o_{3/2}$–^{4}F$_{3/2}$	383.017	0.042	27				
	^{2}P$^o_{3/2}$–^{2}F$_{5/2}$	365.528	0.37	13	0.232	26, D	RT	0.63
	^{2}P$^o_{3/2}$–^{2}P$_{3/2}$	329.364	0.59	17	1.73	53, D	RT	2.93
	^{2}P$^o_{1/2}$–^{2}P$_{1/2}$	330.723	1.43	11	3.35	6, D	RT	2.34

Table 2 – *continued*

Transition	Multiplet	Wavelength (nm)	A_{TW} $(10^8\ \mathrm{s}^{-1})$	U_{TW} (per cent)	A_{Ref} $(10^8\ \mathrm{s}^{-1})$	U_{Ref} (per cent)	Ref	$A_{\mathrm{Ref}}/A_{\mathrm{TW}}$
	$^2P^o_{3/2}-^2P_{1/2}$	336.658	0.24	15	0.409	6, D	RT	1.70
	$^2S^o_{1/2}-^2P_{3/2}$	338.853	0.81	12	1.91	53, D	RT	2.36
	$^2S^o_{1/2}-^2D_{3/2}$	316.137	0.35	45	1.83	56, D	RT	5.23
$(^1D)3d-(^3P_2)4f$	$^2F_{5/2}-^2[3]^o_{7/2}$	316.529	0.038	27				
	$^2F_{7/2}-^2[3]^o_{7/2}$	318.617	0.02	33				
$(^1D)3d-(^3P_1)4f$	$^2F_{5/2}-^2[4]^o_{7/2}$	304.608	0.095	15				
	$^2F_{7/2}-^2[4]^o_{9/2}$	306.689	0.086	14				
$(^1D)4p-(^1D)4d$	$^2F^o_{5/2}-^2F_{5/2}$	335.092	0.90	13	1.48	16, D	RT	1.64
	$^2F^o_{7/2}-^2F_{5/2}$	336.552	0.075	18	0.131	16, D	RT	1.64
	$^2F^o_{7/2}-^2F_{7/2}$	337.644	0.74	13	1.49	2, D	RT	2.01
	$^2P^o_{3/2}-^2P_{3/2}$	366.044	0.73	11	2.22	22, D	RT	3.04
	$^2P^o_{3/2}-^2P_{1/2}$	367.101	0.23	31	0.709	D	RT	3.08
	$^2P^o_{1/2}-^2D_{3/2}$	368.006	0.59	19	1.15	28, D	RT	1.95
$(^1D)4p-(^3P)6s$	$^2P^o_{1/2}-^2P_{3/2}$	367.326	0.11	70				
$(^1D)4p-(^1D)4d$	$^2P^o_{3/2}-^2S_{1/2}$	302.675	1.03	21				
$(^1D)3d-(^3P_1)5f$	$^2D_{3/2}-^2[2]^o_{5/2}$	300.296	0.062	28				
$(^1D)4p - (^1D)4d$	$^2D^o_{5/2}-^2P_{3/2}$	382.567	0.33	55	0.756	22, D	RT	2.29
					0.7600	35	PMDC	2.30
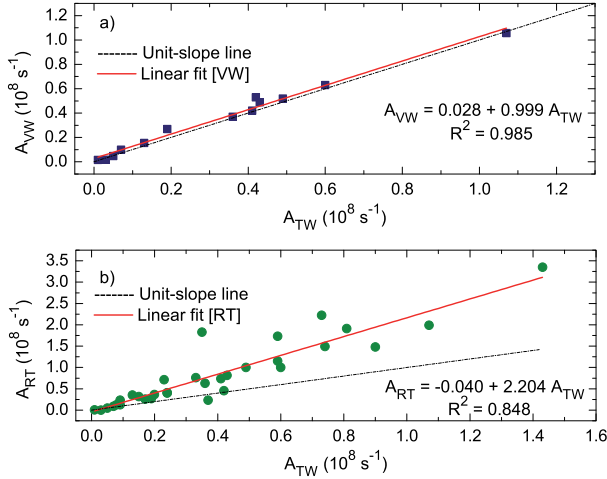
Figure 5. Comparison of the transition probabilities measured in this experiment A_{TW} with (a) those from Vujnović & Wiese (1992) compilation, and (b) those from Rudko & Tang (1967).

Figure 6. Comparison of the transition probabilities measured in this experiment A_{TW} for the multiplet $^4P^o$–^4P from the transition 4p–4d with (a) those from Vujnović & Wiese (1992) compilation, and (b) those from Rudko & Tang (1967).

the comparison between A_{RT} and ours. In this case, the line of fit has a y-intercept of -0.092 ± 0.124 and a slope of 2.491 ± 0.170 with an R^2 value of 0.978, once more higher than that obtained in Fig. 5 (b). The A_{RT}-values for this multiplet are systematically 2.5 times larger than A_{TW} on average. All these analyses agree with some of the ideas suggested by Vujnović & Wiese (1992), according to which atomic lifetime values for 4p and 4d levels from Rudko & Tang (1967) are underestimated. These discrepancies with some of the data from Rudko & Tang (1967) are not contemplated in the erratum from Rudko & Tang (1968).

Finally, our data show very good agreement with the experimental data from Behringer & Thoma (1976). Unfortunately, there are only eight results from these authors, five of them belong to the multiplet 4d^{4}P and are in good agreement with Vujnović & Wiese (1992) data.

4 CONCLUSIONS

This paper reports reliable and new A_{ki}-values for UV Ar II spectral lines extending much further the experimental work performed by Aparicio et al. (1997) in our laboratory. In this experiment, we have measured 43 ionized argon spectral lines in the ultraviolet region from 294 to 386 nm, yielding 11 new transition probabilities for which there are no previous available experimental data, at least up to the authors' knowledge, and 22 A_{ki}-values for which the existing data have uncertainties around 50 per cent.

We have paid special attention to all the possible sources of experimental uncertainty that are likely to affect our transition probability measurements. In addition, the measured A_{ki}-values have been carefully studied and compared with the existing data, finding a significant lack of self-consistency in the Kramida et al. (2014) data base worth analysing.
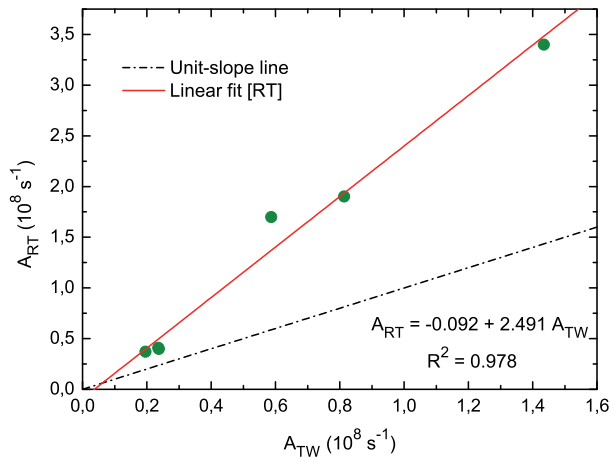
Figure 7. Comparison of A_{TW} with A_{RT} for lines coming from the multiplets with the upper level $(^3P)4d^2P$.

Finally, the results given here can extend the present data base of measured Ar II transition probabilities to the UV region and many of them could be useful in refining new theoretical models.

REFERENCES

Adelman S. J., 1998, MNRAS, 296, 856
Aparicio J. A., 1996, PhD thesis, Universidad de Valladolid
Aparicio J. A., Gigosos M. A., Mar S., 1997, J. Phys. B, 30, 3141
Aparicio J. A., Pérez C., del Val J. A., Gigosos M. A., de la Rosa M. I., Mar S., 1998, J. Phys. B, 31, 4909

Behringer K., Thoma P., 1976, J. Quant. Spectrosc. Radiat. Transfer, 16, 605
de la Rosa García M. I., Pérez García Ma . C., de Frutos Baraja A. M., Mar Sardaña S., 1990, Phys. Rev. A, 42, 7389
del Val J. A., Mar S., Gigosos M. A., de la Rosa I., Pérez C., González V., 1998, Japan. J. Appl. Phys., 37, 4177
Djurovic S., Mar S., Peláez R. J., Aparicio J. A., 2011, MNRAS, 414, 1389
Fedchak J. A., Lawler J. E., 2001, J. Quant. Spectrosc. Radiat. Transfer, 68, 483
García G., Campos J., 1985, J. Quant. Spectrosc. Radiat. Transfer, 34, 85
Gigosos M. A., Mar S., Pérez C., de La Rosa I., 1994, Phys. Rev. E, 49, 1575
Griem H. R., 1963, Phys. Rev., 131, 1170
Griem H. R., 1964, Plasma Spectroscopy. McGraw-Hill, New York
Griem H. R., 1997, Principles of Plasma Spectroscopy. Cambridge Univ. Press, Cambridge
Keenan F. P., Bates B., Dufton P. L., Holmgren D. E., Gilheany S., 1990, ApJ. 348, 322
Lanz T., Cunha K., Holtzman J., Hubeny I., 2008, ApJ. 678, 1342
Lochte-Holtgreven W., 1968, in Lochte-Holtgreven W, ed., Plasma Diagnostics. North-Holland, Amsterdam, p. 135
Lodders K., 2008, ApJ, 674, 607
Lovis C., Pepe F., 2007, A&A, 468, 1115
Luyken B. F. J., 1972, Physica, 60, 432
Murphy M. T., Tzanavaris P., Webb J. K., Lovis C., 2007, MNRAS, 378, 221
Kramida A., Ralchenko Yu., Reader J., NIST ASD Team, 2014, NIST Atomic Spectra Database (version 5.2), Available at: http://physics.nist.gov/asd
Pellerin S., Musiol K., Dzierzega K., Chapelle J., 1997, J. Quant. Spectrosc. Radiat. Transfer, 57, 359
Rudko R. I., Tang C. L., 1967, J. Appl. Phys., 38, 4731
Rudko R. I., Tang C. L., 1968, J. Appl. Phys., 39, 4046
Statz H., Horrigan F. A., Koozekanani S. H., Tang C. L., Koster G. F., 1965, J. Appl. Phys., 36, 2278
Vujnović V., Wiese W. L., 1992, J. Phys. Chem. Ref. Data, 21, 919
Wiese W. L., 1988, J. Quant. Spectrosc. Radiat. Transfer, 40, 421
Wiese W. L., Smith M. V., Miles B. M., 1969, Atomic Transition Probabilities, Vol. II, Sodium Through Calcium, NSRDS-NBS 22. National Stand. Ref. Ser., Nat. Bur. Stand., Washington, DC

This paper has been typeset from a TEX/LATEX file prepared by the author.

Chapter 6

Measurement of Transition Probabilities in Kr II UV spectral lines.

> *"There is a crack in everything.*
> *Thats how the light gets in."*
>
> - Leonard Cohen, *Anthem* -

Krypton is present in many light sources and lasers as the working gas. It is used in fusion experiments and is one of the inert gases employed in spectral lamp production and development. Its importance also extends to the field of astrophysics, where transition probabilities are necessary for the analysis of high-resolution stellar spectra used to estimate chemical abundances in stellar atmospheres, the interstellar medium and the solar wind.

However, there is still a significant shortage of atomic parameters regarding this noble gas. The NIST spectral database reports 410 spectral lines for Kr II within the range 208-360 nm, but there are fewer than ten transitions with known A_{ki}-values. This data highlights the need for new atomic parameters. The goal of this study is to measure accurate transition probabilities of singly ionized Krypton in the ultraviolet region, considerably upgrading the databases with new high quality values. The bibliography and a

detailed description of the recent developments in the field can be found in the accompanying article.

6.1   Experimental details.

The experimental transition probabilities, expressed in absolute units, have been obtained by measuring the relative intensities of the spectral lines emitted by a plasma and using some A_{ki}-values taken from the literature as a reference. The plasmas were generated in a low-pressure-pulsed discharge lamp.

The experimental set-up has already been described in detail in Chapter 2 and, therefore, we will only include a summary of the measurement conditions used in this work. Further experimental details are provided in the accompanying article. The plasma was produced inside a cylindrical tube of Pyrex, 175 mm in length and 19 mm in interior diameter. Krypton at a pressure of 120 Pa flowed continuously at a rate of 0.3 sccm. The pressure of krypton was adjusted to obtain minimal self-absorption and maximum intensity.

Table 6.1: Experimental measurement conditions.

Lamp running conditions	
Xe pressure	120 Pa
Xe flow	0.3 sccm
Discharge voltage	7.8 kV
Optical parameters	
Spectroscopic channel pinholes	$\phi = 2.5$ mm (D1 and D2 in Fig. 2.5)
Width of the entrance slit	35 μm
Diffraction order	1
Acquisition parameters	
Camera	ICCD 4 Quick E S20
Measurement instants	50, 60, 100, 110, 130 μs
Exposure time	2-5 μs
Spectral interval	208-360 nm

Plasma was created by discharging a capacitor bank of 20 μF through the discharge tube. The capacitor bank was charged up to 7.8 kV. The lifespan of the plasma was about

200 μs. Spectral lines were recorded at five different instants from 50 to 130 μs after the beginning of the discharge. All the krypton lines were recorded in the first order of diffraction and the exposure time ranged from 2 to 5 μs, depending on the particularities of each spectrum. For each instant, 10 different spectra were recorded, three of them with the self-absorption control mirror and seven without it. Table 6.1 lists all the measurement conditions used during this experiment.

We carried out both a spectroscopic and interferometric end-on analysis throughout the plasma's lifespan. The excitation temperature, the most important plasma parameter for the measurement of the transition probabilities, was determined by means of several Boltzmann-plots of some measured singly ionized krypton lines for which the transition probabilities were taken from the bibliography. This temperature ranged between 28 000 and 35 000 K with an uncertainty of around 5% calculated from the standard deviation of the slope in a non-weighted linear fit of the Boltzmann-plot. If we include the uncertainties of the reference data by performing a weighted linear fit, this error rises to 25%.
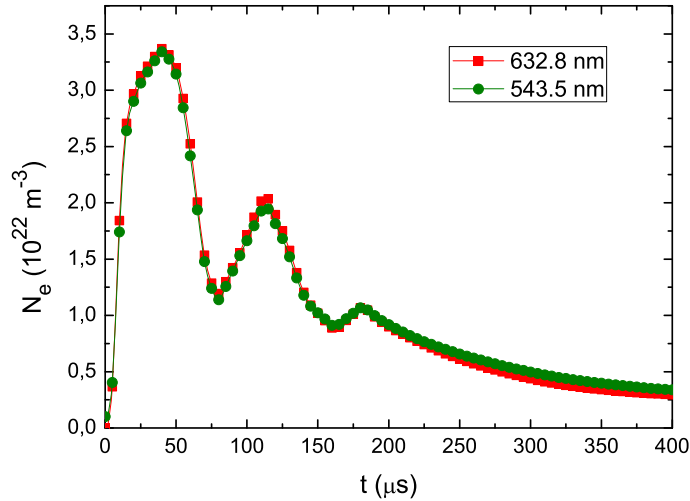
Figure 6.1: Temporal evolution of electron density in the Kr II experiment.

Electron density, in the range of $(1.5 - 3.4) \times 10^{22}$ m^{-3}, was obtained from a two-wavelength interferometric method that allows the change in the refractivity index, caused by the contribution of heavy particles, to be accounted for. The estimated errors of this magnitude ranged between 5 and 10%. Fig 6.1 shows the evolution of the electron density throughout the plasma's lifespan.

Several tests support the assumption that our plasma is well described by a pLTE model, at least within the interval of the upper energy levels considered, from 17.0 to 21.5 eV. One example is the linearity of the fit in Boltzmann plots, the R^2 coefficients of which take values of around 0.99. An additional check suggests that pLTE is satisfied for those atomic states for which the principal quantum number of which is larger than 3 and electron densities are larger than 10^{22} m^{-3}. This corroborates the existence of pLTE for all the upper energy levels considered in this experiment.

6.2   Results and discussion.

This article provides 93 measured transition probabilities (A_{ki}) for singly ionized krypton spectral lines in the ultraviolet region ranging from 208 nm to 360 nm. For 86 of them there is no previous data, at least to the best of the authors' knowledge. We have paid special attention to the calculation of the relative uncertainties introduced by our method of measuring, considering all the possible sources of error. These uncertainties are lower than 15% for almost all of the values reported.

Due to the lack of experimental data for transition probabilities in the UV region, there is only a small number of results from other authors to compare our own findings with. Our values have been contrasted with those from Dzierżega et al. (2001), one of the most comprehensive studies carried out recently into Kr II obtained in a branching ratio-lifetime experiment. The comparison with our data is particularly interesting because it provides a very useful mathematical expression with which to relate the transition probabilities obtained in a *'branching ratio-lifetime'* experiment with those measured with a scale based on a set of pre-existing A_{ki}-values simply by using a factor.

Kr II transition probability measurements for the UV spectral region

M. T. Belmonte,[1][*] L. Gavanski,[2] R. J. Peláez,[3] J. A. Aparicio,[1][*] S. Djurović[2]
and S. Mar[1][*]

[1]*Departamento de Física Teórica, Universidad de Valladolid, Atómica y Óptica, Paseo de Belén 7, E-47011 Valladolid, Spain*
[2]*Faculty of Sciences, Department of Physics, University of Novi Sad, Trg Dositeja Obradovića 4, 21000 Novi Sad, Serbia*
[3]*Laser Processing Group, Instituto de Óptica, CSIC, Serrano 121, E-28006 Madrid, Spain*

ABSTRACT

The determination of radiative transition probabilities or oscillator strengths is of common interest in astrophysics. The analysis of the high-resolution stellar spectra is now available in order to estimate the stellar abundances. In this paper, 93 experimentally obtained transition probability values (A_{ki}) for singly ionized krypton spectral lines belonging to the ultraviolet (UV) wavelength region (208–360) nm are presented. These data, expressed in absolute units, were derived from the measurements of relative spectral line intensities and the values of transition probability data taken from the literature. The results obtained extend considerably the transition probability data base. As a light source, a plasma from a low-pressure pulsed arc was used. Its electron density was in the range of $(1.5–3.4) \times 10^{22}$ m^{-3}, while the temperature was between 28 000 and 35 000 K. A detailed analysis of the results is also given. Only a few relative and a few absolute transition probabilities from other authors, for the mentioned spectral region, are available in the literature.

Key words: line: profiles – plasmas – techniques: spectroscopic.

1 INTRODUCTION

Krypton is present in many light sources and lasers as the working gas (Shimoda 1984), it is one of the inert gases used in spectral lamp production and development (Cayless & Marsden 1983) and it also appears in fusion experiments (Loch et al. 2002). On the basis of the measurements of Planetary Nebulae spectra, it was found that krypton is one of the most abundant elements in the cosmos with $Z > 32$ (Dinerstein 2001; Sharpee et al. 2007). It has been detected in stellar atmospheres (Bidelman 1962), in the interstellar medium (Cardelli, Savage & Ebbets 1991; Cardelli & Meyer 1997), in the solar wind (Morton 2000) and recently in a white dwarf (Werner et al. 2012). Krypton is used as propellant in electric propulsion systems and Kr II spectral lines are used for the characterization of ions' velocity distribution functions by means of laser fluorescence in Hall thrusters (Mazouffre & Pawelec 2009). Transition probabilities data are of fundamental importance in the determination of plasma temperatures from the intensities of the spectral line radiation (Griem 1964). Radiative lifetimes for forbidden transitions of ultraviolet (UV) Kr II lines have been analysed recently (Träbert 2012; Saito et al. 2015), but there are not so many papers devoted to electric dipole UV Kr II transition probability measurements. The papers Marantz, Rudko & Tang (1969), Miller, Roig & Bengtson

(1972), Fonseca & Campos (1982) and Djeniže, Milosavljević & Dimitrijević (2003) report relative transition probabilities, mostly for transitions in the visible part of the spectrum. Only the paper Fonseca & Campos (1982) reports relative results for several UV transitions. Transition probability results in absolute units are given in Podbiralina, Smimov & Stegnova (1973), Helbig (1978), Brandt, Helbig & Nick (1982), Bertuccelli & Di Rocco (1991), Dzierżega et al. (2001), de Castro et al. (2001), Rodríguez et al. (2001) and Mar et al. (2006) and they generally cover the wavelength region between 360 and 714 nm. Results for a wide wavelength region (200–2400 nm) have only been reported in Dzierżega et al. (2001). Some authors report data about lifetime measurements (Fonseca & Campos 1982; Schade et al. 1989; Das & Bhattacharya 1992; Jullien et al. 1993; Das 1997; Lauer et al. 1999).

We can divide the experimental transition probability data found in the bibliography for the UV region into two different groups, depending on the method used for the measurement of the A_{ki} values. Results from Helbig (1978) have been obtained by quantitative spectroscopy of a plasma source in local or partial local thermodynamic equilibrium (pLTE). As mentioned in Dzierżega et al. (2001), this method has to deal with uncertainties around 20 per cent due to the difficulties to either characterize the source or achieve thermal equilibrium conditions. Results from Podbiralina et al. (1973) and Dzierżega et al. (2001) have been obtained by normalizing measured branching ratios with upper-level lifetime data. This method has a disadvantage concerning the necessity of measuring all the possible transitions from this upper level. In this article, we compare our

[*]E-mail: teruca@opt.uva.es (MTB); juanantonio.aparicio@uva.es (JAA); santiago@opt.uva.es (SM)

new data, which have been measured by quantitative spectroscopy, with data from Dzierżega et al. (2001) obtained in a branching ratio experiment. This comparison is especially interesting because it relates data obtained by the two different methods.

In this paper, we continue with the measurements of A_{ki} values carried out in our laboratory (de Castro et al. 2001; Rodríguez et al. 2001; Mar et al. 2006) for Kr II, extending the spectral range to the UV. We report absolute transition probability data for 93 Kr II lines belonging to 69 multiplets within the 208–360 nm spectral range. These values were obtained by measuring the relative intensities of the spectral lines under study. In order to transform our relative measurements into absolute ones, we have selected seven spectral lines and taken their transition probability value from the bibliography (Mar et al. 2006; Kramida et al. 2015). The measurements were carried out by using a plasma produced in a low-pressure pulsed arc as a light source. The electron density, which was in the range of $(1.5–3.4) \times 10^{22}$ m^{-3}, was determined by using a two-wavelength interferometric method. The plasma temperature is the most important plasma parameter for the measurement of the transition probabilities. The excitation temperature, in the range of 28 000–35 000 K, was determined by using the Boltzmann-plot method for seven spectral lines whose transition probabilities were taken from the bibliography (Mar et al. 2006; Kramida et al. 2015). It should also be noted here that the plasma conditions satisfy the pLTE criterion for all the considered instants of measurement.

2 EXPERIMENT

2.1 Set-up

The spectral line intensities have been measured from a low-pressure pulsed arc plasma source. More details concerning the experimental arrangement can be found in Gigosos et al. (1994), Val et al. (1998) and Ćirišan et al. (2011). Here, only a short description will be given for completeness. The discharges were carried out through a cylindrical tube made of Pyrex glass, 175 mm long and 19 mm in internal diameter. Pure krypton at a pressure of 120 Pa was continuously flowing through the discharge tube at a rate of 0.3 sccm. Plasma pulses were created by discharging a capacitor bank of 20 μF through the discharge tube. The capacitor bank was charged up to 7.8 kV. The plasma life was about 200 μs. In order to ensure the plasma reproducibility, the gas in the tube was pre-ionized by using a continuous current of several mA. The discharge tube has been designed to avoid sputtering as much as possible (Val et al. 1998). In spite of this fact, the windows closing the tube were replaced every 800 discharges in order to reduce the optical transmittance loss to values under 5 per cent. Furthermore, the electrodes were polished several times during the experiment.

The spectra were recorded by using a Jobin–Yvon spectrometer, 1.5 m focal length, with a UV holographic grating, 2400 lines mm^{-1}. The spectral resolution of our spectrometer has already been calibrated (Peláez et al. 2012) and it is 3 pm per channel approximately within the working spectral range of this experiment. This resolution gives an idea of the ability of our device to resolve very close spectral lines and it will be important for further discussion. The spectrometer was equipped with an intensified charge-coupled device (ICCD) as a photo-detector. The spectra were taken along the discharge tube, 2 mm off the tube axis, at the instants 50, 60, 100, 110 and 130 μs after the beginning of the discharge. The exposure time varied between 2 and 5 μs and it was adjusted to obtain maximal intensity and avoid the saturation of the ICCD camera. The plasma light was limited by two diaphragms, 3 mm in diame-
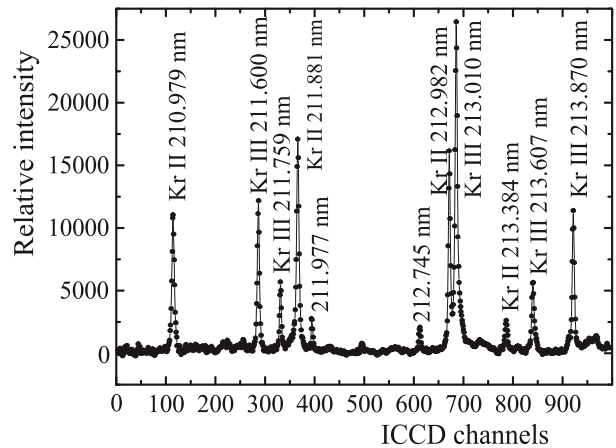

Figure 1. Recorded spectrum of ionized krypton.

ter, and focused by a concave mirror, 150 mm focal length, on to the entrance slit of the spectrometer. This ensures the observation of a homogeneous column along the plasma with a variation in the electron density and temperature less than 5 per cent (Peláez et al. 2005).

The possible self-absorption effect was checked by means of a mirror placed behind the discharge tube. The pressure of the krypton was adjusted to obtain maximal intensity with minimal self-absorption, which allows us to reconstruct the line profile very precisely. All the lines whose self-absorption was higher than 20 per cent were dismissed. For each instant, 10 different runs were recorded in order to increase the signal-to-noise ratio. Three of these profiles were recorded with the self-absorption control mirror and seven without it. The consecutive spectra registered for the same plasma conditions differ in less than 5 per cent. One of the recorded spectra of ionized krypton is shown in Fig. 1. It can be seen from this figure that the recorded spectral line profiles were clear and well defined. This allows us to obtain high-quality experimental parameters.

2.2 Plasma diagnostics

Special care was taken with the plasma diagnostic. Spectroscopic and interferometric end-on measurements have been made simultaneously throughout the plasma life. The measurements have been taken 2 mm off the lamp axis from symmetrical positions referred to it. For the electron density determination, a two-wavelength interferometric technique was applied by making two laser beams of 543.5 and 632.8 nm to pass through the discharge tube in the axial direction. The discharge tube was placed in one of the arms of a Michelson interferometer with a Twyman–Green configuration. This two-wavelength interferometric method allows us to account for the contribution of the heavy particles to the change of the refractivity index (Aparicio et al. 1998). The high-axial homogeneity and the very good cylindrical symmetry of the electron density and the temperature in this lamp (Val et al. 1998) allow this. The electron density, in the range of $(1.5–3.4) \times 10^{22}$ m^{-3}, was obtained with estimated errors between 5 and 10 per cent.

A good determination of the electron temperature is a very important aspect in the measurement of the transition probabilities. The Kr II excitation temperature was obtained from the Boltzmann-plot of some measured Kr II lines for which the transition probabilities were taken from the bibliography. We will refer to

Table 1. Selected wavelengths and transition probabilities from Kramida et al. (2015) – KRA – and Mar et al. (2006) – MAR – for the temperature determination.

Wavelength (nm)	E_k (eV)	g_k	A_{ref} $(10^8\,\text{s}^{-1})$	Ref.	A_{TW} $(10^8\,\text{s}^{-1})$
459.280	21.321	6	0.203	MAR	0.203
460.402	20.070	2	0.272	MAR	0.282
461.529	17.375	4	0.487	KRA	0.471
461.917	17.372	6	0.655	KRA	0.648
482.519	17.571	4	0.240	KRA	0.229
483.208	16.835	2	0.745	KRA	0.832
484.661	17.246	2	0.769	MAR	0.759

these lines as the reference lines. The transition probability values for these lines, A_{ref}, were taken from Kramida et al. (2015) and from Mar et al. (2006). The transition probabilities taken from Kramida et al. (2015) are classified like D by National Institute of Standards and Technology (NIST). The criterion used to select the reference lines was to use data from Kramida et al. (2015) in all cases except for those lines not measured and for which Mar et al. (2006) provide data. It is important to notice that the values from Kramida et al. (2015) belong to the doctoral thesis of Helbig (1978). These values were measured in a wall-stabilized arc and the population densities were calculated under the assumption of local thermodynamic equilibrium (LTE). Regarding the values from Mar et al. (2006), they were also derived by using the absolute scale proposed by Helbig (1978) and measured in an emission spectroscopy experiment by using a similar experimental set-up as the one described in this work, but with a different radiation detector. In Table 1, all the reference lines with their corresponding transition probabilities A_{ref} (Mar et al. 2006; Kramida et al. 2015) and energy values E_k (Kramida et al. 2015) are given. The third column contains the transition probability values measured in this work for the reference lines, A_{TW}. The relative uncertainty of these A_{TW} values introduced by our measuring method is around 10 per cent.

Fig. 2 shows the Boltzmann plots for each measurement instant throughout the life of the plasma, as well as the excitation temperature for the different instants. According to van der Mullen (1990), the excitation temperature takes similar values to the kinetic temperature in collision-dominated plasmas, like the plasma produced in this experiment. The linearity of the Boltzmann plots, with R^2 values of around 0.99, supports the assumption that our plasma is well described by a pLTE model, at least within the interval of the upper energy levels considered (17–21.5 eV). An additional check shows that pLTE is satisfied in this experiment for the atomic states whose principal quantum number is larger than 3 and for electron densities larger than 10^{22} m^{-3} (Griem 1963, 1997). This supports the existence of pLTE for all the upper energy levels considered in this work. The uncertainty in the temperature was calculated from the standard deviation of the slope in a non-weighted linear fit of the Boltzmann plot and it turned to be 5 per cent. If we include the uncertainties of the reference data by performing a weighted linear fit, this uncertainty raises up to 25 per cent.

3 TRANSITION PROBABILITY DATA DETERMINATION

The transition probability values were obtained by measuring the relative intensities of the spectral lines under study and using the transition probability data taken from the bibliography (Mar et al. 2006; Kramida et al. 2015) for the seven lines used as a reference.
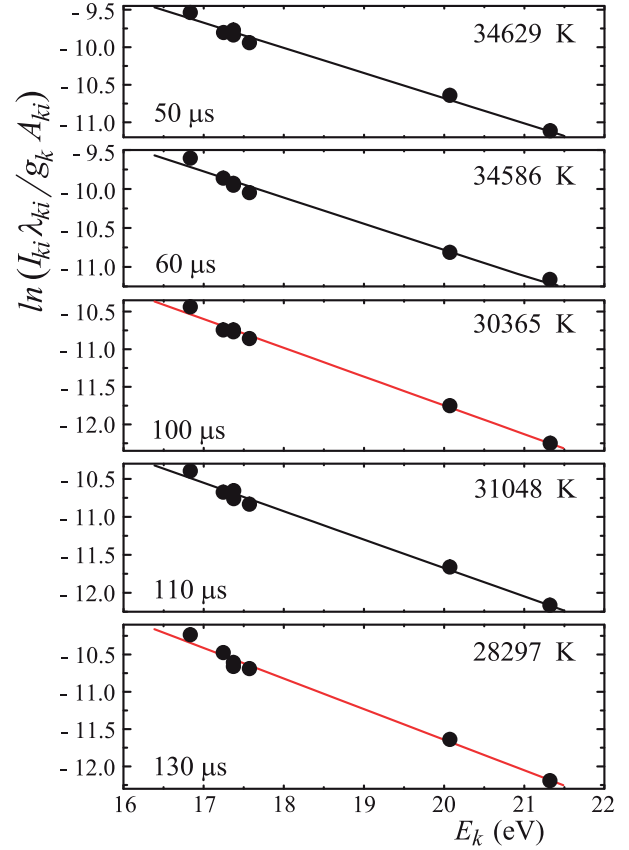

Figure 2. Boltzmann plots for different plasma instants.

Before carrying on with any calculations, the recorded spectra were corrected by the spectral response of the optical and the spectroscopic system. For that purpose, we used an calibrated incandescent lamp which emits like a blackbody at 3041 K for the visible region and a calibrated deuterium lamp for the UV. The uncertainty of the transmittance curve was estimated to be lower than 4 per cent. The corrected spectra were fitted to sums of Lorentzian functions, which represent the spectral line profiles, and a linear function, which represents the emission from the continuum (Djurović et al. 2006). The areas under the profiles were considered as the relative line intensities that were used for the determination of the transition probabilities. From the ratio between the intensity of two spectral lines of the same species and stage of ionization (the line under study and a reference line) and considering the equilibrium assumption, it is possible to obtain the equation 34 in Konjević (1999). Rearranging this equation, we can isolate the unknown transition probability value and express it as a function of known quantities:

$$A_{\text{ki}} = A_{\text{ref}} \frac{I_{\text{ki}}}{I_{\text{ref}}} \frac{\lambda_{\text{ki}}}{\lambda_{\text{ref}}} \frac{g_{\text{ref}}}{g_{\text{k}}} \exp^{\frac{E_{\text{ki}} - E_{\text{ref}}}{\text{kT}}}, \tag{1}$$

where g are the statistical weights and E the upper energy level of the considered transitions. This procedure was repeated for the five instants of the plasma life for which spectroscopic measurements were performed and using the intensities of the seven spectral lines used as reference (Table 1) and whose transition probabilities, A_{ref}, were taken from the bibliography (Mar et al. 2006; Kramida et al. 2015). As a whole, we obtained 35 values of A_{ki} for each of the spectral lines. The final A_{ki} result for each line was determined by

means of a weighted arithmetic mean. We calculated the weights from the uncertainty associated with our measurement of the area for every spectral line (Belmonte et al. 2014). This relative uncertainty was calculated by taking into account different aspects, such us the accuracy of the fitting, the self-absorption of the spectral line, the ratio between the background intensity and the maximum height of the line and the overlapping with the adjacent spectral lines. All these factors were added in quadrature to get the final value of the relative uncertainty.

4 EXPERIMENTAL RESULTS AND DISCUSSION

The experimentally obtained transition probability data for the Kr II spectral lines are given in Table 2. The table is arranged in order of increasing wavelength. The first column contains the wavelengths of the observed spectral lines, followed by the configuration, term and J value of the upper and lower energy levels of each transition. The notation for most of them has been taken from Kramida et al. (2015). The last column includes our transition probability results, A_{TW}, with their relative uncertainties in per cent shown in parentheses. As explained before, these relative uncertainties have been carefully calculated by following the method described in Belmonte et al. (2014). We would like to emphasize that the relative uncertainties included in Table 2 are the ones introduced by our experimental procedure and they do not take into account the uncertainty of the transition probabilities used as reference. The absolute uncertainty could be calculated by adding in quadrature our relative uncertainty and the one estimated by NIST for the reference A_{ki} values.

Several of the transitions in Table 2 present some characteristics and peculiarities which are worth mentioning.

(1) The line 210.979 nm is notated as $4s^24p^4(^3P)4d^4D_{3/2} - 4s^24p^4(^3P_2)4f^2[2]^o_{3/2}$ in our Table 2 and it has a relative intensity of 5 in Kramida et al. (2015). In this data base, there is an additional and very close line (210.988 nm) with the transition $4s^24p^4(^3P)5s^2P_{1/2} - 4s^24p^4(^3P_2)4f^2[2]^o_{3/2}$ and a relative intensity of 3. However, there is only one line at this wavelength, 210.981 nm, in Striganov & Sventitskii (1968) with the transition $4d^4D_{3/2} - 5f^2F^o_{3/2}$. From our recorded spectrum and fitting procedure, and keeping in mind that the spectral resolution of our spectrometer is around 3 pm per channel (Peláez et al. 2012), we can conclude that only one spectral line appears in our experiment (see Fig. 1).

(2) The terms and J values for the lower energy levels of 12 spectral lines are missing. Although the LS-coupling scheme has been used to describe the $4s^24p^4(^3P)4d$ levels, the coupling is not a pure LS one due to the mixing obtained with most of the levels of this configuration (El Sherbini & Farrag 1976). The maximum percentage of the components in the composition of these levels is 35 per cent. For this reason, the levels are not dominated by a particular component and they are only described by the total angular momentum.

(3) The configuration, term and J value for the upper and lower energy levels of seven of the spectral lines given in Table 2 are missing in Kramida et al. (2015). In this case, we used the notation from Striganov & Sventitskii (1968), even though it is also incomplete.

Due to the lack of experimental data for transition probabilities in the UV region (208–360 nm), there is only a small number of results from other authors to compare with our results. Some relative transition probability values are given in Fonseca & Campos (1982) and some absolute ones in Podbiralina et al. (1973) and Dzierżega

et al. (2001). The comparison among the absolute values is given in Table 3. The absolute results from Dzierżega et al. (2001) are in a relative good agreement with ours and they will be analysed in detail later. The comparison with Podbiralina et al. (1973) shows considerable discrepancies with both Dzierżega et al. (2001) and A_{TW}.

In Fig. 3, we compare our transition probability results, A_{TW}, with the experimental ones from Dzierżega et al. (2001), A_{DZ}. The work of Dzierżega et al. (2001) provides absolute transition probabilities for transitions from 5p and 5p' levels between 200 and 2400 nm determined by normalizing the experimentally measured branching ratios with a weighted mean of published upper level lifetime data. As can be seen from Fig. 3, the A_{DZ} values show a very good agreement with ours. The linear regression fit has a y-intercept of 0.036 ± 0.034 and a slope of 1.27 ± 0.085. It is possible to observe how the A_{ki} values in Fig. 3 are, in general, randomly distributed along the linear regression fit line, giving a R^2 value of 0.98. The fact that the y-intercept is almost zero seems natural since the transition probability values of the lines under study range between almost zero to one. This y-intercept reveals, among other things, that the spectral lines have been properly identified. The fact that the R^2 value is so close to one reflects the fact that our values (A_{TW}) and those from Dzierżega et al. (2001) (A_{DZ}) are in a relative good agreement. We can observe how the values from Dzierżega et al. (2001) and from our work could be taken as equivalent if we consider the 20 per cent of uncertainty inherent to the quantitative spectroscopy methods.

Two different aspects should be born in mind when trying to evaluate this discrepancy between our values and those from Dzierżega et al. (2001): the quality of the measurements made and the scale used to transform these measurements into absolute transition probability values. These two aspects can be evaluated both for A_{DZ} and A_{TW}. On the one hand, regarding A_{TW}, the relative intensities of the spectral lines were carefully measured to avoid any kind of systematic error. In this case, the values from the thesis of Helbig (1978) constitute the absolute scale selected by us to transform our relative measurements to absolute ones, since all the data measured in our laboratory (de Castro et al. 2001; Rodríguez et al. 2001; Mar et al. 2006) come from this scale. The A_{ki} values from the thesis of Helbig (1978) have been traditionally considered to be some of the most accurate data available for Kr II (Ward et al. 1985), as proves the fact that they have been selected for several compilations and handbooks of basic atomic spectroscopic data (Fuhr & Wiese 1996, 1998; Sansonetti & Martin 2005). On the other hand, the branching ratios measured by Dzierżega et al. (2001) were normalized to absolute transition probabilities by using a weighted mean value calculated from very carefully chosen values of upper-level lifetimes. This set of lifetimes defines the Dzierżega et al. (2001) scale.

Both types of experiments, Dzierżega et al. (2001) and this work, have strengths and weaknesses and it is very difficult to establish which the absolute scale is. However, Fig. 3 reveals that both absolute scales are not so different and it makes it possible to relate them in a precise and simple way. Since the y-intercept is almost null within its error bar and the R^2 is close to 1, both sets of values A_{DZ} and A_{TW} are simply related by a factor, which implies that rescaling our data to those from Dzierżega et al. (2001) can be done easily just by using the slope of the fitting in Fig. 3. The data from Helbig (1978) and Mar et al. (2006) and therefore, ours in this work, present a good agreement and can be adjusted to another absolute scale by using an appropriate scaling factor. The Boltzmann plots with all our measured A_{ki} data for every instant have been used as a way of checking the general behaviour of our results. Fig. 4 shows

Table 2. Measured transition probability data for the Kr II spectral transitions.

λ (nm)	E_{upper} (eV)	E_{lower} (eV)	Upper level Conf.	Term	J	Lower level Conf.	Term	J	A_{TW} (10^8 s^{-1})
208.673	20.844	14.904	$4s^24p^4(^3P_2)4f$	$^2[4]^o$	7/2	$4s^24p^4(^3P)4d$	^4D	7/2	0.24(11)
208.815	20.840	14.904	$4s^24p^4(^3P_2)4f$	$^2[4]^o$	9/2	$4s^24p^4(^3P)4d$	^4D	7/2	0.700(11)
209.337	20.852	14.931	$4s^24p^4(^3P_2)4f$	$^2[3]^o$	5/2	$4s^24p^4(^3P)4d$	^4D	5/2	0.36(11)
209.623	20.844	14.931	$4s^24p^4(^3P_2)4f$	$^2[4]^o$	7/2	$4s^24p^4(^3P)4d$	^4D	5/2	0.600(11)
210.979	20.877	15.002	$4s^24p^4(^3P_2)4f$	$^2[2]^o$	3/2	$4s^24p^4(^3P)4d$	^4D	3/2	0.52(11)
211.881	20.852	15.002	$4s^24p^4(^3P_2)4f$	$^2[3]^o$	5/2	$4s^24p^4(^3P)4d$	^4D	3/2	0.51(11)
221.172	21.465	15.861	$4s^24p^4(^3P_1)4f$	$^2[3]^o$	7/2	$4s^24p^4(^3P)4d$	^4F	7/2	0.022(15)
221.296	21.421	15.820	$4s^24p^4(^3P_1)4f$	$^2[2]^o$	5/2	$4s^24p^4(^1D)5s$	^2D	3/2	0.033(14)
222.793	21.425	15.861	$4s^24p^4(^3P_1)4f$	$^2[4]^o$	9/2	$4s^24p^4(^3P)4d$	^4F	7/2	0.24(11)
228.779	21.27	15.85	$4s^24p^4(^1D)5d$	6°	7/2	5s'	^2D	5/2	0.49(11)
230.174	21.465	16.080	$4s^24p^4(^3P_1)4f$	$^2[3]^o$	7/2	$4s^24p^4(^3P)4d$	^4F	5/2	0.069(11)
231.202	18.875	13.514	$4s^24p^4(^1D)5p$	$^2P^o$	1/2	$4s4p^6$	^2S	1/2	0.084(11)
231.424	21.414	16.058	$4s^24p^4(^3P_1)4f$	$^2[2]^o$	3/2	$4s^24p^44d$		1/2	0.22(11)
231.553	21.534	16.182	$4s^24p^4(^3P_0)4f$	$^2[3]^o$	5/2	$4s^24p^4(^3P)4d$	^4F	3/2	0.34(11)
234.438	21.468	16.182	$4s^24p^4(^3P_1)4f$	$^2[3]^o$	5/2	$4s^24p^4(^3P)4d$	^4F	3/2	0.32(11)
235.287	20.890	15.622	$4s^24p^4(^3P_2)4f$	$^2[5]^o$	9/2	$4s^24p^4(^3P)4d$	^4F	9/2	0.013(14)
236.275	21.534	16.289	$4s^24p^4(^3P_0)4f$	$^2[3]^o$	5/2	$4s^24p^4(^3P)4d$	^2P	3/2	0.11(11)
237.369	20.844	15.622	$4s^24p^4(^3P_2)4f$	$^2[4]^o$	7/2	$4s^24p^4(^3P)4d$	^4F	9/2	0.042(11)
237.553	20.840	15.622	$4s^24p^4(^3P_2)4f$	$^2[4]^o$	9/2	$4s^24p^4(^3P)4d$	^4F	9/2	0.17(11)
239.279	21.468	16.289	$4s^24p^4(^3P_1)4f$	$^2[3]^o$	5/2	$4s^24p^4(^3P)4d$	^2P	3/2	0.12(13)
240.852	21.751	16.604	$4s^24p^4(^3P)6d$	^4D	5/2	$4s^24p^4(^3P)5p$	$^4P^o$	5/2	0.12(12)
240.907	21.465	16.320	$4s^24p^4(^3P_1)4f$	$^2[3]^o$	7/2	$4s^24p^4(^3P)4d$	^2F	7/2	0.054(11)
241.381	21.739	16.604	$4s^24p^4(^3P)6d$	^4D	7/2	$4s^24p^4(^3P)5p$	$^4P^o$	5/2	0.14(11)
241.840	21.414	16.289	$4s^24p^4(^3P_1)4f$	$^2[2]^o$	3/2	$4s^24p^4(^3P)4d$	^2P	3/2	0.11(13)
245.607	21.533	16.486	$4s^24p^4(^3P_0)4f$	$^2[3]^o$	7/2	$4s^24p^4(^3P)4d$	^4P	5/2	0.29(11)
246.477	20.890	15.861	$4s^24p^4(^3P_2)4f$	$^2[5]^o$	9/2	$4s^24p^4(^3P)4d$	^4F	7/2	0.700(13)
247.885	20.861	15.861	$4s^24p^4(^3P_2)4f$	$^2[3]^o$	7/2	$4s^24p^4(^3P)4d$	^4F	7/2	0.043(11)
250.387	21.27	16.32		6°	7/2	4d	^2F	7/2	0.29(10)
255.591	20.907	16.058	$4s^24p^4(^3P_2)4f$	$^2[1]^o$	1/2	$4s^24p^44d$		1/2	0.24(14)
255.636	21.533	16.684	$4s^24p^4(^3P_0)4f$	$^2[3]^o$	7/2	$4s^24p^4(^3P)4d$	^2F	5/2	0.085(11)
255.910	21.534	16.691	$4s^24p^4(^3P_0)4f$	$^2[3]^o$	5/2	$4s^24p^44d$		3/2	0.13(11)
259.125	22.030	17.246	$4s^24p^4(^1D)5d$	^2P	3/2	$4s^24p^4(^3P)5p$	$^2P^o$	1/2	0.047(13)
259.248	21.465	16.684	$4s^24p^4(^3P_1)4f$	$^2[3]^o$	7/2	$4s^24p^4(^3P)4d$	^2F	5/2	0.74(11)
259.440	21.468	16.691	$4s^24p^4(^3P_1)4f$	$^2[3]^o$	5/2	$4s^24p^44d$		3/2	0.045(12)
259.536	20.86	16.09	5p"	$^2P^o$	1/2	4d	^4F	3/2	0.300(11)
259.773	20.852	16.080	$4s^24p^4(^3P_2)4f$	$^2[3]^o$	5/2	$4s^24p^4(^3P)4d$	^4F	5/2	0.073(11)
260.211	20.844	16.080	$4s^24p^4(^3P_2)4f$	$^2[4]^o$	7/2	$4s^24p^4(^3P)4d$	^4F	5/2	0.048(11)
261.671	21.421	16.684	$4s^24p^4(^3P_1)4f$	$^2[2]^o$	5/2	$4s^24p^4(^3P)4d$	^2F	5/2	0.12(11)
262.775	20.946	16.229	$4s^24p^4(^1S)5p$	$^2P^o$	3/2	$4s^24p^4(^3P)4d$	^4P	1/2	0.075(12)
264.306	20.918	16.229	$4s^24p^4(^3P_2)4f$	$^2[1]^o$	3/2	$4s^24p^4(^3P)4d$	^4P	1/2	0.31(11)
264.927	20.907	16.229	$4s^24p^4(^3P_2)4f$	$^2[1]^o$	1/2	$4s^24p^4(^3P)4d$	^4P	1/2	0.42(13)
266.097	21.528	16.870	$4s^24p^4(^3P)7s$	^4P	3/2	$4s^24p^4(^3P)5p$	$^4D^o$	5/2	0.16(12)
266.400	21.487	16.835	$4s^24p^4(^3P)7s$	^4P	5/2	$4s^24p^4(^3P)5p$	$^4D^o$	7/2	0.11(11)
266.661	20.877	16.229	$4s^24p^4(^3P_2)4f$	$^2[2]^o$	3/2	$4s^24p^4(^3P)4d$	^4P	1/2	0.063(11)
268.355	20.907	16.289	$4s^24p^4(^3P_2)4f$	$^2[1]^o$	1/2	$4s^24p^4(^3P)4d$	^2P	3/2	0.300(12)
269.570	20.886	16.289	$4s^24p^4(^3P_2)4f$	$^2[2]^o$	5/2	$4s^24p^4(^3P)4d$	^2P	3/2	0.18(13)
271.240	20.890	16.320	$4s^24p^4(^3P_2)4f$	$^2[5]^o$	9/2	$4s^24p^4(^3P)4d$	^2F	7/2	0.37(10)
271.449	20.886	16.320	$4s^24p^4(^3P_2)4f$	$^2[2]^o$	5/2	$4s^24p^4(^3P)4d$	^2F	7/2	0.028(13)
271.616	20.852	16.288	$4s^24p^4(^3P_2)4f$	$^2[3]^o$	5/2	$4s^24p^4(^3P)4d$	^2P	3/2	0.046(11)
272.946	20.861	16.320	$4s^24p^4(^3P_2)4f$	$^2[3]^o$	7/2	$4s^24p^4(^3P)4d$	^2F	7/2	0.082(11)
273.233	21.534	16.998	$4s^24p^4(^3P_0)4f$	$^2[3]^o$	5/2	$4s^24p^44d$		5/2	0.020(14)
273.326	21.533	16.998	$4s^24p^4(^3P_0)4f$	$^2[3]^o$	7/2	$4s^24p^44d$		5/2	0.21(11)
274.256	20.840	16.320	$4s^24p^4(^3P_2)4f$	$^2[4]^o$	9/2	$4s^24p^4(^3P)4d$	^2F	7/2	0.098(11)
275.902	22.064	17.571	$4s^24p^4(^3P)7s$	^2P	3/2	$4s^24p^4(^3P)5p$	$^4S^o$	3/2	0.038(16)
277.260	21.468	16.998	$4s^24p^4(^3P_1)4f$	$^2[3]^o$	5/2	$4s^24p^44d$		5/2	0.025(11)
279.581	21.431	16.998	$4s^24p^4(^3P_1)4f$	$^2[4]^o$	7/2	$4s^24p^44d$		5/2	0.28(10)
280.320	20.907	16.486	$4s^24p^4(^3P^2)4f$	$^2[1]^o$	1/2	$4s^24p^44d$		3/2	0.18(11)

the Boltzmann plot for the instant 60 µs after the beginning of the discharge. The deviation from the line obtained by a least-square fitting procedure is within ± 3 per cent. It is similar for any other instant of the plasma life for which measurements were taken. These results confirm the validity and self-consistency of our experimental transition probability data.

From the slope of the Boltzmann plot shown in Fig. 4, we obtain an electron temperature of 34 585 K. This temperature is in

Table 2 – *continued*

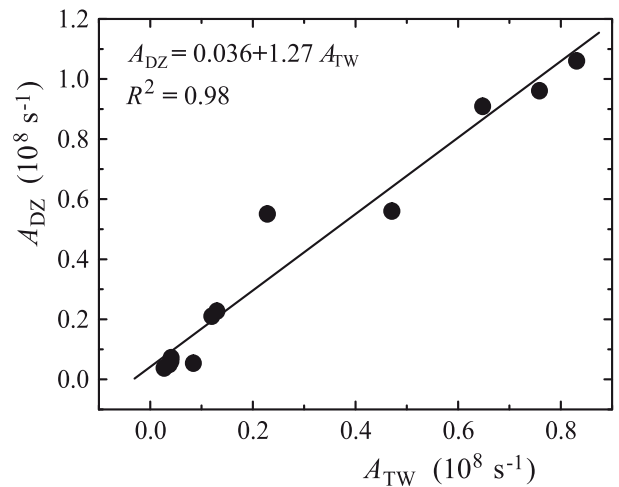| λ (nm)	E_{upper} (eV)	E_{lower} (eV)	Upper level Conf.	Upper level Term	J	Lower level Conf.	Lower level Term	J	A_{TW} (10^8 s^{-1})
280.360	20.91	16.48	5f	$^2D^o$	3/2		1	5/2	0.022(24)
281.646	20.886	16.486	$4s^24p^4(^3P_2)4f$	$^2[2]^o$	5/2	$4s^24p^44d$		3/2	0.300(11)
281.687	20.886	16.486	$4s^24p^4(^3P_2)4f$	$^2[2]^o$	5/2	$4s^24p^4(^3P)4d$	^4P	5/2	0.14(12)
283.300	20.861	16.486	$4s^24p^4(^3P_2)4f$	$^2[3]^o$	7/2	$4s^24p^4(^3P)4d$	^4P	5/2	0.29(10)
283.879	20.852	16.486	$4s^24p^4(^3P_2)4f$	$^2[3]^o$	5/2	$4s^24p^44d$		3/2	0.057(11)
284.446	20.844	16.486	$4s^24p^4(^3P_2)4f$	$^2[4]^o$	7/2	$4s^24p^4(^3P)4d$	^4P	5/2	0.028(11)
284.738	18.623	14.270	$4s^24p^4(^1D)5p$	$^2P^o$	3/2	$4s^24p^4(^3P)5s$	^4P	3/2	0.041(11)
295.835	22.73	18.54		13°	5/2	4d'	^2D	5/2	0.088(12)
296.725	20.861	16.684	$4s^24p^4(^3P_2)4f$	$^2[3]^o$	7/2	$4s^24p^4(^3P)4d$	^2F	5/2	0.14(11)
297.404	20.852	16.684	$4s^24p^4(^3P_2)4f$	$^2[3]^o$	5/2	$4s^24p^4(^3P)4d$	^2F	5/2	0.035(11)
297.887	20.852	16.691	$4s^24p^4(^3P_2)4f$	$^2[3]^o$	5/2	$4s^24p^44d$		3/2	0.049(11)
306.084	20.70	16.65		11°	5/2		^2D	3/2	0.073(11)
315.094	18.623	14.689	$4s^24p^4(^1D)5p$	$^2P^o$	3/2	$4s^24p^4(^3P)5s$	^2P	3/2	0.12(11)
320.040	18.875	15.002	$4s^24p^4(^1D)5p$	$^2P^o$	1/2	$4s^24p^4(^3P)5s$	^2P	1/2	0.13(11)
320.828	17.378	13.514	$4s^24p^4(^3P)5p$	$^4D^o$	1/2	$4s4p^6$	^2S	1/2	0.12(12)
322.657	22.66	18.82		10°	3/2		^2P	3/2	0.058(17)
328.209	18.875	15.099	$4s^24p^4(^1D)5p$	$^2P^o$	1/2	$4s^24p^4(^3P)4d$	^4D	1/2	0.040(11)
337.903	21.041	17.372	$4s^24p^4(^3P)5d$	^2D	5/2	$4s^24p^4(^3P)5p$	$^2D^o$	5/2	0.040(12)
338.111	21.041	17.375	$4s^24p^4(^3P)5d$	^2D	5/2	$4s^24p^4(^3P)5p$	$^2P^o$	3/2	0.073(11)
338.523	20.818	17.157	$4s^24p^4(^3P)5d$	^2P	3/2	$4s^24p^4(^3P)5p$	$^4D^o$	3/2	0.055(11)
342.373	18.623	15.002	$4s^24p^4(^1D)5p$	$^2P^o$	3/2	$4s^24p^4(^3P)5s$	^2P	1/2	0.027(11)
342.771	17.605	13.989	$4s^24p^4(^3P)5p$	$^2D^o$	3/2	$4s^24p^4(^3P)5s$	^4P	5/2	0.037(11)
343.098	20.769	17.157	$4s^24p^4(^3P)5d$	^4P	5/2	$4s^24p^4(^3P)5p$	$^4D^o$	3/2	0.042(12)
346.541	21.148	17.571	$4s^24p^4(^3P)5d$	^2D	3/2	$4s^24p^4(^3P)5p$	$^4S^o$	3/2	0.030(13)
347.005	20.818	17.246	$4s^24p^4(^3P)5d$	^2P	3/2	$4s^24p^4(^3P)5p$	$^2P^o$	1/2	0.29(11)
350.325	22.033	18.495	$4s^24p^4(^1D)5d$	^2F	5/2	$4s^24p^4(^1D)5p$	$^2F^o$	5/2	0.29(11)
353.535	20.155	16.649	$4s^24p^4(^3P)5d$	^4D	1/2	$4s^24p^4(^3P)5p$	$^4P^o$	3/2	0.49(10)
354.414	21.148	17.651	$4s^24p^4(^3P)5d$	^2D	3/2	$4s^24p^4(^3P)5p$	$^2S^o$	1/2	0.49(14)
354.454	22.058	18.561	$4s^24p^4(^1D)5d$	^2F	7/2	$4s^24p^4(^1D)5p$	$^2F^o$	7/2	0.36(12)
355.349	20.093	16.604	$4s^24p^4(^3P)5d$	^4D	3/2	$4s^24p^4(^3P)5p$	$^4P^o$	5/2	0.14(11)
355.554	22.109	18.623	$4s^24p^4(^1D)5d$	^2D	5/2	$4s^24p^4(^1D)5p$	$^2P^o$	3/2	0.16(12)
357.268	21.041	17.571	$4s^24p^4(^3P)5d$	^2D	5/2	$4s^24p^4(^3P)5p$	$^4S^o$	3/2	0.061(11)
358.625	20.061	16.604	$4s^24p^4(^3P)6s$	^2P	3/2	$4s^24p^4(^3P)5p$	$^4P^o$	5/2	0.042(11)
358.965	20.699	17.246	$4s^24p^4(^3P)5d$	^2P	1/2	$4s^24p^4(^3P)5p$	$^2P^o$	1/2	0.83(10)
359.686	20.818	17.372	$4s^24p^4(^3P)5d$	^2P	3/2	$4s^24p^4(^3P)5p$	$^2D^o$	5/2	0.028(15)
359.921	20.818	17.375	$4s^24p^4(^3P)5d$	^2P	3/2	$4s^24p^4(^3P)5p$	$^2P^o$	3/2	0.26(12)

Table 3. Comparison of the transition probabilities from this work (TW) with the absolute results from Dzierżega et al. (2001) – DZ – and Podbiralina et al. (1973) – PSS.

Wavelength (nm)	Absolute A_{ki} (10^8 s^{-1}) TW	DZ	PSS
231.202	0.084	0.054	
342.771	0.037	0.049	
284.738	0.041	0.072	0.130
315.094	0.12	0.210	0.045
320.040	0.13	0.227	
342.373	0.027	0.038	
328.209	0.040	0.060	

Figure 3. Comparison between the absolute transition probabilities from Dzierżega et al. (2001), A_{DZ}, and those from this work, A_{TW}.

a very good agreement with the one obtained from the measurements of the excitation temperature. This is the confirmation that our experimental procedure has been performed properly.

5 CONCLUSIONS

As a final conclusion, this work reports transition probability values for a set of 93 Kr II lines in the spectral region ranging from 208 to 360 nm, extending considerably the transition probability data base
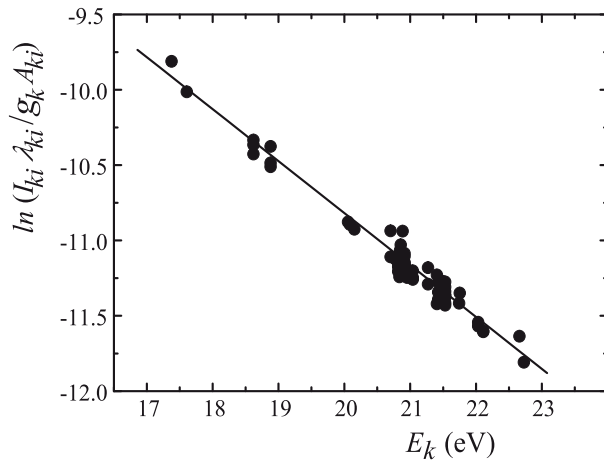
Figure 4. One of the Boltzmann plots obtained from all the new transition probability data presented in this work.

in the UV. For 86 of them there are not previous data, at least up to the authors' knowledge. The relative uncertainties of the A_{ki} values introduced by our method of measuring have been carefully calculated by taking into account different sources of error and they are lower than 15 per cent for almost all of them. Furthermore, this work analyses the differences found between data from Dzierżega et al. (2001), which constitutes one of the most comprehensive works done recently in A_{ki} values for Kr II, and the new values presented in this work. Since a careful revision of lifetime experiments was made in Dzierżega et al. (2001), the comparison with our data provides a useful mathematical expression to relate the A_{ki} values normalized with a scale based on lifetime measurements with those obtained from a scale based on plasma emission spectroscopy measurements. However, a very precise measurement of the value of at least one absolute transition probability would provide a way to establish the most appropriate absolute scale.

REFERENCES

Aparicio J. A., Gigosos M. A., González V. R., Pérez C., de la Rosa M. I., Mar S., 1998, J. Phys. B: At. Mol. Opt. Phys., 31, 1029
Belmonte M. T., Djurović S., Peláez R. J., Aparicio J. A., Mar S., 2014, MNRAS, 445, 3345
Bertuccelli G., Di Rocco H. O., 1991, Spectrosc. Lett., 24, 1039
Bidelman W. P., 1962, ApJ, 67, 111
Brandt T., Helbig V., Nick K.-P., 1982, J. Phys. B: At. Mol. Phys., 15, 2139
Cardelli J. A., Meyer D. M., 1997, ApJ, 477, L57
Cardelli J. A., Savage B. D., Ebbets D. C., 1991, ApJ, 383, L23
Cayless M. A., Marsden A. M., 1983, Lamps and Lighting, 3rd edn. Edward Arnold, London
Ćirišan M., Peláez R. J., Djurović S., Aparicio J. A., Mar S., 2011, Phys. Rev. A, 83, 012513
Das M. B., 1997, J. Quant. Spectrosc. Radiat. Transfer, 57, 237
Das M. B., Bhattacharya R., 1992, Z. Phys., 22, 699

de Castro A., Aparicio J. A., del Val J. A., González V. R., Mar S., 2001, J. Phys. B: At. Mol. Opt. Phys., 34, 3275
del Val J. A., Mar S., Gigosos M. A., de la Rosa M. I., Pérez C., González V. R., 1998, Japan. J. Appl. Phys., 37, 4177
Dinerstein H. L., 2001, ApJ, 550, L223
Djeniže S., Milosavljević V., Dimitrijević M. S., 2003, Eur. Phys. J. D, 27, 209
Djurović S., Peláez R. J., Ćirišan M., Aparicio J. A., Mar S., 2006, J. Phys. B: At. Mol. Opt. Phys., 39, 2901
Dzierżega K., Griesmann U., Nave G., Bratasz L., 2001, Phys. Scr., 63, 209
El Sherbini T. M., Farrag A. A., 1976, J. Phys. B: At. Mol. Opt. Phys., 9, 2797
Fonseca V., Campos J., 1982, J. Phys. B: At. Mol. Phys., 15, 2349
Fuhr J. R., Wiese W. L., 1996, in Lide D. R., Frederikse H. P. R., eds, CRC Handbook of Chemistry and Physics, 77th edn., CRC Press. Inc., Boca Raton, p. 128
Fuhr J. R., Wiese W. L., 1998, in Lide D. R., ed., CRC Handbook of Chemistry and Physics, 78th edn. CRC Press. Inc., Boca Raton, p. 154
Gigosos M. A., Mar S., Pérez C., de la Rosa I., 1994, Phys. Rev. E, 49, 1575
Griem H. R., 1963, Phys. Rev., 131, 1170
Griem H. R., 1964, Plasma Spectroscopy. McGraw-Hill Book Company, New York
Griem H. R., 1997, Principles of Plasma Spectroscopy. Cambridge Univ. Press, Cambridge
Helbig V., 1978, PhD thesis, Kiel Univ.
Jullien S., Lemaire J., Fenistein S., Heninger M., Mauclaire G., Marx R., 1993, Chem. Phys. Lett., 212, 340
Konjević N., 1999, Phys. Rep., 316, 339
Kramida A., Ralchenko Yu., Reader J., NIST ASD Team, 2015, NIST Atomic Spectra Database (version 5.2), (Available at http://physics.nist.gov/asd)
Lauer S., Liebel H., Vollweiler F., Schmoranzer H., Lagutin B. M., Demekhin Ph. V., Petrov I. D., Sukhorukov V. L., 1999, J. Phys. B: At. Mol. Phys., 32, 2015
Loch S. D. et al., 2002, Phys. Rev. A, 66, 052708
Mar S., del Val J. A., Rodríguez F., Peláez R. J., González V. R., Gonzalo A. B., de Castro A., Aparicio J. A., 2006, J. Phys. B: At. Mol. Phys., 39, 3709
Marantz H., Rudko R. I., Tang C. L., 1969, IEEE J. Quantum Electron., 5, 38
Mazouffre S., Pawelec E., 2009, J. Phys. D: Appl. Phys., 42, 015203
Miller M. H., Roig R. A., Bengtson R. D., 1972, J. Opt. Soc. Am., 62, 1027
Morton D. C., 2000, ApJS, 130, 403
Peláez R. J., Pérez C., González V. R., Rodríguez F., Aparicio J. A., Mar S., 2005, J. Phys. B., 38, 2505
Peláez R. J., Mar S., Aparicio J. A., Belmonte M. T., 2012, Appl. Spectrosc., 66, No. 8
Podbiralina V. P., Smirnov Yu. M., Stegnova N. V., 1973, Opt. Spectrosc., 34, 467
Rodríguez F., Aparicio J. A., de Castro A., del Val J. A., González V. R., Mar S., 2001, A&A, 372, 338
Saito M., Ojima N., Itoi S., Haruyama Y., 2015, Phys. Rev. A, 91, 012508
Sansonetti J. E., Martin W. C., 2005, J. Phys. Chem. Ref. Data, 34, 1559
Schade W., Stryla Z. W., Helbig V., Langhans G., 1989, Phys. Scr., 39, 246
Sharpee B., Zhang Y., Williams R., Pellegrini E., Cavagnolo K., Badwin J. A., Phillips M., Lui X. W., 2007, ApJ, 659, 1265
Shimoda K., 1984, Introduction to Laser Physics. Springer Series in Optical Sciences, Springer, Berlin
Striganov A. R., Sventitskii N. S., 1968, Tables of Spectral Lines of Neutral and Ionized Atoms. Plenum, New York
Träbert E., 2012, Phys. Scr., 85, 048101
van der Mullen J. A. M., 1990, Phys. Rep. 191, 109
Ward L., Wännström A., Arnesen A., Hallin R., Vogel O., 1985, Phys. Scr., 31, 149
Werner K., Rauch T., Ringat E., Kruk J. W., 2012, ApJ, 753, L7

This paper has been typeset from a TEX/LATEX file prepared by the author.

Conclusions

1) One of the main contributions of this work has been the development of a general mathematical expression that quantifies the relative uncertainties introduced in our transition probability measurements. A detailed analysis of all the possible sources of error present in our experiment has been carried out, establishing not only their presence, but also their relevance and how they affect the total intensity of a spectral line.

2) Stark parameters (widths and shifts) for singly ionized Argon (Ar II) have been measured in the spectral region between 265 and 405 nm. A set of 126 half-widths and 111 shifts are reported, mostly for 4p4d and 3d4f transitions, 53 half-width and 44 shift values being new, at least to the best of the authors' knowledge. Careful plasma diagnostics were performed, obtaining an electron density in the range of $(0.20 - 1.15) \times 10^{23}$ m^{-3} and an excitation temperature ranging from 16 000 to 26 000 K.

The obtained Stark parameters showed a clear linear dependence on electron density and were compared with both experimental and theoretical results from other authors. A very detailed analysis of Stark parameter regularities within multiplets, supermultiplets and transition arrays was performed. Most of the existing irregularities have been explained from the study of the Ar II complex energy level structure

3) A set of 43 reliable transition probabilities for single ionized Argon (Ar II) in the UV spectral region 294 - 386 nm is reported, yielding 11 new A_{ki}-values and 22 for which the existing data have uncertainties of around 50%, extending the experimental work previously carried out in our laboratory much further. Plasma electron densities of $(3.5 - 9.0) \times 10^{22}$ m^{-3} and temperatures between 19 000 and 22 000 K were obtained by performing careful plasma diagnostics.

The method used is based on the measurement of relative intensities of spectral lines emitted from a low-pressure-pulsed discharge lamp. Accurate transition probabilities of

11 spectral lines were taken from the literature and used to establish an absolute scale. The measured A_{ki}-values have been carefully studied and compared with the existing data, finding a significant lack of self-consistency with some of the values in the NIST spectral database which is worth analysing.

4) Transition probabilities of singly ionized Krypton (Kr II) have been measured, extending the spectral range of the previous measurements carried out in our laboratory to the ultraviolet. A set of 93 Kr II transition probabilities within the spectral range 208 - 360 nm is reported, 86 of them being new as far as the authors are aware. The electron density was in the range of $(1.5 - 3.4) \times 10^{22}$ m^{-3} and the plasma temperature ranged from 28 000 to 35 000 K.

Transition probabilities were obtained by measuring the relative intensities of the spectral lines under study. In order to transform our relative measurements into absolute ones, we have selected seven spectral lines and taken their A_{ki}-value from the bibliography. The A_{ki}-values reported have been compared with measurements obtained from branching ratio and lifetime measurements, providing a very useful mathematical expression to relate the transition probability values obtained with a scale based on lifetime measurements to those obtained from a scale based on plasma emission spectroscopy measurements. The measurement of at least one very precise absolute transition probability value would provide a way of establishing the most appropriate absolute scale.

Appendices

Appendix A

Medidas de probabilidades de transición y parámetros Stark de gases nobles una vez ionizados.

"Y cuando la mirada es sólo un catalejo,
para viajar por laberintos donde el dato es religión,
aún creo en la pregunta 'qué hay tras el espejo'
en donde se produce la osadía de la reflexión"

- Luis Eduardo Aute, *La inocencia* -

Introducción y objetivos.

La medida de parámetros atómicos, tales como las probabilidades de transición y las anchuras y desplazamientos Stark, es de gran importancia no solo en el campo de la física teórica y atómica, sino también para el diagnóstico de cualquier fuente emisora de radiación tales como lámparas convencionales, láseres, plasmas industriales y de fusión o en el campo de la Astrofísica, en donde las probabilidades de transición son necesarias para el cálculo de abundancias químicas de los distintos elementos en las estrellas. Sin embargo, las necesidades actuales no se ven cubiertas por los datos disponibles hoy en día,

siendo esta falta especialmente acusada en la región del ultravioleta, en donde existe una gran carencia de datos experimentales de buena calidad para átomos ionizados.

El objetivo de esta tesis doctoral es la medida de nuevos datos atómicos mediante una técnica de espectroscopía de emisión de plasmas. En concreto, este trabajo se ha centrado en:

1) Medida de nuevos valores de probabilidades de transición de calidad para líneas espectrales de Argon y Kripton una vez ionizados en la región del ultravioleta, prestando especial atención al cálculo de sus incertidumbres.

2) Medida de anchuras y desplazamientos Stark de líneas espectrales de Argon una vez ionizado en la región del ultravioleta.

Este trabajo aporta y analiza una cantidad significativa de datos nuevos y de sus incertidumbres, contribuyendo así a una mejora y modernización de las bases de datos atómicos existentes a partir de nuevos datos de gran calidad.

El trabajo de esta tesis doctoral se ha llevado a cabo en el Laboratorio de Espectroscopía de Plasmas de la Universidad de Valladolid. Este grupo lleva trabajando en la medida de parámetros atómicos más de treinta aos y tiene una gran experiencia en el mundo de la espectroscopía de plasmas fruto de las muchas horas de intenso trabajo invertidas por todas aquellas personas que forman y han formado parte de él. El dispositivo experimental y los métodos de diagnóstico del plasma utilizado en este trabajo han sido desarrollados durante todos estos aos, siendo este profundo conocimiento del experimento lo que ha permitido llevar a cabo medidas de gran calidad.

Este manuscrito se ha estructurado en seis capítulos diferentes. Los primeros tres están dedicados a la descripción del marco teórico, el dispositivo experimental y el procesado de los datos. La segunda mitad de este manuscrito está formado por otros tres capítulos, cada uno de los cuales contiene uno de los artículos ya publicados que contituyen esta tesis doctoral e incluyen el estado del arte, los detalles de cada uno de los experimentos llevados a cabo, as como los resultados y conclusiones.

El **Capítulo 1** contiene un resument de los conceptos teóricos fundamentales relacionados con la medida de probabilidades de transición de parámetros Stark y define todos los términos que se utilizarán a lo largo del manuscrito. El **Capítulo 2** contiene una descripción exhaustiva del dispositivo experimental, desde la generación de los plas-

mas hasta la adquisición de los espectros, prestando especial atención a la calibración del canal espectroscópico. El **Capítulo 3** se centra en el proceso de los datos y en el estudio de la determinación de las incertidumbres asociadas a la medida de los parámetros atómicos. Los **Capítulos 4**, **5** y **6** contienen los detalles experimentales y los resultados y conclusiones de los experimentos de medidas de parámetros Stark en Ar II y medidas de probabilidades de transición de Ar II y Kr II en la región del ultravioleta, respectivamente.

Metodología.

Para la medida de probabilidades de transición y parámetros Stark se han generado plasmas de argon y kripton en una lámpara pulsada a baja presión mediante la descarga de una batería de condensadores de 20 μF a través de un tubo cilíndrico de Pyrex de 175 mm de longitud y 19 mm de diámetro interno. La batería de condensadores se cargó hasta 7.8 kV. Se hizo fluir gas puro a través del tubo de descarga, ajustándose la presión para obtener máxima intensidad y mínima autoabsorción. Para asegurar la repetitividad del plasma, se preionizó el gas contenido en la lámpara de descarga aplicando una corriente continua de varios mA. El tiempo de vida de los distintos plasmas generados fue de unos 200 μs, aproximadamente.

Los plasmas generados están bien caracterizados. Se ha realizado un cuidadoso diagnóstico del plasma para obtener la temperatura y la densidad electrónica del mismo mediante la técnica del Boltzmann-plot y un método de interferometría a dos longitudes de onda, respectivamente. En todos los experimentos realizados, los distintos parámetros del plasma cumplían los criterios de equilibrio termodinámico local parcial (pLTE) para todos los instantes de medida considerados. En todas las medidas se ha realizado un chequeo muy cuidadoso de la autoabsorción de las líneas espectrales, desechando todas aquellas cuyas autoabsorciones eran mayores del 20%.

Resultados y conclusiones.

Una de las principales contribuciones de este trabajo ha sido el desarrollo de una expresión matemática general que cuantifica las incertidumbres relativas introducidas en nuestras medidas de probabilidades de transición. Para obtener esta expresión, se ha realizado

un análisis detallado de todas las posibles fuentes de error presentes en nuestro experimento estableciendo no solo su presencia, sino también su relevancia y cómo afectan a la intensidad de las líneas espectrales.

Los resultados experimentales obtenidos en cada uno de los experimentos que componen esta tesis doctoral y las conclusiones de los mismos se detallan a continuación:

1) Se han medido parámetros Stark (anchuras y desplazamientos) de líneas espectrales del Argon una vez ionizado en la región espectral entre los 265 y los 405 nm. Este trabajo aporta un conjunto de 126 semianchuras y 111 desplazamientos, la mayor parte correspondientes a transiciones 4p-4d y 3d-4f, siendo 53 valores de semianchuras y 44 de desplazamientos nuevos. Se ha realizado un cuidadoso diagnstico del plasma, obteniendo una densidad electrónica en el rango $(0.20 - 1.15) \times 10^{23}$ m^{-3} y una temperatura de excitación de 16 000 a 26 000 K.

Los parámetros Stark obtenidos muestran una clara dependencia con la densidad electrónica y han sido comparados con resultados tanto experimentales como teóricos de otros autores. Se ha realizado un análisis muy detallado de las regularidades de los parámetros Stark dentro de multipletes, submultipletes y transiciones. La mayor parte de las irregularidades encontradas han sido explicadas en base a un estudio de la compleja estructura de niveles del energía del Ar II.

2) Este trabajo aporta un conjunto de 43 valores de probabilidades de transición para el Argon una vez ionizado en la región del ultravioleta entre los 294-386 nm, proporcionando 11 nuevos valores y 22 medidas para las cuales los datos existentes tenían incertidumbres alrededor del 50%, extendiendo de esta manera los trabajos experimentales realizados con anterioridad en nuestro laboratorio. El diagnóstico del plasma permitió obtener la densidad electrónica, la cual oscilaba entre $(3.5 - 9.0) \times 10^{22}$ m^{-3} y la temperatura entre los 19 000 y los 22 000 K.

El método experimental utilizado para el cálculo de las probabilidades de transición se basa en la medida de las intensidades relativas de líneas espectrales emitidas por un plasma generado en una lámpara de descarga pulsada a bajas presiones. Para establecer una escala absoluta de medida se utilizaron 11 valores de probabilidades de transición cogidos de la bibliografía. Los valores obtenidos de A_{ki} han sido analizados cuidadosamente y comparados con los datos existentes, encontrando una falta de consistencia significativa con algunos de los valores incluídos en la base de datos atómicos del NIST que merece la pena analizar.

3) Se han medido valores de probabilidades de transición del Kripton una vez ionizado (Kr II), extendiendo hacia el ultravioleta el rango espectral de las medidas llevadas a cabo con anterioridad en nuestro laboratorio. Se aporta un conjunto de 93 probabilidades de transición del Kr II en el rango espectral 208-360 nm, siendo 86 de estos valores nuevos. La densidad electrónica de los plasmas generados osciló entre $(1.5 - 3.4) \times 10^{22}$ m^{-3} y la temperatura electrónica entre 28 000 y 35 000 K.

Las probabilidades de transición se obtuvieron a partir de la medida de intensidades relativas de las líneas espectrales de interés. Para transformar nuestras medidas relativas en absolutas, se seleccionó un conjunto de siete líneas espectrales cuyos valores de probabilidades de transición fueron cogidos de la bibliografía. Los valores de A_{ki} aportados han sido comparados con valores obtenidos a partir de medidas de branching ratios y tiempos de vida. A partir de esta comparación, se ha obtenido una expresión matemática muy útil que permite relacionar las probabilidades de transición obtenidas a partir de ua escala basada en medidas de tiempos de vida con aquellas obtenidas a partir de experimentos de espectroscopía de emisión de plasmas. La medida de al menos un valor de probabilidad de transición proporcionaría un modo de establecer cuál de las escalas absolutas mencionadas anteriormente es la más apropiada.

Appendix B

Reconstruction of self-absorbed profiles.

The general idea about the correction of the self-absorbed profiles has already been introduced in Chapter 3. In this appendix, the mathematical expressions used by the code "General" are included for completeness.
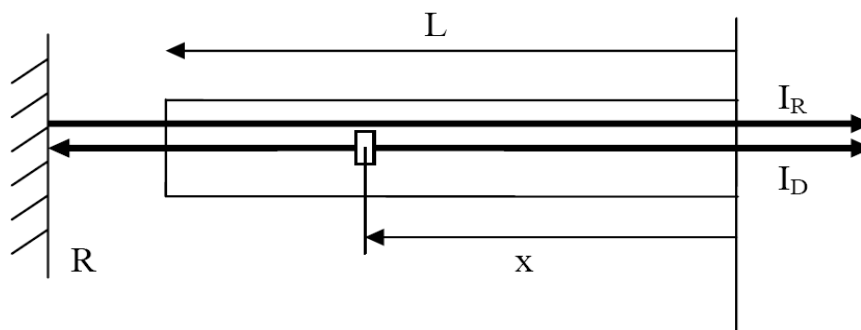
Figure B.1: Schematic idea of the self-absorption correction.

The direct irradiance, I_D, can be expressed as:

$$I_D(\lambda) = \int_0^L \varepsilon_\lambda e^{\kappa_\lambda x} dx = \frac{\varepsilon_\lambda}{\kappa_\lambda}(1 - e^{-L \ \kappa_\lambda}) = S_\lambda(1 - e^{-\tau_\lambda}) \qquad (\text{B.1})$$

where:

$\varepsilon_\lambda \rightarrow$ emission coefficient.

$\kappa_\lambda \rightarrow$ absorption coefficient.

$L \rightarrow$ length of the lamp.

$\tau_\lambda \rightarrow$ optical depth.

$S_\lambda \rightarrow$ source function.

The dependence of S_λ on the wavelength is smooth, it being the blackbody dependence if the plasma is in local thermodynamic equilibrium (LTE). In the vicinities of a spectral line, we will assume that the source function is practically constant, S.

The irradiance recorded when the mirror is operating, I_M, is given by:

$$I_M(\lambda) = I_D(\lambda) + I_R(\lambda) = I_D(\lambda) + R I_D(\lambda) e^{-\tau_\lambda} \tag{B.2}$$

where R is the *effective reflectivity*. It is useful to define now the quantity r_λ as:

$$r_\lambda \equiv \frac{I_M(\lambda) - I_D(\lambda)}{I_D(\lambda)} = R e^{-\tau_\lambda} \tag{B.3}$$

It is possible to see how if $\tau_\lambda \rightarrow 0$, $r_\lambda \rightarrow R$. The corrected value of the irradiance, once the self-absorption effect has been eliminated, is given by:

$$I_c(\lambda) = S\tau_\lambda = I_D(\lambda)\frac{\tau_\lambda}{1 - e^{-\tau_\lambda}} \tag{B.4}$$

where:

$$\tau_\lambda = -\ln(\frac{1 - I_D(\lambda)}{S}) \tag{B.5}$$

In order to reconstruct a self-absorbed profile, it is necessary to evaluate the source function S and this requires knowing R, the effective reflectivity. The code "General" includes different options for the calculation of R depending on how noisy r_λ is. The most useful methods are as follows:

a) Mode E (Exact): it is used in conditions of low noise. In this method, S and R are obtained simultaneously by performing a linear fit of r_λ against $I_D(\lambda)$.

$$r_\lambda = Re^{-\tau_\lambda} = R - \frac{R}{S}I_D(\lambda) \tag{B.6}$$

b) Mode P (Parabolic): this mode is used in cases of normal noise. S and R are obtained simultaneously performing a cuadratic fitting of $I_M(\lambda)$ against $I_D(\lambda)$. The expression used for the fitting is:

$$I_M(\lambda) = I_D(\lambda) + I_D(\lambda)R(1 - \frac{I_D(\lambda)}{S}) = (1+R)I_D(\lambda) - \frac{R}{S}I_D^2(\lambda) \tag{B.7}$$

c) Mode D (Débil = Weak): this is used for situations of high noise. In this case, R should be known and S is calculated from data of the peak of the spectral line.

$$I_D(\lambda) = S(1 - e^{-\tau_\lambda}) = S(1 - \frac{r_\lambda}{R}) \tag{B.8}$$

which results in:

$$S = \frac{I_D(\lambda)}{1 - \frac{r_\lambda}{R}} = \frac{I_D(max)}{1 - \frac{r_\lambda}{R}} \tag{B.9}$$

where

$$r_\lambda(max) = \frac{I_M(max) - I_D(max)}{I_D(max)} \tag{B.10}$$

The precision of this method is usually defined by that one of R.

Appendix C

Co-authors' permission.

ACEPTACIÓN DE LOS COAUTORES

D. **SANTIAGO MAR SARDAÑA**, con DNI 17176147T, como coautor de las publicaciones:

1. M. T. Belmonte; L. Gavanski; R. J. Pelaez; J. A. Aparicio; S. Djurovic; S. Mar. *"Kr II transition probability measurements for the UV spectral region"*. Monthly Notices of the Royal Astronomical Society (MNRAS), 456, 518-524 (2016).
2. M. T. Belmonte, S. Djurovic, R. J. Peláez, J. A. Aparicio and S. Mar. *"Improved and expanded measurements of transition probabilities in UV Ar II spectral lines"*. Monthly Notices of the Royal Astronomical Society (MNRAS), 445, 3345-3351 (2014).
3. S. Djurovic, M. T. Belmonte, R. J. Peláez, J. A. Aparicio and S. Mar. *"Stark parameter measurement of Ar II UV spectral lines"*. Monthly Notices of the Royal Astronomical Society (MNRAS), 433, 1082-1093 (2013).

doy mi consentimiento para que éstas formen parte de la Tesis Doctoral en la modalidad de "compendio de publicaciones" presentada en la Universidad de Valladolid por Dña. **MARÍA TERESA BELMONTE SAINZ-EZQUERRA** y titulada *"Experimental transition probabilities and Stark parameters of singly ionized noble gases"*, asimismo renuncio a la presentación de las publicaciones como parte de otra tesis doctoral.

Fecha y firma

VALLADOLID, 3 MAYO 2016

CO-AUTHOR PERMISSION

Mr **SANTIAGO MAR SARDAÑA** , with ID 17176147T, as co-author of the articles:

1. M. T. Belmonte; L. Gavanski; R. J. Pelaez; J. A. Aparicio; S. Djurovic; S. Mar. *"Kr II transition probability measurements for the UV spectral region"*. Monthly Notices of the Royal Astronomical Society (MNRAS), 456, 518-524 (2016).
2. M. T. Belmonte, S. Djurovic, R. J. Peláez, J. A. Aparicio and S. Mar. *"Improved and expanded measurements of transition probabilities in UV Ar II spectral lines"*. Monthly Notices of the Royal Astronomical Society (MNRAS), 445, 3345-3351 (2014).
3. S. Djurovic, M. T. Belmonte, R. J. Peláez, J. A. Aparicio and S. Mar. *"Stark parameter measurement of Ar II UV spectral lines"*. Monthly Notices of the Royal Astronomical Society (MNRAS), 433, 1082-1093 (2013).

I give my full consent for its/their use as part of the PhD Thesis elaborated as "compendium of publications" presented at the University of Valladolid by Ms **MARÍA TERESA BELMONTE SAINZ-EZQUERRA** entitled *"Experimental transition probabilities and Stark parameters of singly ionized noble gases"*, renouncing as well to present them as part of any other PhD thesis.

Date and signature

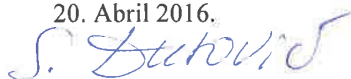VALLADOLID, 3 MAY 2016

ACEPTACIÓN DE LOS COAUTORES

D. **STEVICA DJUROVIĆ**, con pasaporte n°(007005962) , como coautor de las publicaciones:

1. M. T. Belmonte; L. Gavanski; R. J. Pelaez; J. A. Aparicio; S. Djurovic; S. Mar. *"Kr II transition probability measurements for the UV spectral region"*. Monthly Notices of the Royal Astronomical Society (MNRAS), 456, 518-524 (2016).
2. M. T. Belmonte, S. Djurovic, R. J. Peláez, J. A. Aparicio and S. Mar. *"Improved and expanded measurements of transition probabilities in UV Ar II spectral lines"*. Monthly Notices of the Royal Astronomical Society (MNRAS), 445, 3345-3351 (2014).
3. S. Djurovic, M. T. Belmonte, R. J. Peláez, J. A. Aparicio and S. Mar. *"Stark parameter measurement of Ar II UV spectral lines"*. Monthly Notices of the Royal Astronomical Society (MNRAS), 433, 1082-1093 (2013).

doy mi consentimiento para que éstas formen parte de la Tesis Doctoral en la modalidad de "compendio de publicaciones" presentada en la Universidad de Valladolid por Dña. **MARÍA TERESA BELMONTE SAINZ-EZQUERRA** y titulada *"Experimental transition probabilities and Stark parameters of singly ionized noble gases"*, asimismo renuncio a la presentación de las publicaciones como parte de otra tesis doctoral.

Fecha y firma

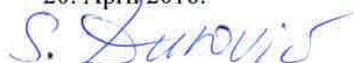20. Abril 2016.

CO-AUTHOR PERMISSION

Mr **STEVICA DJUROVIĆ**, with passport (007005962), as co-author of the articles:

1. M. T. Belmonte; L. Gavanski; R. J. Pelaez; J. A. Aparicio; S. Djurovic; S. Mar. *"Kr II transition probability measurements for the UV spectral region"*. Monthly Notices of the Royal Astronomical Society (MNRAS), 456, 518-524 (2016).
2. M. T. Belmonte, S. Djurovic, R. J. Peláez, J. A. Aparicio and S. Mar. *"Improved and expanded measurements of transition probabilities in UV Ar II spectral lines"*. Monthly Notices of the Royal Astronomical Society (MNRAS), 445, 3345-3351 (2014).
3. S. Djurovic, M. T. Belmonte, R. J. Peláez, J. A. Aparicio and S. Mar. *"Stark parameter measurement of Ar II UV spectral lines"*. Monthly Notices of the Royal Astronomical Society (MNRAS), 433, 1082-1093 (2013).

I give my full consent for its/their use as part of the PhD Thesis elaborated as "compendium of publications" presented at the University of Valladolid by Ms **MARÍA TERESA BELMONTE SAINZ-EZQUERRA** entitled *"Experimental transition probabilities and Stark parameters of singly ionized noble gases"*, renouncing as well to present them as part of any other PhD thesis.

Date and signature

20. April 2016.

ACEPTACIÓN DE LOS COAUTORES

D. **JUAN ANTONIO APARICIO CALZADA**, con DNI 12372576W, como coautor de las publicaciones:

1. M. T. Belmonte; L. Gavanski; R. J. Pelaez; J. A. Aparicio; S. Djurovic; S. Mar. *"Kr II transition probability measurements for the UV spectral region"*. Monthly Notices of the Royal Astronomical Society (MNRAS), 456, 518-524 (2016).
2. M. T. Belmonte, S. Djurovic, R. J. Peláez, J. A. Aparicio and S. Mar. *"Improved and expanded measurements of transition probabilities in UV Ar II spectral lines"*. Monthly Notices of the Royal Astronomical Society (MNRAS), 445, 3345-3351 (2014).
3. S. Djurovic, M. T. Belmonte, R. J. Peláez, J. A. Aparicio and S. Mar. *"Stark parameter measurement of Ar II UV spectral lines"*. Monthly Notices of the Royal Astronomical Society (MNRAS), 433, 1082-1093 (2013).

doy mi consentimiento para que éstas formen parte de la Tesis Doctoral en la modalidad de "compendio de publicaciones" presentada en la Universidad de Valladolid por Dña. **MARÍA TERESA BELMONTE SAINZ-EZQUERRA** y titulada *"Experimental transition probabilities and Stark parameters of singly ionized noble gases"*, asimismo renuncio a la presentación de las publicaciones como parte de otra tesis doctoral.

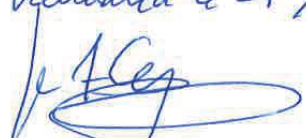Fecha y firma *Valladolid, 25/4/16*

CO-AUTHOR PERMISSION

Mr **JUAN ANTONIO APARICIO CALZADA**, with ID 12372576W, as co-author of the articles:

1. M. T. Belmonte; L. Gavanski; R. J. Pelaez; J. A. Aparicio; S. Djurovic; S. Mar. *"Kr II transition probability measurements for the UV spectral region"*. Monthly Notices of the Royal Astronomical Society (MNRAS), 456, 518-524 (2016).
1. M. T. Belmonte, S. Djurovic, R. J. Peláez, J. A. Aparicio and S. Mar. *"Improved and expanded measurements of transition probabilities in UV Ar II spectral lines"*. Monthly Notices of the Royal Astronomical Society (MNRAS), 445, 3345-3351 (2014).
2. S. Djurovic, M. T. Belmonte, R. J. Peláez, J. A. Aparicio and S. Mar. *"Stark parameter measurement of Ar II UV spectral lines"*. Monthly Notices of the Royal Astronomical Society (MNRAS), 433, 1082-1093 (2013).

I give my full consent for its/their use as part of the PhD Thesis elaborated as "compendium of publications" presented at the University of Valladolid by Ms **MARÍA TERESA BELMONTE SAINZ-EZQUERRA** entitled *"Experimental transition probabilities and Stark parameters of singly ionized noble gases"*, renouncing as well to present them as part of any other PhD thesis.

Date and signature *Valladolid a 25/4/16*

ACEPTACIÓN DE LOS COAUTORES

D. **RAMÓN J. PELÁEZ DE FUENTES**, con DNI nº09343185-X , como coautor de las publicaciones:

1. M. T. Belmonte; L. Gavanski; R. J. Pelaez; J. A. Aparicio; S. Djurovic; S. Mar. *"Kr II transition probability measurements for the UV spectral region"*. Monthly Notices of the Royal Astronomical Society (MNRAS), 456, 518-524 (2016).
2. M. T. Belmonte, S. Djurovic, R. J. Peláez, J. A. Aparicio and S. Mar. *"Improved and expanded measurements of transition probabilities in UV Ar II spectral lines"*. Monthly Notices of the Royal Astronomical Society (MNRAS), 445, 3345-3351 (2014).
3. S. Djurovic, M. T. Belmonte, R. J. Peláez, J. A. Aparicio and S. Mar. *"Stark parameter measurement of Ar II UV spectral lines"*. Monthly Notices of the Royal Astronomical Society (MNRAS), 433, 1082-1093 (2013).

doy mi consentimiento para que éstas formen parte de la Tesis Doctoral en la modalidad de "compendio de publicaciones" presentada en la Universidad de Valladolid por Dña. **MARÍA TERESA BELMONTE SAINZ-EZQUERRA** y titulada *"Experimental transition probabilities and Stark parameters of singly ionized noble gases"*, asimismo renuncio a la presentación de las publicaciones como parte de otra tesis doctoral.

Fecha y firma
Madrid a 21 de abril de 2016

CO-AUTHOR PERMISSION

Mr **RAMÓN J. PELÁEZ DE FUENTES**, with ID 09343185-X, as co-author of the articles:

1. M. T. Belmonte; L. Gavanski; R. J. Pelaez; J. A. Aparicio; S. Djurovic; S. Mar. *"Kr II transition probability measurements for the UV spectral region"*. Monthly Notices of the Royal Astronomical Society (MNRAS), 456, 518-524 (2016).
2. M. T. Belmonte, S. Djurovic, R. J. Peláez, J. A. Aparicio and S. Mar. *"Improved and expanded measurements of transition probabilities in UV Ar II spectral lines"*. Monthly Notices of the Royal Astronomical Society (MNRAS), 445, 3345-3351 (2014).
3. S. Djurovic, M. T. Belmonte, R. J. Peláez, J. A. Aparicio and S. Mar. *"Stark parameter measurement of Ar II UV spectral lines"*. Monthly Notices of the Royal Astronomical Society (MNRAS), 433, 1082-1093 (2013).

I give my full consent for its/their use as part of the PhD Thesis elaborated as "compendium of publications" presented at the University of Valladolid by Ms **MARÍA TERESA BELMONTE SAINZ-EZQUERRA** entitled *"Experimental transition probabilities and Stark parameters of singly ionized noble gases"*, renouncing as well to present them as part of any other PhD thesis.

Date and signature
Madrid, April 21st 2016
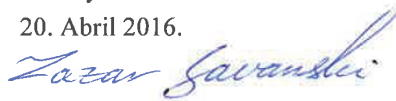
ACEPTACIÓN DE LOS COAUTORES

D. **LAZAR GAVANSKI**, con pasaporte nº(007774162) , como coautor de las publicaciones:

1. M. T. Belmonte; L. Gavanski; R. J. Pelaez; J. A. Aparicio; S. Djurovic; S. Mar. *"Kr II transition probability measurements for the UV spectral region"*. Monthly Notices of the Royal Astronomical Society (MNRAS), 456, 518-524 (2016).

doy mi consentimiento para que éstas formen parte de la Tesis Doctoral en la modalidad de "compendio de publicaciones" presentada en la Universidad de Valladolid por Dña. **MARÍA TERESA BELMONTE SAINZ-EZQUERRA**   y titulada *"Experimental transition probabilities and Stark parameters of singly ionized noble gases"*, asimismo renuncio a la presentación de las publicaciones como parte de otra tesis doctoral.

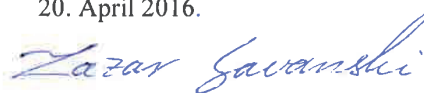Fecha y firma
20. Abril 2016.

CO-AUTHOR PERMISSION

Mr **LAZAR GAVANSKI**, with passport (007774162), as co-author of the articles:

1. M. T. Belmonte; L. Gavanski; R. J. Pelaez; J. A. Aparicio; S. Djurovic; S. Mar. *"Kr II transition probability measurements for the UV spectral region"*. Monthly Notices of the Royal Astronomical Society (MNRAS), 456, 518-524 (2016).

I give my full consent for its/their use as part of the PhD Thesis elaborated as "compendium of publications" presented at the University of Valladolid by Ms **MARÍA TERESA BELMONTE SAINZ-EZQUERRA** entitled *"Experimental transition probabilities and Stark parameters of singly ionized noble gases"*, renouncing as well to present them as part of any other PhD thesis.

Date and signature
20. April 2016.

Appendix D

Publications and Conference Papers.

Short Stays

Visiting PhD Student Imperial College London (United Kingdom).
Space and Atmospheric Physics Department. 3 months, September- December 2015.

Visiting PhD Student University of Novi Sad (Serbia). Physics Department.
3 months, August- November 2014.

Visiting PhD Student University of Novi Sad (Serbia). Physics Department.
3 months, September- December 2013.

Publications

"Experimental Stark halfwidths of the ionized oxygen and silicon spectral lines" L. Gavanski, M. T. Belmonte, I. Savić and S. Djurović. Monthly Notices of the Royal Astronomical Society (MNRAS), 457, 4038-4050 (2016).

"Kr II transition probability measurements for the UV spectral region". M. T. Belmonte, L. Gavanski, R. J. Peláez, J. A. Aparicio, S. Djurović and S. Mar. Monthly Notices of the Royal Astronomical Society (MNRAS), 456, 518-524 (2016).

"Improved and expanded measurements of transition probabilities in UV Ar

II spectral lines". M. T. Belmonte, S. Djurović, R. J. Peláez, J. A. Aparicio and S. Mar. Monthly Notices of the Royal Astronomical Society (MNRAS), 445, 3345-3351 (2014).

"Stark parameter measurement of Ar II UV spectral lines". S. Djurović, M. T. Belmonte, R. J. Peláez, J. A. Aparicio and S. Mar. Monthly Notices of the Royal Astronomical Society (MNRAS), 433, 1082-1093 (2013).

"Integration of an ICCD camera for accurate spectroscopic measurements". R. Peláez, S. Mar, J.A Aparicio, M.T. Belmonte. Applied Spectroscopy, 66, 8, 970-978 (2012).

Conferences

Oral contribution ***"Estimación de la incertidumbre de probabilidades de transición medidas mediante espectroscopia de emisión en un plasma pulsado"***. M. T. Belmonte, L. Gavanski, R. J. Peláez, J. A. Aparicio, S. Djurović and S. Mar. XXXV Bienal de la Real Sociedad Espaola de Física (Gijón, Spain) "Young Researchers in Plama and its applications": 13-17 July 2015.

"Transition Probabilities Measurements of several UV ArII lines". M. T. Belmonte, J. A. Aparicio, R. J. Peláez, S. Djurović and S. Mar. SPIG 2014 (27th Summer School and International Symposium on the Physics of Ionized Gases. Belgrado, Serbia). 26-29 August 2014.

Oral contribution ***"Medida de las probabilidades de transición del Argon ionizado en la región del ultravioleta"***. M. T. Belmonte, R. J. Peláez, S. Djurović, J. A. Aparicio and S. Mar. X Reunión Nacional de Óptica (Zaragoza, Spain). 4-7 September 2012.

"Transition Probabilities Measurements of several XeII lines". M. T. Belmonte, J. A. Aparicio, R. J. Peláez, S. Djurović and S. Mar. SPIG 2012 (26th Summer School and International Symposium on the Physics of Ionized Gases. Zrenjanin, Serbia). 27-31 August 2012.

"Experimental transition probability measurements in pulsed lamps: critical points.". J. A. Aparicio, M. T. Belmonte, R. J. Peláez, S. Djurović and S. Mar. SPIG 2012 (26th Summer School and International Symposium on the Physics of Ionized Gases. Zrenjanin, Serbia). 27-31 August 2012.

Bibliography

Ali A. W. and Griem H. R., 1965, Phys. Rev., 140, 1044.

Ali A. W. and Griem H. R., 1966, Phys. Rev., 144, 366.

Alpher R. A. and White D. R., 1965, *Plasma diagnostic techniques*,(ed. H. Huddlestone, S. L. Leonard), Academic Press.

Aparicio J. A., 1996, *Medidas de parámetros atómicos en un plasma pulsado de argón*, PhD Thesis, University of Valladolid.

Aparicio J. A., Gigosos M. A., González V. R., Pérez C., de la Rosa M. I., Mar S., 1998, J. Phys. B: At. Mol. Opt. Phys., 31, 1029.

Baranger M., 1962, Spectral Line Broadening in Plasmas, *Atomic and Molec. Processes* (ed. Bates), Academic Press.

Bittencourt J. A., 2004, *Fundamentals of Plasma Physics*, Ed. Springer, Third edition.

Canon C. J., 1985, *The transfer of spectral line radiation*, ed. Cambridge University Press.

Chen F. F., 1974, *Introduction to Plasma Physics*, Plenum Press, New York.

Cooper J., 1966, *Plasma Spectroscopy*, Rep. Prog. Phys., 29, 35.

Corney A., 1970, *The measurement of Lifetimes of Free Atoms, Molecules and ions*, Adv. in Electronics and Electrn Phys. 29, 115.

Crossley R. J. S., 1969, *Calculation of Atomic Transition Probabilities*, Adv. in Atomic and Molecular Phys., 5, 237.

Crookes W., 1897, *On Radiant Matter*, Lecture delivered before the British Association for the Advancement of Science at Sheffield, Friday, 22 August 1879. The Popular Science Monthly, Volume 16., 157, D. Appleton.

Davis J. T. and Vaughan J. M, 1963, Astrophys. J., 137, 1302.

Djurović S., Peláez R. J., Ćirišan M., Aparicio J. A., Mar S., 2006, J. Phys. B: At. Mol. Phys. Opt., 39, 2901

Dzierżega K., Griesmann U., Nave G., Bratasz L., 2001, Phys. Scr. 63, 209.

Fantz U., 2006, Plasma Sources Sci. Technol., 15, 137.

Fujimoto T. and Whirter R. W. P., 1990, Phys. Rev. A, 42, 6588.

Gigosos M. A., Mar S., Pérez C. and de la Rosa I., 1994, Phys. Rev. E, 49, 2, 1575.

González V. R., 1999, *Medida de parámetros atómicos en un plasma de silicio*, PhD Thesis,University of Valladolid.

Griem H. R., 1963, Phys. Rev., 131, 3, 1170.

Griem H. R., 1964, *Plasma Spectroscopy*, Mc Graw-Hill Book Company, New York.

Griem H. R., 1974. *Spectral line broadening by Plasmas*, McGraw-Hill, New York.

Griem H. R., 1997, *Principles of Plasma Spectroscopy*, Ed. Cambridge University Press.

Hibbert A. and Hansen, J. E., 1994, J. Phys. B, 27, 3325.

Huber M. C. E. and Sandeman R. J., 1986, Rep. Prog. Phys, 49, 397.

Huddlestone R. H. and Leonard S. L, 1965, *Plasma Diagnostic Techniques*, Edited by Huddlestone, R. H. and Leonard, S. L, Academic Press.

Hutchinson I. H., 1987, *Principles of Plasma Diagnostics*, Cambridge University Press, New York.

Kock M., 1996, Phys. Scripta, 65,43.

Konjević N., 1999, Physics Reports 316, 339.

Kramida A., Ralchenko Yu., Reader J., NIST ASD Team, 2015, NIST Atomic Spectra Database(version5.2), [Online]. Available:http://physics.nist.gov/asd

Kuhn H. G., 1969, *Atomic Spectra*, Longmans.

Layzer D. and Garstang R. H., 1968, *Theoretical Atomic Transition Probabilities*, Ann. Rev. of Astron. and Astrophys., 6, 449.

Lochte-Holtgreven W., 1968, *Plasma Diagnostics*, Ed. North-Holland, Amsterdam; Interscience (Wiley), New York

Marr G., 1968, *Plasma Spectroscopy*, Elsevier.

Miles B. M. and Wiese W. L, 1970, Bibliography on Atomic Transition Probabilities, N.B.S. Spec. Pub. 320 (1916-1969)

Nicholls R. W. and Steward A. L., 1962, Allowed Transitions, *Atomic and Molec. Processes* (ed. Bates), Academic Press.

Peláez R. J., 2008, Doctoral Thesis, University of Valladolid.

Peláez R. J., Mar S., Aparicio J. A, Belmonte M. T., 2012, Appl. Spectrosc., 66, No. 8

Ritcher J., 1968, *Plasma diagnostics*, (ed. by Lochte-Holtgreven), North-Holland Publishing Company, Amsterdam.

de la Rosa M. I., 1989, *Medida de la refractividad de un plasma pulsado. Influencia de las especies no electrónicas*, PhD Thesis, University of Valladolid.

de la Rosa M. I., Pérez C., de Frutos, A. M. and Mar, S., 1990, Phys. Rev. A, 42, 7389.

de la Rosa M. I., Pérez. C, de Frutos A. M. and Mar S., 1990, Appl. Opt., 29, 4725.

Ruffoni M. P., 2013, Comput. Phys. Commun., 184, 1770.

Sikström C. M., Nilsoon H., Litzén U., Blom A. and Lundberg H., 2002, J. Quant. Spectrosc. Radiat. Transfer, 74, 355.

Spitzer L., 1956, *Physics of Fully Ionized Gases*, Interscience Publishers, New York.

Striganov A. R., Sventitskii N. S., 1968, Tables of Spectral Lines of Neutral and Ionized Atoms, Plenum, New York.

Taylor B. N. and Kuyatt C. E., 1994, *Guidelines for evaluating and expressing the uncertainty of NIST measurement results*, National Institute of Standards and Technology.

Thorne A. P., 1974, *Spectrophysics*, Chapman and Hall Ltd, London.

del Val J. A., 1993, *Medida de la Distribución Espacial y Temporal de la Densidad Electrónica y de la Temperatura en un Plasma Pulsado*, Tesina de Licenciatura, University of Valladolid.

del Val J. A., 1997, *Determinación de parámetros atómicos en plasmas de neón*, PhD Thesis, University of Valladolid.

del Val J. A., Mar S., Gigosos M. A., de la Rosa M. I., Pérez C., González V. R., 1998, Japan J. Appl. Phys., 37, 4177.

Van der Mullen J. A. M., 1990, Phys. Rep., 191, 109.

Vujnović V., Wiese W. L., 1992, J. Phys. Chem. Ref. Data, 21, 5, 919.

Wiese W. L., Smith M. W. and Glennon B. M., *Atomic Transition Probabilities*, N.S.R.D.S. N.B.S 4 vol. I H-Ne,1966; N.B.S. 22 vol. II Na-Ca, 1969.

Wies, W. L., 1987, J. Quant. Spectrosc. Radiat. Transfer, 40, 3, 421.

Wiese W. L. and Kelleher D. E., 1998, The Critical Assesment of Atomic Transition Probabilities, *Atomic and Molec. Data and their appl.*, (ed. Mohr & Wiese).